

Antonio Šiber

 ${\bf A.\ \check{S}iber},\ Theory\ of\ thermal\ energy\ inert\ atom\ scattering\ from\ surface\ vibrations$

A. Šiber, Teorija neelastičnog raspršenja inertnih atoma na vibracijama kristalnih površina

The work decribed in this book is based on A. Šiber's Master of Science Thesis which has been done at the Institute of Physics, Zagreb, under the tutorship of Dr. Branko Gumhalter within the framework of the Postgraduate Physics Study at the Physics Department of the Faculty of Natural Sciences and Mathematics of the University of Zagreb.

THEORY OF THERMAL ENERGY INERT ATOM SCATTERING FROM SURFACE VIBRATIONS

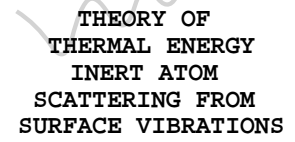
Antonio Šiber

You are viewing the electronic version 2.1 of the manuscript, created on 11th of January 2000 by Antonio Šiber.

Contents

1	Introduction			
2	Basic concepts in			
3	Inte	eraction of inert atoms	13	
	3.1	Static component of the	14	
		3.1.1 Pairwise summation procedure	14	
		3.1.2 Other procedures for obtaining the static compo-		
		nent of the interaction potential	20	
		3.1.3 Some general properties of the static component		
		of the interaction potential	21	
	3.2	Dynamic component of the	24	
	3.3	Convenient approximations to	25	
4	Nor	rmal modes and phonons	29	
	4.1	Small oscillations	30	
	4.2	Normal modes in	33	
	4.3	Normal modes in semi-infinite	36	
	4.4	Force constants and the	40	
	4.5	Quantization of normal modes	43	
5	Sho	ort survey of atom-surface	47	
6	DW	/BA:	53	
	6.1	Derivation of the DWBA	54	
	6.2	Probability of elastic	67	
	6.3	Additional comments concerning	69	
7	For	ced oscillator model or	73	
	7.1	Essentials of time dependent	74	
	7.2	Derivation of the trajectory	76	
	7.3		83	

	7.4	Comparison of the elastic
8	Exp	onentiated Born 87
	8.1	Dyson form as the
	8.2	Alternative approach to the
	8.3	The alternative approach
	8.4	EBA: 97
	8.5	Additional comments
9	Con	aparison of theoretical 105
	9.1	$\mathrm{He} \to \mathrm{Cu}(001)$
	9.2	Ne, Ar, $\stackrel{\frown}{\mathrm{Kr}} \rightarrow \mathrm{Cu}(111)$
	9.3	$\text{He} \rightarrow \text{Xe/Cu(111)} \dots \dots$
	9.4	$\mathrm{He} \to \mathrm{Xe/Cu}(001)$
	9.5	$\text{He} \rightarrow \text{Xe}(111)$
	9.6	Debye-Waller factor and exponent
		9.6.1 Ne, Ar, Kr \rightarrow Cu(111)
		9.6.2 He $\to Cu(001)$
		9.6.3 He $\to Xe(111)$
	9.7	
		9.7.1 He $\to \text{Xe/Cu}(111)$
		9.7.2 He $\to \text{Xe/Cu}(001)$
		9.7.3 He $\to Cu(001)$
		9.7.4 He \to Xe(111)
	9.8	Mean energy transfer
		9.8.1 He $\to \text{Xe/Cu}(111)$
		9.8.2 He $\to Cu(001)$
		9.8.3 Ne, Ar, Kr \to Cu(111)
	9.9	Comments on the applicability of
10	Poss	sible future investigations 129
11	Sun	nmary 133



Antonio Šiber

 ${\bf A.\ \check{S}iber},\ Theory\ of\ thermal\ energy\ inert\ atom\ scattering\ from\ surface\ vibrations$

A. Šiber, Teorija neelastičnog raspršenja inertnih atoma na vibracijama kristalnih površina

Chapter 1 Introduction

 $A \ thousand \ miles \ journey, \\ starts \ with \ a \ single \ step$

Lao Tse

THEORY OF
THERMAL ENERGY
INERT ATOM
SCATTERING FROM
SURFACE VIBRATIONS

Antonio Šiber

In this thesis we study the scattering of inert, thermal energy atoms from vibrations of semi infinite crystals. Scattering of inert atoms (especially helium) from surfaces has developed over the past 15 years ¹ into an indispensable technique for the studies of surface dynamics, i.e. phonons. However, the theory needed for detailed interpretation of the experiments has not been developed to a satisfactory extent, particularly for experiments performed in the multiphonon scattering regime. The aim of this work is to contribute to the understanding of microscopic processes involved in inelastic scattering of thermal energy inert atoms from surfaces.

The presentation of the subject follows the outline given below.

Basic notions in the theoretical descriptions of atom-surface collisions are explained in *Chapter 2*. A short survey of the theoretical approaches is given in terms of the basic principles which are further illustrated within a simplified, one dimensional model description of the problem. Several standard approaches used in the field of atom-surface scattering (forced oscillator model - trajectory approximation and Langevin equation approach) are explained using a simple, one dimensional model of the problem.

The potentials governing both the static and dynamic components of the interaction of atoms with surfaces are explained in *Chapter 3*. Model potentials employed in the calculations are discussed.

Normal vibrational modes typical of infinite and semi-infinite crystals are discussed in $Chapter\ 4$. A general approach to the system of N mutually interacting bodies is presented first. The lattice dynamics approach to the problem of finding the normal modes (phonons) is briefly outlined. The notation and nomenclature typical of the so-called "slab calculations" is introduced. Quantization of normal modes is presented in the last section of this chapter.

Typical scattering experiments, including the description of experimental equipment used, are further explained in *Chapter 5*. Basic principles of the time-of-flight (TOF) technique are explained. A relatively detailed account of the various experimental parameters is given. The detection of scattered projectile atoms is briefly discussed. The geometrical dimensions of experimental apparatus, typical ranges of experimental scattering parameters and the physics underlying the detection of scattered atoms turn out to be of essential importance for comparison of the calculated and measured spectra.

First order perturbation theory approach as applied to the problem

¹For very readable, popular text on this subject see [1].

of atom-surface scattering is outlined in *Chapter 6*. This approximation falls into the class known as the Distorted Wave Born Approximation (DWBA). A rather detailed derivation of the DWBA for the case of uncorrugated surface is given. Some comments on the appropriateness of the use of DWBA for comparison with experiments are given in the last section of this chapter.

Nonperturbative approach which treats the projectile dynamics classically, but still uses Schrödinger equation for the description of target phonons is sketched in *Chapter 7*. This class of approximations is known as the forced oscillator model or the trajectory approximation.

A derivation of a more complete and powerful approximation to treat the scattering problem, which approximately includes contributions to all orders in the perturbation expansion, is presented in *Chapter 8*. This approximation has become known as the Exponentiated Born Approximation (EBA). Some additional comments on the validity of EBA are presented in the last section of this chapter. The thus developed EBA has been adopted as a basic theoretical tool for all calculations presented in this work.

A basic description of the scattering systems studied, concerning their vibrational and interaction properties (*Chapters 4* and 3) is given at the beginning of *Chapter 9*. Furthermore, comparison of experimental results with the results obtained within the EBA is presented for the representative scattering systems.

Some drawbacks and limitations of the calculations in their present form and possible perspectives for improvements are shortly summarized in *Chapter 10*.

A short summary of the work presented in this thesis is given in *Chapter 11*.

Notations and conventions specific to the surface and solid state physics (such as the labeling of crystal planes and directions in the Brilluoin zone, types of crystal structures etc.) have been chosen to agree with references [2, 3] wherever possible.

Chapter 2

Basic concepts in atom-surface scattering

 $Lack\ of\ skill\ dictates\ the\ economy\ of\ style.$

Joey Ramone

THEORY OF
THERMAL ENERGY
INERT ATOM
SCATTERING FROM
SURFACE VIBRATIONS

Antonio Šiber

The title of this thesis contains the expression "inert atoms". This simply means that in the process of scattering of inert atoms from surfaces we can safely disregard all the processes in which a transfer or strong rearrangement of charge leading to chemical bonding may occur¹. These processes require much more energy than available in the course of collision since the oscillations of the target are characterized by energies of the order of 10 meV and the atoms scattered from surfaces are expected to have the energies of the same order of magnitude (experiments typically operate in the range of 5-120 meV of incident projectile energy - these energies are commonly called "thermal energies").

The basic physics of thermal energy atom-surface scattering can be explained in simple terms even to an undergraduate reader ². The atom used as a projectile has a specific charge distribution, namely the nucleus and the electronic "cloud". The target sample also has a specific charge distribution. Thus, the surfaces of simple metals have a characteristic "jellium-like" type of charge distribution where the nearly free electrons "spill out" across the jellium edge ³ with their density exponentially decaying into the vacuum [2]. On the other hand, the charge distribution at crystal surfaces made up of condensed noble gas atoms is expected to be realistically described by a superposition of atomic charge distributions, since one does not expect that the charge delocalization phenomena would be important in this case. Here, the charge distribution is expected to be inhomogeneous, reflecting the crystalline, geometrical arrangement of the noble gas atoms.

Upon approaching the surface, the inert projectile atom whose scattering is studied will experience effective repulsive potential at distances at which the two charge distributions overlap. This distance is typically of the order 2-3 Å⁴. That is why the inert projectile atoms of thermal

¹Recent results point to certain amount of hybridization of the inert atom orbitals with the target orbitals [4].

²It is not an intention of this chapter to give a detailed overview of the various theoretical approaches to the problem of atom-surface scattering. An extremely limited point of view is taken here in order to explain the nature of the problem in simple and clear terms. More detailed accounts of the various theoretical approaches can be found in [5, 6].

³Jellium edge is located a/2 above the centers of the topmost atom crystal plane, where a is the normal distance between the equivalent crystal planes (of the same structure as the surface or the topmost plane of atoms).

⁴The classical "turning point" of the projectile atoms is located at the distance where the velocity of the projectile in the direction perpendicular to the surface vanishes. This distance depends on the static atom-surface potential and the incident energy of the projectile atom [7].

energies are reflected from the surface. These atoms do not penetrate into the sample and they are most sensitive to the topmost layer of atoms (surface) [1].

At distances far from the surface, there is a net attraction between the atom and the surface arising as a consequence of the dynamic dipole-dipole interactions. The dynamic dipole component of the atomic charge distribution induces a similar dipole "image" in the whole metallic sample, which results in a net attraction. For noble gas crystals, this "image" is formed in each atom of the sample and a superposition of such atomic van der Waals interactions is expected to realistically describe the total van der Waals potential.

For samples of other types, the physical picture of interaction lies somewhere in between the two extreme cases discussed so far.

If the atoms of the target were fixed at their positions, they would exert a time independent, static force on the projectile atom and hence, all the projectile atoms would be reflected elastically, i.e. with the outgoing energy equal to the incident energy. The fact that the atoms in the crystal move even at zero temperature makes the interaction potential time dependent. Dynamic interactions lead to processes in which the energy of separate constituents of the system studied is generally not conserved [8]. This gives rise to a transfer of energy from the projectile atom to the target or vice versa, with the total energy of the whole system (projectile atom + target) conserved. The processes in which nonzero energy transfer occurs are called inelastic processes.

The points emphasized so far can be easily illustrated on a simple classical example. We shall represent the projectile atom as a material point of mass m and energy ϵ_i moving towards a mass M (representing the target) on a spring characterized by the stiffness constant k. The effective potential between the two bodies will be assumed to depend only on the relative distance between the geometrical centers of the bodies. One has to solve two coupled Newton equations describing the motion of both bodies. The coupling is introduced through the interaction potential. Only one dimension will be considered, i.e. the projectile atom motion is constrained to the line connecting the two point masses. Figure 2.1 shows the temporal evolution of the positions of the two bodies. It is seen that the transfer of energy does occur here, since the oscillator has a finite amplitude of oscillation (i.e. nonzero energy) after the scattering event has been completed (after the bodies have separated so that their interaction can be neglected). This is a

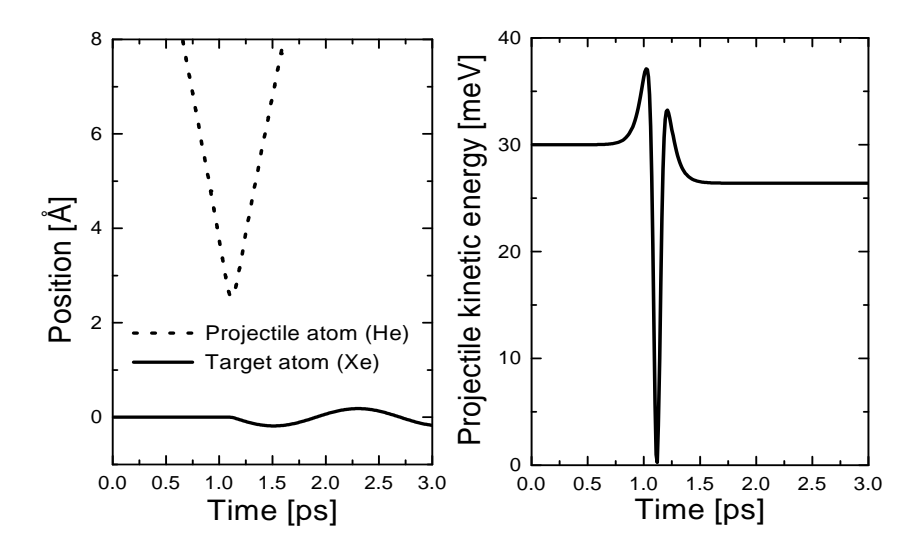


Figure 2.1: Left: Temporal evolution of positions of projectile atom and one dimensional harmonic oscillator. Right: The kinetic energy of projectile atom as a function of time.

typical example of an inelastic scattering event ⁵.

The parameters of this calculation were adjusted to model the He \rightarrow Xe/Cu(111) scattering system. Therefore, the projectile atom mass was set to 4 amu, the target atom mass to 131.29 amu, characteristic frequency of vibration was set to 2.62 meV (this is a perpendicular frequency of Xe/Cu(111) vibration - see section 9.3), which corresponds to k = 3.47 N/m, while the parameters of the interaction potential can be found in section 9.5. They were taken to be the same as for the $He \rightarrow Xe(111)$ scattering system (the substrate Cu(111) does not appear in this calculation, but the frequency of perpendicular vibration is determined by the substrate properties). Initial He atom energy is 30 meV. The target oscillator was assumed to be at the equilibrium point with the velocity equal to zero at time t=0. Note that the point where the velocity of the projectile atom vanishes is located at 2.54 A^6 . Although this example looks rather oversimplified for application to atom-surface scattering (the oscillator and the projectile atom are assumed to behave classically), there have been attempts to solve the

⁵Note that the scale of the interaction time is a picosecond.

 $^{^6}$ This is *not* the turning point to be introduced in *Chapter 6* since the target is allowed to move.

problem of atom-surface scattering following this line of thought. Of course, all three dimensions are included in the problem, the surface is represented by many coupled oscillators and a set of coupled Newton's equations is solved. This approach has become known as a generalized Langevin equation approach or stochastic classical trajectory approximation [2] and is well known in the literature on atom-surface scattering [9, 10]. It is expected to work well in applications to heavy projectile atoms when the quantum corrections are expected to be small (at least for the projectile atom, whereas the problem of a classical treatment of the target vibrations still remains). Note that this approach conserves the total energy in the system.

A simplified quantum approach to the problem will be explained next. Let us assume that the projectile atom can be treated as a time dependent force acting on quantized vibrations of the sample atoms. The time dependence of this force can be obtained by "freezing" the atoms in the sample and obtaining the classical, elastic trajectory of the projectile atom which is then inserted back into the interaction potential making it time dependent. In one dimension this simply means that if we know the dependence of the atom-target interaction potential, V(z), on the relative distance between the two "bodies", z, we can obtain the time dependence of the interaction by inserting the elastic trajectory z(t) (obtained by solving the Newton equation for the projectile in potential V(z) and subjected to appropriate initial conditions) back in the potential, which yields V(z(t)). The response of the target to time dependent perturbation can then be easily calculated following the well established schemes [8, 11]. The information one acquires from this type of calculation is the time evolution of populations of vibrational states of the target. The method is further illustrated on a one-dimensional prototype model with the interaction and vibrational parameters equal to the ones in figure 2.1. The left part of the figure 2.2 represents the time evolution of populations of harmonic oscillator levels. The results presented in figure 2.2 were obtained by numerically solving the coupled differential equations which result from the formal solution to the time dependent perturbation acting on a system described by a solvable hamiltonian.

The oscillator was assumed to be in the lowest energy eigen-state (denoted by "0" in the figure) prior to collision. One can obtain the energy transferred to the harmonic oscillator by subtracting its initial energy from its energy after the interaction has terminated (see the right part of the figure 2.2). Note that the energy transferred (3.78 meV) is quite close to the value calculated classically (in figure 2.1, 3.6 meV).

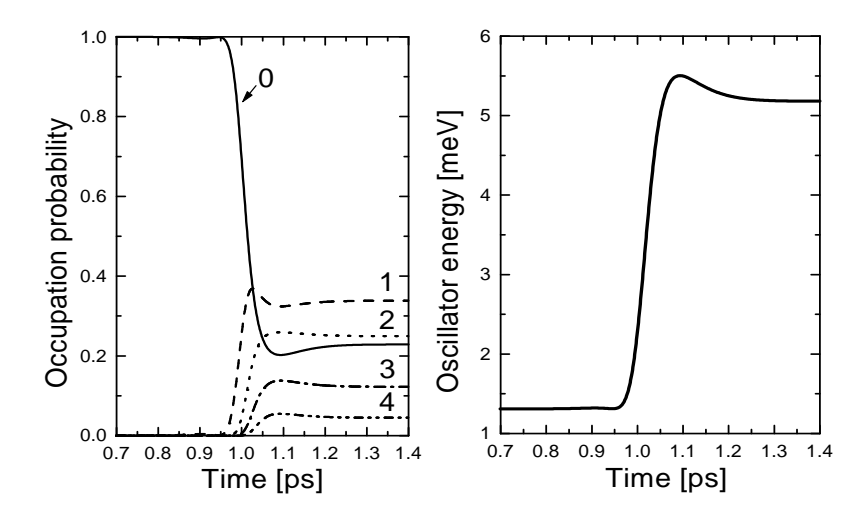


Figure 2.2: Left: Temporal evolution of population of the levels of a one dimensional harmonic oscillator. Numbers above the curves correspond to quantum numbers of the harmonic oscillator. Right: Temporal evolution of the harmonic oscillator energy.

The populations of the levels follow the Poisson distribution law [12] (see figure 2.3, interaction and vibrational parameters are the same as in figures 2.1 and 2.2). This is a characteristic of all so called *independent boson models* forced by external, recoilless perturbation [12, 13]. It is also interesting to note that the energy of the target harmonic oscillator is *not* a monotonously growing function of time which is something one could expect. At $t \approx 1.1$ ps, the oscillator energy has a maximum, which is a consequence of the interplay of the populations of harmonic oscillator levels and level excitation and de-excitation probabilities.

This type of approximation has become known as the forced oscillator model or the recoilless trajectory approximation. Although it treats the target vibrations in a quantum mechanical manner, it has several drawbacks. What is most important, the law of energy conservation is not satisfied: the atoms in the sample gain energy from the projectile atom which is assumed to scatter elastically without recoil. However, as this type of calculation has been widely used for description of atom-surface scattering [14, 15, 16, 17, 18, 19, 21], a variety of schemes has been proposed for remedying the drawbacks inherent in this approach [20, 21]. A realistic application of the trajectory approximation to the problem of atom-surface scattering will be outlined in Chapter 7.

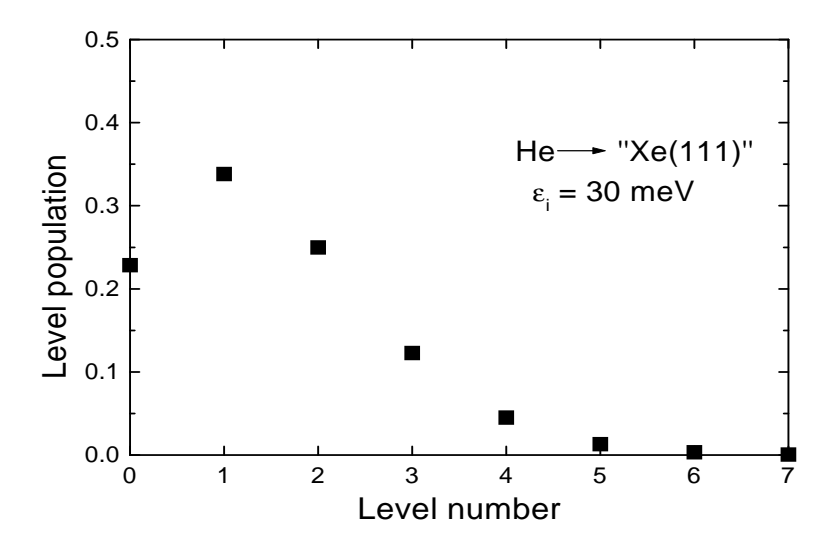


Figure 2.3: The populations of quantum harmonic oscillator levels after the interaction has terminated.

In the following two chapters I shall describe two prerequisites needed even for simple calculations as those presented above, namely the atom-target interaction potentials and the model of vibrational dynamics of the target (phonons in the discussed two simple models were represented by a single classical (quantal) oscillator with characteristic frequency of 2.62 meV). These two ingredients of the model form a base necessary for calculating the scattering transition rates in all atom-surface scattering theories.

Chapter 3

Interaction of inert atoms with crystalline surfaces

If I kiss you, that is a psychological interaction.

On the other hand, if I hit you over the head with a brick, that is also a psychological interaction.

The difference is that one is friendly and the other is not so friendly.

The crucial point is if you can tell which is which.

_

Dolph Sharp, "I'm O.K., You're Not So Hot"

THEORY OF
THERMAL ENERGY
INERT ATOM
SCATTERING FROM
SURFACE VIBRATIONS

Antonio Šiber

3.1 Static component of the atom-target interaction potential

The knowledge of a precise atom-target potential is of essential importance even for simple calculations as those presented in the preceding chapter. In the present chapter I shall address the problem of obtaining information on the interaction potential. The simplest case, for which a rather accurate answer to the problem can be given, is the atom-surface scattering system in which the target is a noble gas crystal ¹. There, the charge delocalization is expected to be of minor importance and we can expect that the atom-target interaction potential, $V(\mathbf{r})$, can be constructed as a superposition of atomic potentials, $v(|\mathbf{r} - \mathbf{r}_j|)$ (here \mathbf{r}_j are the positions of the target atoms), known very accurately from the crossed molecular beam scattering experiments ² [22]. The same holds for ionic crystals such as LiF due to the closed shell electronic structure of ions making up the crystal and the absence of a delocalized electronic charge [26].

3.1.1 Pairwise summation procedure

When the target is noble gas or ionic crystal, we can write the total potential as a pairwise sum of projectile-atom(ion) potentials:

$$V(\mathbf{r}) = \sum_{j} v(||\mathbf{r} - \mathbf{r}_{j}||). \tag{3.1}$$

Here \mathbf{r} is the radius vector of the projectile atom, $\{j\}$ is the set of indices enumerating the atoms in the sample and \mathbf{r}_{j}^{0} is the radius vector of atom j in its equilibrium position. Note that we have a priori assumed spherical symmetry of the pair potentials, v, which is reflected in the fact that these potentials depend only on the modulus of the relative radius vector. We shall further illustrate the procedure of pairwise summation on He \rightarrow Xe(111) potential. The He-Xe atomic potential is known rather accurately from the scattering experiments in the gasphase [22, 23]. We take the functional form of this potential from

¹A typical example, which is going to be throughly examined in this section, is the scattering from Xe(111) surface, see section 9.5.

²The comparisons of the theoretical and experimental differential collision cross section for the elastic scattering serve as an excellent test of various interaction potential models.

reference [23]:

$$v(r_r) = Ae^{-\alpha r_r} - \left(\frac{C_6}{r_r^6} + \frac{C_8}{r_r^8} + \frac{C_{10}}{r_r^{10}}\right) \exp\left[-\left(1.28\frac{r_m}{r_r} - 1\right)^2\right]$$
(3.2)

where r_r is the distance between the He and Xe nuclei. The last exponential term in equation (3.2) which "damps" the attractive part of the potential applies only if $r_r < 1.28r_m$. The parameters of this potential are specified in the table below ³:

Parameter	Units	Value
A	meV	8116570
α	$1/ ext{Å}$	3.93
C_6	$\mathrm{meV}\ \mathrm{\AA}^6$	11014
C_8	${ m meV~\AA^8}$	56766
C_{10}	$\mathrm{meV}\ \mathrm{\AA^{10}}$	334761
r_m	Å	5.03

The potential $V(\mathbf{r})$ in equation (3.1) depends on three spatial variables, so it is generally difficult to represent in all details in just one plot. In figure 3.1 we plot the He \rightarrow Xe(111) potential, $V(\mathbf{r})$, as a function of two coordinates (x, y) in the surface plane and for two values of coordinate z which is perpendicular to the surface plane. The origin of coordinate system (x = 0, y = 0, z = 0) is chosen to be in the center of the Xe atom in the topmost layer. The summation over the Xe(111) crystal sites has been performed by taking into account 128×128 atoms in the topmost Xe(111) layer and the same number of atoms in the Xe(111) layer located below the topmost layer. The nearest neighbor Xe-Xe distance has been set to a = 4.37 Å. Figure 3.1 displays the result of this calculation. Note that this figure represents the static part of the potential, because the positions of the atoms in the target were fixed to their equilibrium points. To perform the summation in equation (3.1) one has to take care about the crystallographic structure of the target. Due to the specific functional dependence of the repulsive component of the atom-atom potential, the layers below the topmost layer of atoms contribute significantly only to the attractive part of the total potential, while the repulsive part of the potential is influenced mainly by the topmost layer (in fact, only by very few crystal atoms closest to the projectile atom).

Figure 3.1 illustrates an interesting feature, characteristic of all inert atom-surface potentials. Namely, the equipotential surfaces have

³Consult reference [24] for other possible choices of He-Xe pair potential.

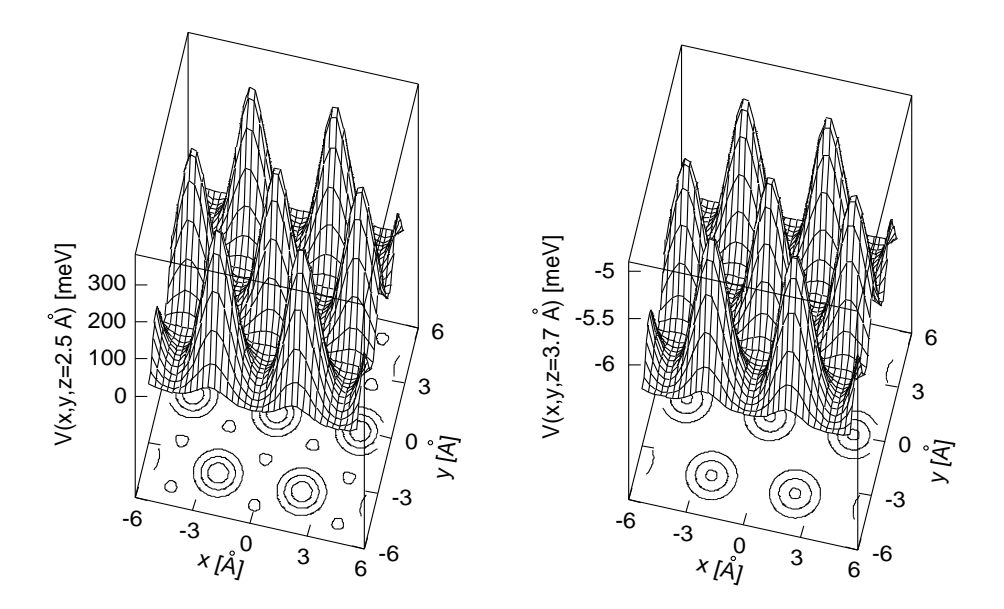


Figure 3.1: Left: He \rightarrow Xe(111) interaction potential as a function of x and y coordinates for z=2.5 Å. Right: Same for z=3.7 Å. Note the scales on the z-axis. Equipotential contours are drawn for the values of the potential denoted by labels on the z-axis.

the appearance of a corrugated tin roof. This wavy-like behavior of the equipotential surfaces is in fact known in the literature as the corrugation of the potential. This is a consequence of the inhomogeneous, discrete nature of the crystal. Such a periodic modulation of the atomtarget potential also implies that the projectile atoms will diffract under the influence of this potential if their wavelengths are comparable to the period of the spatial modulation. This indeed happens in the scattering of thermal energy inert atoms from surfaces since at these incident energies atomic de Broglie wavelengths become comparable to the lattice parameter of the target. Diffracted projectile atoms continue to move in the final direction which is fixed by the requirements of parallel momentum and energy conservation, which means that diffraction is an elastic event because the energy of the projectile atom after diffraction remains equal to the initial energy 4. Thus, the diffracted projectile atoms will be experimentally detected only if the source and the detector are in the "right" positions. This happens for the discrete set of relative angles between the source and the detector of the projectile atoms. This kind of measurement can be used to determine the two-

⁴A comprehensive review of atomic beam diffraction from solid surfaces can be found in reference [25].

dimensional geometry of the target [2, 25]. In fact, the nearest neighbor Xe-Xe distance, a, which was set to 4.37 Å in the calculations above was determined from such a measurement (figure 3.2). Figure 3.2 displays the experimental diffraction spectrum obtained by scattering of He atoms from Xe(111) target. Magnitude of the diffraction peaks depends on the corrugation of the target surface. We can say that the Xe(111) surface is moderately corrugated 5 . We can represent the periodic, corrugated nature of the static component of the interaction potential in a more "natural" way. Imagine that we send a beam of classical particles impinging along the target surface normal. The particles all have fixed kinetic energy E_i . The particles will reflect from the surface at the point T where

$$E_i = V(x_T, y_T, z_T).$$
 (3.3)

If we vary x_T and y_T coordinates of the impinging projectile, the remaining turning-point coordinate, z_T is also going to vary since all three coordinates must satisfy equation (3.3). Thus, we can plot z_T as a function of x_T and y_T with incident energy, E_i as the parameter of this plot. This kind of plot is called the turning point profile plot. Figure 3.3 represent this plot for He \rightarrow Xe(111) scattering system for two characteristic incident energies. A parameter which can be used to quickly estimate the magnitude of the potential corrugation is the so-called "peak-to-peak-corrugation parameter" which is given by the difference between the farthest and the closest turning point. This parameter's value depends on the projectile incident energy. This is illustrated in figure 3.4. Another way of representing the interaction potential is to plot the z-dependence of the potential with x and y coordinates fixed. Figure 3.5 displays such plot for three characteristic points in (x, y)-surface plane of Xe(111). It is seen that the potential has a minimum at some distance above the plane passing through the centers of topmost atoms (surface plane). This feature results from an interplay between the attractive and repulsive parts of the potential which produces a minimum typically at 3-4 Å above the surface plane.

Illustrative examples of the procedure of pairwise addition of the potentials can be found in references [26, 27, 28, 29].

⁵Surfaces of alkali halides (such as LiF) exhibit much stronger intensities in HAS [26] indicating strongly corrugated surface potentials probed by He atoms.

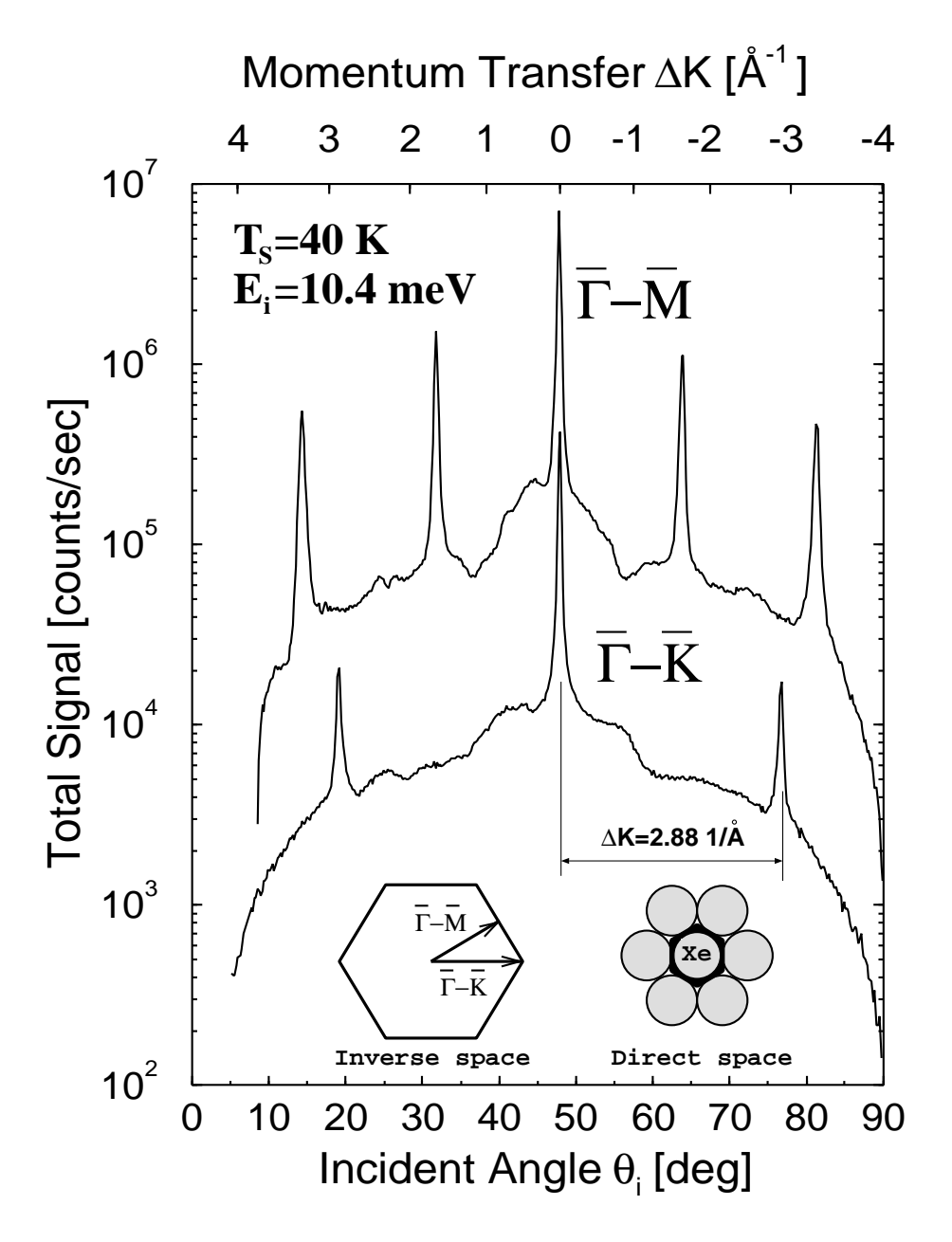


Figure 3.2: He-atom angular distribution along the Γ -M and Γ -K azimuths of Xe(111) surface. The left sketch at the bottom represents the surface Brillouin zone of the Xe(111) surface. The right sketch displays the structure of Xe(111) surface in the direct space. Full thick line denotes the surface Wigner-Seitz cell of Xe(111).

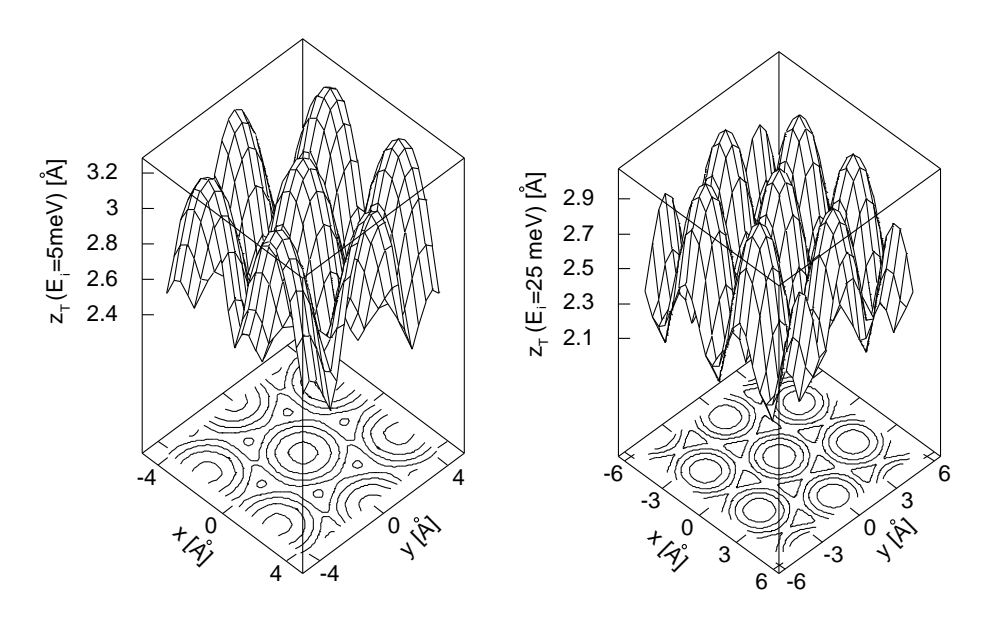


Figure 3.3: Left: He \to Xe(111) turning point profile plot for $E_i=5$ meV . Right: Same for $E_i=25$ meV. Contours are drawn for the values of the turning point denoted by labels on the z-axis.

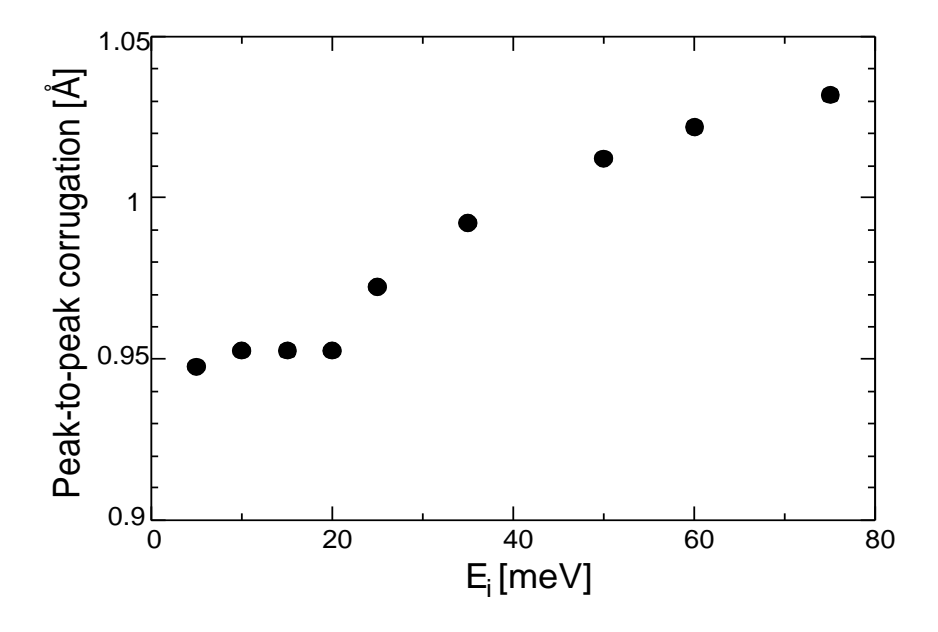


Figure 3.4: Dependence of the peak-to-peak corrugation parameter on the incident He energy for He \rightarrow Xe(111) scattering system.

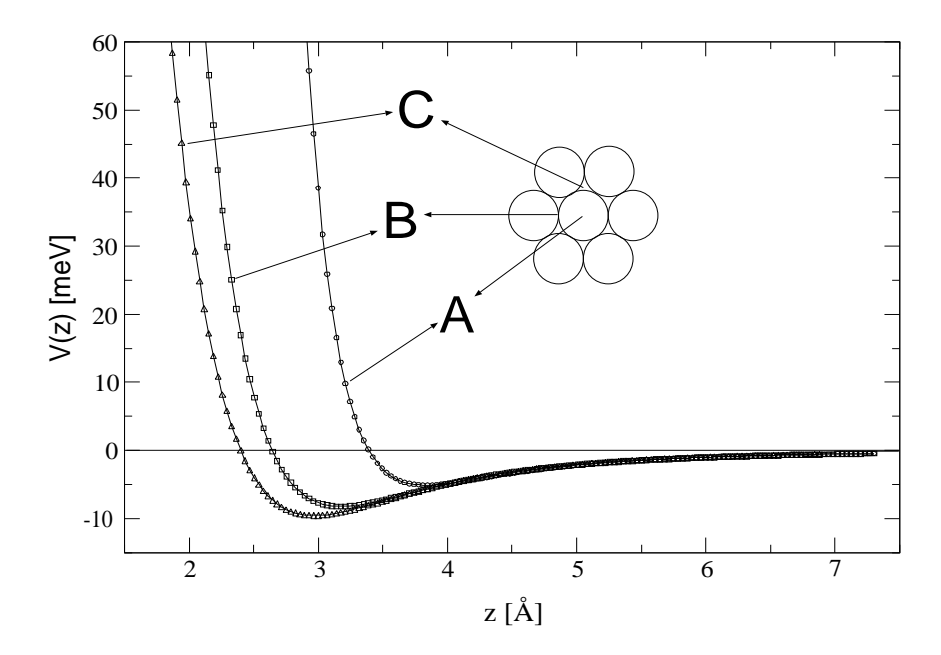


Figure 3.5: He \to Xe(111) interaction potential as a function of coordinate perpendicular to Xe(111) surface, z, for three characteristic points in (x, y) plane as denoted in the inset.

3.1.2 Other procedures for obtaining the static component of the interaction potential

The simple approach of pairwise summation of atomic potentials is less reliable for metallic surfaces, for which we expect that the electrons in the outer shells of metal atoms are largely delocalized. This means that there is a contribution to the electronic charge distribution of the metal spread over the crystal sites. In this case one has to perform a total energy calculation as a function of the distance of the projectile atom from the surface. Various approximation schemes have been used in order to obtain the atom-target potentials. Historically, the earliest ones were based either on the jellium model [2, 30] or Linear Combination of Atomic Orbitals model (LCAO). The calculations of self-consistent Hartree-Fock type have been reported in reference [31]. Recent advanced schemes such as the various types of density functional approaches combine the discrete nature of the metal with the improved accounts of correlation effects [30, 32, 33, 34]. All of these calculations are beyond the scope of this work. It is tempting to extend the simple approach of pairwise summation to the case of metallic surfaces. The pair potentials, v, we need in this case are *not* the gas-phase potentials.

They must be suitably constructed to at least approximately include the effects of delocalized negative charge. In this case, we think of pair potentials v as the effective projectile-site potentials. This approach has been used in the literature with success. In reference [28], the pair potentials, v, have been constructed to reproduce the results consistent with the experimental data for both the bound state energy levels of $V_0(z)$ and the diffraction probabilities. The potentials v used in this reference depend only on modulus of relative distance between the projectile and a particular site. To model the anisotropic rearrangement of the atomic electron cloud, one has to assume that the pairwise potentials are also anisotropic. A superposition of ellipsoidal pairwise potentials has proven to be quite successful (see e.g. reference [36]).

Regardless of the actual approach utilized to obtain the interaction potential, the resulting potential must reflect the periodicity of the crystal lattice.

3.1.3 Some general properties of the static component of the interaction potential

Quite generally, due to the periodicity of the total potential in the directions parallel to the surface, the static part of the total potential can be written as 2D Fourier series:

$$V_{static}(\mathbf{r}) = V_0(z) + \sum_{\mathbf{G} \neq 0} V_{\mathbf{G}}(z) e^{i\mathbf{G} \cdot \mathbf{R}}.$$
 (3.4)

Here, $\mathbf{R} = (x, y)$ is the vector in the surface plane and \mathbf{G} is a 2D reciprocal lattice vector (see e.g. [2]) in the surface plane. The term $\mathbf{G} = 0$ has to be excluded from the summation in (3.4) because it has been explicitly written as $V_0(z)$. This term is the *laterally averaged* static component of the interaction potential. This can be seen right away since

$$V_{\mathbf{G}}(z) = \frac{1}{L_S^2} \int d^2 R e^{-i\mathbf{G} \cdot \mathbf{R}} V_{static}(\mathbf{r}), \qquad (3.5)$$

where L_S^2 is the total area of the surface of the sample. Since the equation above holds also for $\mathbf{G} = 0$, we see that $V_0(z)$ is nothing but an average of the interaction potential over the target surface plane. When the total interaction potential can be written as a superposition of pair potentials, as in equation (3.1), relation (3.5) additionally simplifies according to

$$V_{\mathbf{G}}(z) = \frac{1}{L_S^2} \int d^2R e^{-i\mathbf{G}\cdot\mathbf{R}} \sum_{j} v(\mathbf{r} - \mathbf{r}_j)$$

$$= \frac{1}{L_S^2} \sum_{l,\kappa} \int d^2 R e^{-i\mathbf{G} \cdot \mathbf{R}} v(\mathbf{r} - \mathbf{r}_{l,\kappa})$$

$$= \frac{1}{L_S^2} \sum_{l,\kappa} \int d^2 R e^{-i\mathbf{G} \cdot \mathbf{R}} v(\mathbf{R} - \mathbf{R}_l + z\mathbf{z}_0 - \mathbf{S}_{\kappa}). \quad (3.6)$$

Here, index j was replaced with two indices (l, κ) which count the atoms within the crystal plane and the crystal planes themselves, respectively. Vector \mathbf{S}_{κ} connects the centers of the two-dimensional Wigner-Seitz cells in the topmost crystal plane and the crystal plane κ . \mathbf{z}_0 is the unit vector pointing in z-direction.

Assuming that the pair potential, v, does not depend on the angle in the surface plane, ϕ , equation (3.6) simplifies to

$$V_{\mathbf{G}}(z) = \frac{2\pi}{A_c} \sum_{\kappa} e^{i\mathbf{G} \cdot \mathbf{S}_{\kappa}} \int_0^{\infty} R J_0(|\mathbf{G}|R) v \left(\sqrt{R^2 + (z - (\mathbf{S}_{\kappa} \cdot \mathbf{z}_0))^2} \right) dR,$$
(3.7)

where we have used the integral representation of the zeroth order Bessel function J_0 ,

$$J_0(w) = \frac{1}{\pi} \int_0^{\pi} \cos(w \cos \phi) d\phi. \tag{3.8}$$

 A_c is the area of the two dimensional (2D) Wigner-Seitz cell of the target given by

$$A_c = \frac{L_S^2}{N_{2D}},\tag{3.9}$$

where N_{2D} is the number of 2D Wigner-Seitz cells in each crystal plane, κ . Note also that $\mathbf{S}_{\kappa} \cdot \mathbf{z}_0 < 0$. Figure 3.6 represents the Fourier components $V_{\mathbf{G}}(z)$ of the He \to Xe(111) potential which was obtained as in the previous subsection.

A convenient (but approximate - see figure 3.5) representation of the static part of the interaction potential is

$$V_{static}(\mathbf{r}) = V(z - \xi(\mathbf{R})), \tag{3.10}$$

where $\xi(\mathbf{R})$ is called the effective static corrugation function. Proper choice of $\xi(\mathbf{R})$ leads to quite a satisfactory description of the potential corrugation profile obtained from the experimental diffraction spectra [25].

The present state of the art regarding the theory of interaction potentials is that the part of the potential, written explicitly as $V_0(z)$, is generally represented by a sum of two terms [6], one of which is

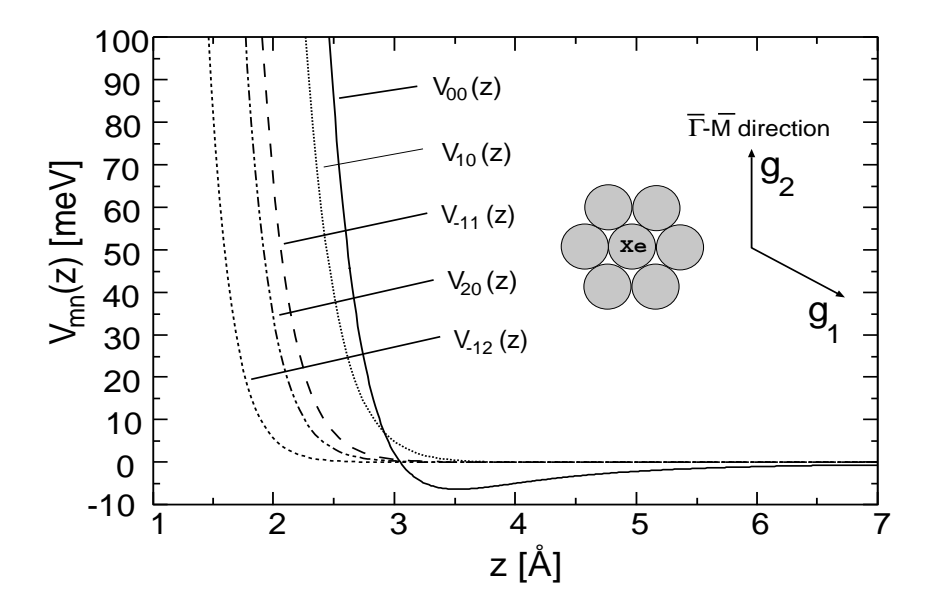


Figure 3.6: Fourier components of He \to Xe(111) interaction potential as a function of coordinate perpendicular to Xe(111) surface, z. The choice of basis for the inverse space is denoted in the inset. The notation is: $V_{mn}(z) = V_{\mathbf{G}}(z)$, $\mathbf{G} = m\mathbf{g}_1 + n\mathbf{g}_2$, $|\mathbf{g}_1| = |\mathbf{g}_2| = 1.66$ 1/Å.

repulsive and the other is attractive. The repulsive part of the interaction potential originates from the overlap of the surface electronic wave functions with the closed shell projectile atom orbitals. The attractive part is due to van der Waals forces. The laterally averaged projectile atom - surface repulsion is generally well approximated by [6]

$$V_{rep,0}(z) = V_r e^{-\alpha z}. (3.11)$$

At large distances from the surface, the attractive part of the potential can be represented as [6]

$$V_{att,0}(z) = -\frac{C_3}{(z - z_{eff})^3},$$
(3.12)

where the coefficient C_3 can be related to the projectile atom polarizability and the surface response function [6, 31]. The values of z_{eff} appearing in the equation above are typically 1 Å for low indexed metal surfaces [31]. Although expression (3.12) is valid only at large distances z, it is quite common to extend its validity to all z distances of interest (i.e. for z several atomic units away from z_{eff}) and write the potential $V_0(z)$ as

$$V_0(z) = V_r e^{-\alpha z} - \frac{C_3}{(z - z_{eff})^3}.$$
 (3.13)

It is also possible to "damp" the attractive part of the potential as it was done in equation (3.2), which guarantees physical behavior of $V_0(z)$ even for very small values of z.

3.2 Dynamic component of the atom-target interaction potential

The full atom-surface interaction potential is time dependent since the atoms in the target oscillate around their equilibrium positions. Assuming that we can apply the pairwise summation procedure described earlier to the oscillating atoms as well and expanding the interaction potential up to first order in atomic displacements (assuming that atomic displacements are small relative to the equilibrium interatomic distances), we can write

$$V(\mathbf{r}, \{\mathbf{u}_i\}) = V_{static}(\mathbf{r}) + \sum_{j} \nabla_{\mathbf{r}_j} v(||\mathbf{r} - \mathbf{r}_j||) \cdot \mathbf{u}_j + O(\{\mathbf{u}_j^2\})$$

$$= V_{static}(\mathbf{r}) - \sum_{j} \nabla_{\mathbf{r}} v(||\mathbf{r} - \mathbf{r}_j||) \cdot \mathbf{u}_j + O(\{\mathbf{u}_j^2\})(3.14)$$

Here, \mathbf{u}_{j} is the time dependent displacement of the j-th atom in the crystal from its equilibrium position. All the derivatives of pair potentials are needed in $\mathbf{r}_i = \mathbf{r}_i^0$. The question of finding the time dependence of \mathbf{u}_i still remains unanswered. The answer to this question will be given in Chapter 4. It must be noted that here we have resorted to the assumption that the time dependence of the total potential is governed solely by the motion of crystal sites. A simple appearance of equation (3.14) is the result of this assumption. The problem of metallic targets for which we can expect that the electrons do not adiabatically follow the motion of the ion cores is a more difficult one. Namely, there is an additional term in the change of the potential which is associated with the rearrangement of the electronic density around a particular site. This issue has been discussed in the literature [35, 36, 37]. One could assume that the ion cores in their motion rigidly "drag" their part of the physical space. The pair potentials must be suitably modeled for this case. This procedure has been used in the literature with very satisfying results [28, 36]. Another approach assigns new degrees of freedom to the nearly free metal electrons i.e. the Born-Openheimer approximation for the motion of the electrons is relaxed. One then has to solve the coupled equations of motion for appropriately defined so called "pseudocharges" and the ion cores. This poses a more difficult problem, but some results have been achieved using this approach

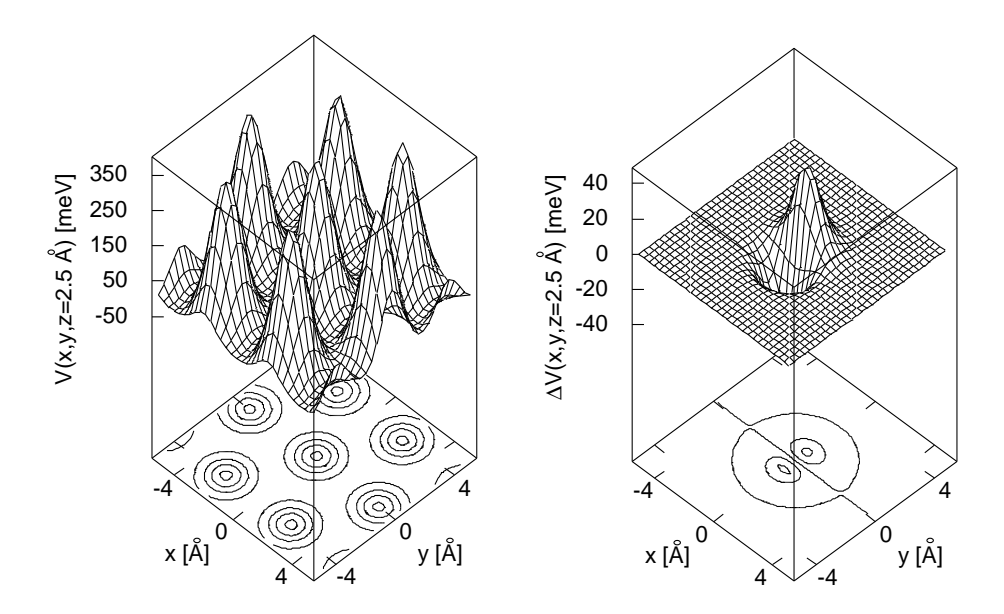


Figure 3.7: Left: The static component of He \rightarrow Xe(111) interaction potential with one Xe atom at (0,0.15 Å,0) (i.e. moved within the surface plane). Right: The difference introduced in the interaction potential with respect to the case when the Xe atom is at (0,0,0).

[37, 35]. We shall further illustrate the change of the interaction potential when a particular site is moved on He \rightarrow Xe(111) scattering system where we can expect that equation (3.14) holds.

We can envisage that the interaction potential changes in different ways when a particular site is moved within the surface plane and perpendicular to the surface plane. This is illustrated in figures 3.7 and 3.8.

It is quite clear from these figures that the movement of Xe atom in the direction perpendicular to the surface plane produces much larger change in the absolute value of the interaction potential. Therefore, we can anticipate that He atoms are going to be much more "sensitive" to movements of Xe atoms perpendicular to the Xe(111) surface than to the Xe-atom movements within the Xe(111) surface.

3.3 Convenient approximations to the interaction potential

In this section I shall specify some convenient approximations to the static and dynamic components of the interaction potential that will

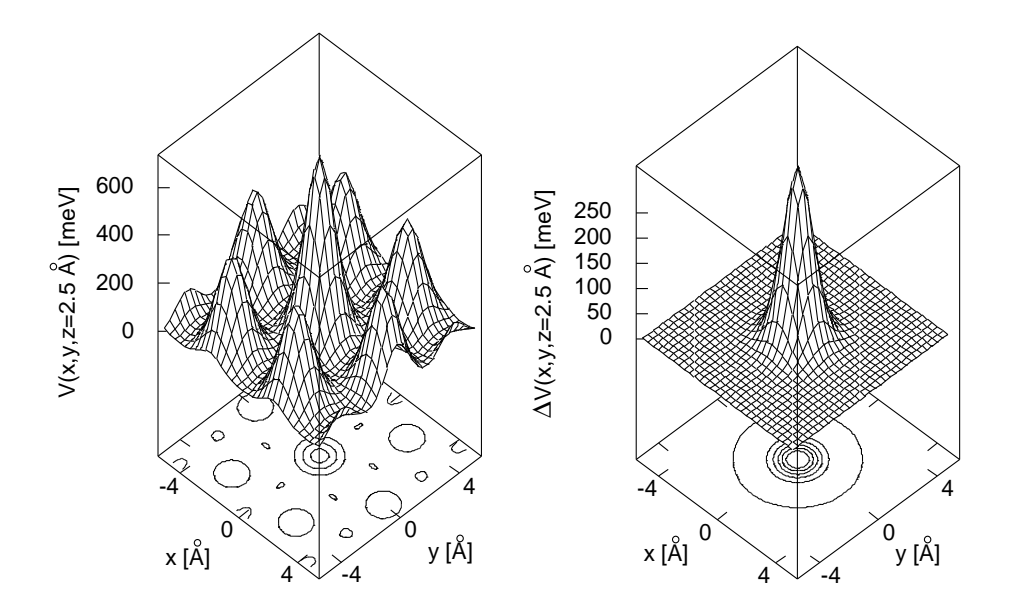


Figure 3.8: Left: The static component of He \rightarrow Xe(111) interaction potential with one Xe atom at (0,0,0.15 Å) (i.e. moved perpendicular to the surface plane). Right: The difference introduced in the interaction potential with respect to the case when the Xe atom is at (0,0,0).

be adopted in the calculations presented in Chapter 9.

For mildly corrugated surfaces one could neglect all the components $V_{\mathbf{G}}$ of the static potential in equation (3.4) with \mathbf{G} different from zero. This means that in the treatment of inelastic processes we consider the static potential as completely flat in the directions parallel to the surface plane. This, however, does not mean that we disregard the dynamic corrugation of the interaction potential which is introduced by vibrations of the target crystal sites (see figures 3.7 and 3.8). The $\mathbf{G} \neq 0$ components of the potential play a major role in the diffraction spectra of elastically scattered projectile atoms, but are expected to have minor influence on the inelastic events which are the subject of this thesis.

It is quite convenient to approximate the remaining part of the potential, $V_0(z)$, with the Morse potential:

$$V_0(z) = D\left[\exp(-2\frac{z - z_0}{d}) - 2\exp(-\frac{z - z_0}{d})\right].$$
 (3.15)

Here, D is the depth of the potential well at distance z_0 from the surface plane and d/2 is the range of the repulsive part of the potential. The reason for this simplification is that the transition matrix elements

needed in inelastic atom-surface scattering calculations (see Chapter 6) can be expressed in a closed analytic form for the Morse potential [38, 39], both for the transitions to continuum and bound states of the interaction potential, but must be calculated numerically otherwise. The latter does not pose a major problem but it slows down the calculations (Chapter 9). Additionally, if we chose $V_0(z)$ to be represented by the Morse potential, the coupling of the projectile atoms to the atomic vibrations in all crystal slabs can be easily calculated (see section 6.3) when the targets are noble gas crystals. The use of the Morse potential instead of the potentials given numerically has been shown to be a good approximation if the energies of the projectile atom are not too low (below 1 meV) [40]. For low energies, the precise functional dependence of the attractive van der Waals component of the interaction potential becomes a crucial factor (this is extremely important for the quantum reflection phenomena in sticking [41]). The attractive part of the Morse potential decays exponentially with distance z while the true potential decays as third inverse power of distance. Therefore, we can expect that the Morse potential approximation will be inadequate for projectile atoms with very low incident energies [40]. In this case, the projectile atoms "spend a lot of time" in the attractive region of the interaction potential and are, therefore, very differently accelerated in the exponential and $1/z^3$ potentials. On the other hand, the repulsive part of the Morse potential has a proper functional dependence, since the exponential repulsion has been shown to be a good approximation to the repulsive interactions calculated for the systems with overlapping charge distributions. For atom-surface scattering, in the absence of hybridization effects (see reference [4]) the repulsive component of interaction, V_{rep} can be approximated by [42]

$$V_{rep.}(r) = A\rho(r), \tag{3.16}$$

where A is a constant $(A \approx 45 - 90 \text{ eV Å}^3 \text{ [6]})$, only weakly dependent on the target characteristics, and $\rho(r)$ is the unperturbed target electronic density. The electronic densities of the systems in which electrons are bounded in a finite region of space by a potential should decay approximately exponentially in the region where the confining potential exceeds electronic energies.

Figure 3.9 represents a comparison of the Morse potential and $V_0(z)$ part of the He \rightarrow Xe(111) potential. The Morse potential parameters were set to D=6.4 meV, d=0.641 Å and $z_0=3.49$ Å. It is clear that the potentials are very similar, except in the region of distances where the long range character of the van der Waals interaction gives

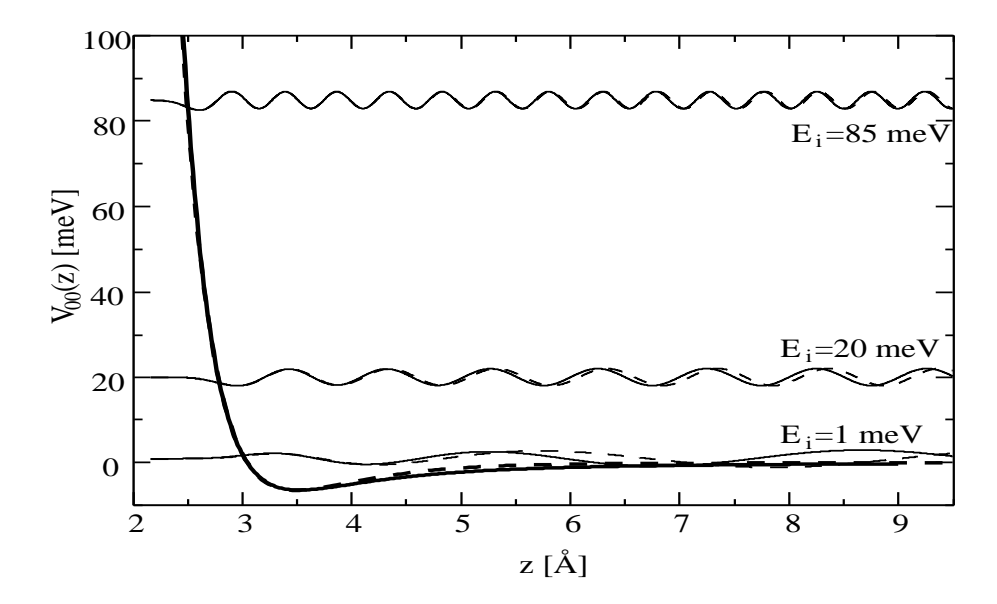


Figure 3.9: A comparison of the Morse interaction potential (dashed line) and $V_0(z)$ part of He \rightarrow Xe(111) potential (full line) and their scattering wave-functions for three characteristic values of incident energy.

the dominant contribution to the total potential. Note, however, that the corresponding scattering wave-functions of the two potentials show clear differences, especially for low incident energy of the projectile (He).

A word of caution concerning the fitting of the Morse potential to the calculated data seems to be appropriate here: It is very difficult to fit the sum of exponential functions to the dataset. However, for scattering calculations, the Morse potential should agree with the true potential in two crucial aspects. First, both potentials should have the same derivative around the projectile turning point and second, both potentials should have the same (z, V(z)) position of the minimum. The reason for this will become clear in chapters which follow.

Chapter 4

Normal modes and phonons in infinite and semi-infinite crystals

He had that rare weird electricity about him – that extremely wild and heavy presence that you only see in a person who has abandoned all hope of ever behaving "normally".

Hunter S. Thompson, "Fear and Loathing '72"

THEORY OF
THERMAL ENERGY
INERT ATOM
SCATTERING FROM
SURFACE VIBRATIONS

Antonio Šiber

The preceding chapter has brought to the fore the problem of finding solutions of equations governing the time dependence of atomic positions in the target. This is an old question of finding the normal modes of a system of interacting particles which has been addressed many times in the literature both classically [43] and quantum mechanically [11, 44]. However, the answers pertain mostly to infinite, three dimensional systems exhibiting discrete translational invariance in all three spatial directions. The target used in atom-surface scattering experiments is somewhat different: it is at best a semi-infinite solid since its surface is exposed to the beam of projectile atoms. In this chapter I shall briefly outline the concept of normal modes and its application to the geometry of infinite and semi-infinite crystals.

4.1 Small oscillations and normal modes

Consider a system of N mutually interacting bodies. If the bodies are arranged in the a dimensional space, we will need 3N coordinates $\{q_1, q_2, ..., q_{3N}\}$ to specify the positions in the system plus 3N conjugate momenta $\{p_1, p_2, ..., p_{3N}\}$ to specify completely the position of the system in the phase space. The system is said to be in equilibrium when the generalized forces acting on the system (i.e. on each particular constituent) vanish:

$$F_i = \left\{ \frac{\partial V}{\partial q_i} \right\}_0 = 0. \tag{4.1}$$

Here F_i is the force deriving from the change in the *i*-th coordinate (i = 1, 2, ..., 3N) and V is the potential energy of the system for which we assume to depend only on the set of q's. We shall be interested in the motion of the system within the immediate neighborhood of the configuration of a stable equilibrium. If we displace the system from the point of stable equilibrium, it will remain close to this point at all times during its motion in the phase space, performing small oscillations around the point of stable equilibrium. The deviations of the generalized coordinates q from equilibrium will be denoted by η_i :

$$q_i = q_i^0 + \eta_i. (4.2)$$

Expanding the potential energy about the point of stable equilibrium

we obtain

$$V(q_1, ..., q_{3N}) = V(q_1^0, ..., q_{3N}^0) + \sum_i \left\{ \frac{\partial V}{\partial q_i} \right\}_0 \eta_i$$

$$+ \sum_{i,j} \frac{1}{2} \left\{ \frac{\partial^2 V}{\partial q_i \partial q_j} \right\}_0 \eta_i \eta_j + \mathcal{O}(\eta^3)$$
(4.3)

The terms linear in η_i vanish as a consequence of the equilibrium condition in equation (4.1) and we are therefore left with quadratic terms as the first approximation to V^{-1} . Shifting the arbitrary zero of the potential to $V(q_1^0, ..., q_{3N}^0)$ we have

$$V = \frac{1}{2} \sum_{i,j} \left\{ \frac{\partial^2 V}{\partial q_i \partial q_j} \right\}_0 \eta_i \eta_j = \frac{1}{2} V_{ij} \eta_i \eta_j. \tag{4.4}$$

It is obvious from the definition above that the V_{ij} 's are symmetric with respect to i and j i.e. $V_{ij} = V_{ji}$.

A similar series expansion can be obtained for the kinetic energy T:

$$T = \frac{1}{2} \sum_{i,j} m_{ij} q_i' q_j' = \frac{1}{2} \sum_{i,j} m_{ij} \eta_i' \eta_j'. \tag{4.5}$$

Here the primes denote first derivatives with respect to time t. In general, the coefficients m_{ij} are functions of the coordinates q_k , but they may be expanded in a Taylor series about the equilibrium configuration:

$$m_{ij}(q_1, ..., q_{3N}) = m_{ij}(q_1^0, ..., q_{3N}^0) + \sum_k \left\{ \frac{\partial m_{ij}}{\partial q_k} \right\}_0 \eta_k + ...$$
 (4.6)

As equation (4.5) is already quadratic in the η_i 's we need to keep only the values of m_{ij} 's at equilibrium configuration. Denoting $T_{ij} = m_{ij}(q_1^0, ..., q_{3N}^0)$ we can write the kinetic energy as

$$T = \frac{1}{2} \sum_{i,j} T_{ij} \eta_i' \eta_j'. \tag{4.7}$$

The coefficients T_{ij} are also symmetrical, $T_{ij} = T_{ji}$. The Lagrangian of the system is therefore given by

$$L = T - V = \frac{1}{2} \sum_{i,j} (T_{ij} \eta_i' \eta_j' - V_{ij} \eta_i \eta_j)$$
 (4.8)

 $^{^{1}}$ Keeping only the second term in expansion (4.3) is called *the harmonic approximation*.

which leads to the following Euler-Lagrange equations of motion:

$$\sum_{j} (T_{ij}\eta_{j}'' + V_{ij}\eta_{j}) = 0. \tag{4.9}$$

If we try a solution of the form

$$\eta_i = a_i e^{-i\omega t} \tag{4.10}$$

then the equations of motion lead to the following equation for the amplitude factors a_i 's:

$$\sum_{j} V_{ij} a_j - \omega^2 T_{ij} a_j = 0. (4.11)$$

This system of linear homogeneous equations for the a_i 's can have a solution only if the determinant of the system vanishes:

$$Det\{V_{ij} - \omega^2 T_{ij}\} = 0. (4.12)$$

This determinantal condition yields an algebraic equation of 3N-th degree for ω^2 . The allowed frequencies ω_k^2 which result as a solution to equation (4.12) are called resonant frequencies of the system or eigenfrequencies. It can be shown that all ω_k^2 are real which is a consequence of the hermitian property of \mathbf{T} (kinetic energy) and \mathbf{V} (potential energy) matrices. Every value of ω_k yields a set (vector) of coefficients $a_i, i = 1, 2, ..., 3N$ which we call eigenvector \mathbf{a}_k . If we arrange all 3N eigenvectors (the possible degeneracy in ω is excluded here) as the columns of a matrix, we obtain a square matrix $\mathbf{A} = [a_{ij}]$. The vector \mathbf{a}_k is not uniquely determined by the value of a particular ω_k . Additional condition can be obtained by further requiring that $\mathbf{A}^{-1}\mathbf{T}\mathbf{A} = 1$ (therefore, the masses appear in the normalization) which is convenient since then the matrix \mathbf{A} diagonalizes both the kinetic and potential energy matrices. Since the eigenvectors are orthogonal, the matrix \mathbf{A} has an inverse \mathbf{A}^{-1} which is equal to its transposed matrix $\tilde{\mathbf{A}}$, $\mathbf{A}^{-1} = \tilde{\mathbf{A}}$.

A complete solution of the equations of motion involves a *superpo*sition of oscillations with all the resonant frequencies:

$$\eta_i = \sum_k C_k a_{ik} e^{-i\omega_k t} \tag{4.13}$$

We define a new set of coordinates ξ_j related to the original coordinates by equations

$$\eta_i = \sum_j a_{ij} \xi_j; \quad \eta = \mathbf{A}\xi, \tag{4.14}$$

where ξ (η) is a vector with ξ_i (η_i) as components. It can be relatively easily shown [43] that the Lagrangian expressed in the new coordinates is

$$L = \frac{1}{2} \sum_{k} (\xi_k' \xi_k' - \omega_k^2 \xi_k^2). \tag{4.15}$$

Each of the new coordinates is thus a periodic function of time involving only one of the resonant frequencies. We call the ξ 's the normal coordinates of the system. The complete motion of the system can be constructed as a sum of the normal modes weighted with appropriate amplitude and phase factors contained in C_k (equation (4.13)). It is important to note that normal coordinates act as independent harmonic oscillators. Therefore, we can in principle excite a particular normal mode without exciting other normal modes.

A simple, one dimensional, surface-science-related application of the normal modes calculation is given in Appendix A.

4.2 Normal modes in infinite crystals - phonons

In this section we shall extend the general formalism of the previous section to infinite crystals. In crystals, the atoms occupy positions (crystal sites) which are arranged as the knots in a three dimensional grid. To be less pictorial and more exact, all the crystal cells can be reached from any other fixed crystal cell with a translation specified as ²:

$$\mathbf{r}(n_1, n_2, n_3) = n_1 \mathbf{L}_1 + n_2 \mathbf{L}_2 + n_3 \mathbf{L}_3. \tag{4.16}$$

Here $\mathbf{r}(n_1, n_2, n_3)$ is the vector specifying the translation needed, n_1, n_2 and n_3 are integers $(n_{1,2,3} = -\infty, ..., -2, -1, 0, 1, 2, ..., \infty)$ and $\mathbf{L_1}$, $\mathbf{L_2}$ and $\mathbf{L_3}$ are vectors specifying the nature of the crystallographic "grid" or lattice vectors.

This discrete translational invariance of the crystal simplifies the calculations of the normal modes. The general coordinates we chose here are the displacements of the atoms from their equilibrium positions. The equilibrium position of an atom (site) in a general lattice is specified by the cell indices n_1, n_2 and n_3 and an additional index, a = 1, 2, ..., J, labeling the different atoms within a unit crystal cell

²The crystal cell can, however, contain more than one atom, so that the additional index for labeling the different atoms within a unit cell may be needed for specifying the exact position of the atoms (crystal sites) themselves.

composed of J atoms. Therefore, the set of generalized coordinates is $\{\mathbf{u}(n_1, n_2, n_3, a)\}$. This set corresponds to the set of η 's in equation (4.2). The displacements are of course vectors since we can expect every atom of the crystal to move in all three directions. The kinetic energy of the a-th atom in crystal cell $p = (n_1^p, n_2^p, n_3^p)$ is given by

$$T(a,p) = \frac{M_a}{2} \mathbf{u}'(p,a)^2.$$
 (4.17)

Here, M_a is the mass of the a-th atom in crystal cell p. The total kinetic energy is given by the sum of energies in equation (4.17) over the crystal sites

$$T = \sum_{p,a} \frac{M_a}{2} \mathbf{u}'(p,a)^2, \tag{4.18}$$

The Euler-Lagrange equations of motion (4.9) reduce to

$$M_a u_{\alpha}''(p,a) = -\sum_{p',a',\beta} \left\{ \frac{\partial^2 V}{\partial u_{\alpha}(p,a)\partial u_{\beta}(p',a')} \right\}_0 u_{\beta}(p',a'), \tag{4.19}$$

where $\alpha, \beta = x, y, z$ and subscript 0 means that the derivatives should be taken in the equilibrium configuration of the crystal. It is quite convenient to introduce a new notation for the second derivatives of the potential energy:

$$V_{\alpha,\beta}(p, p', a, a') = V_{\alpha,\beta}(p - p', a, a')$$

$$= \left\{ \frac{\partial^2 V}{\partial u_{\alpha}(p, a) \partial u_{\beta}(p', a')} \right\}_0. \tag{4.20}$$

The first identity in the equation above follows from the fact that the second derivative depends only on the relative cell index p - p' and not on the indices p and p' individually. We now use Bloch's theorem which allows us to explicitly employ the three dimensional periodicity of the crystal [11]. The normal mode solutions have the form of 3D Bloch functions:

$$\mathbf{u}(p,a) = \frac{1}{\sqrt{NM_a}} \mathbf{e}(\mathbf{q}, a) u_0 e^{i(\mathbf{q} \cdot \mathbf{r}(p) - \omega(\mathbf{q})t)}.$$
 (4.21)

Here, $\mathbf{r}(p)$ is the vector specifying the position of the atom of the crystal unit cell p, i.e.

$$\mathbf{r}(p) = n_1^p \mathbf{L}_1 + n_2^p \mathbf{L}_2 + n_3^p \mathbf{L}_3. \tag{4.22}$$

N is the number of unit cells in the crystal, $\mathbf{e}(\mathbf{q}, a)$ is the polarization vector of the normal mode characterized by the wave vector \mathbf{q} , frequency $\omega(\mathbf{q})$ and associated with a-th atom within the crystal unit cell.

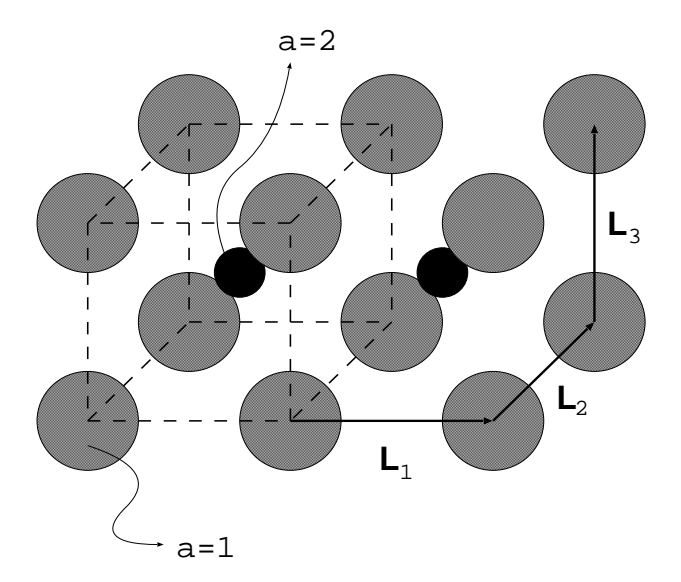


Figure 4.1: Geometry and the notation used in this section, explained on a CsCl type of crystal which has two atoms per unit cell (J = 2).

The polarization vector specifies the vector character of the displacements i.e. it specifies in which directions atoms oscillate. The time dependence of collective variables (normal modes) is explicitly written as $e^{-i\omega(\mathbf{q})t}$. The normalization of $\mathbf{u}(p,a)$ with respect to atom mass, M_a , has been introduced for later convenience. Inserting equation (4.21) in (4.19) we obtain an algebraic set of equations for the polarization vectors, $\mathbf{e}(\mathbf{q},a)$:

$$\omega^{2} e_{\alpha}(a) - \sum_{\beta, a'} D_{\alpha, \beta}(\mathbf{q}, a, a') e_{\beta}(a') = 0.$$
 (4.23)

Here

$$D_{\alpha,\beta}(\mathbf{q}, a, a') = D_{\beta,\alpha}(\mathbf{q}, a', a)^* = D_{\alpha,\beta}(-\mathbf{q}, a, a')^*$$

$$= \frac{1}{\sqrt{M_a M_{a'}}} \sum_{p'} V_{\alpha,\beta}(p - p', a, a') e^{i\mathbf{q} \cdot (\mathbf{r}(p') - \mathbf{r}(p))},$$
(4.24)

is called the $dynamical\ matrix$. Note that index (crystal cell) p can be chosen at will, since the elements of the dynamical matrix do not depend on this choice.

In order that the nontrivial solution exists for the system of equations in (4.23), its determinant must vanish. Therefore, we have:

$$|\omega^{2}(\mathbf{q})\delta_{\alpha,\beta}\delta_{a,a'} - D_{\alpha,\beta}(\mathbf{q}, a, a')| = 0.$$
(4.25)

The above equation yields the dispersion relations of the system i.e. dependence of the mode's frequency on the wave vector of the mode. Equation (4.25) generally yields 3J real solutions (or phonon branch-es) $\omega(\mathbf{q}, s)$ for a particular \mathbf{q} where $s = 1, 2, ..., 3J^3$. Each of them has a different polarization vector specifying the way atoms oscillate. Polarization vectors $\mathbf{e}(\mathbf{q}, a)$ are easily found (by the matrix diagonalization procedures) as the eigenvectors of the matrix $\omega^2(\mathbf{q})\delta_{\alpha,\beta}\delta_{a,a'} - D_{\alpha,\beta}(\mathbf{q}, a, a')$. The number of modes we obtain by the diagonalization procedure is 3J for each \mathbf{q} in question. We label the normal modes by index s, s = 1, ..., 3J. Additional normalization condition needed for the unique solution is imposed on the polarization vectors of the same wave vector modes as 4 :

$$\sum_{a} \mathbf{e}^{*}(\mathbf{q}, a, s) \cdot \mathbf{e}(\mathbf{q}, a, s') = \delta_{s, s'}; \quad s, s' = 1, ..., 3J.$$
 (4.26)

and

$$\sum_{s} e_{\alpha}^{*}(\mathbf{q}, a, s) e_{\beta}(\mathbf{q}, a', s) = \delta_{\alpha, \beta} \delta_{a, a'}$$
(4.27)

The modes found in the way described are called *phonons* and they diagonalize the Lagrangian of the problem in the same way as in equation (4.15), therefore the modes behave as independent harmonic oscillators. This means that the phonons do not mutually interact. They begin to interact if we include the derivatives of the interaction potential of orders higher than second, going beyond the harmonic approximation [45]. Figure 4.2 represents the dispersion relations of Xe crystal calculated along the triangular path in the inverse space (Γ -L-X- Γ). Note that the normal modes can be degenerate along the high-symmetry directions in the inverse space. Note also that the normal modes were divided in *longitudinal* and *transversal* modes. The longitudinal (transversal) modes are the ones characterised by the vibration of atoms which is parallel (perpendicular) to the direction of mode propagation (defined by \mathbf{q}). The method which was used to obtain this figure will be discussed in more detail in section 4.4.

4.3 Normal modes in semi-infinite crystals - slab method approach and surface phonons

 $^{^3}$ The reality of the solutions is a consequence of hermiticity of the D matrix.

⁴Additional condition needed to completely specify the polarization vectors is of course completely arbitrary. It is more or less a question of convenience.

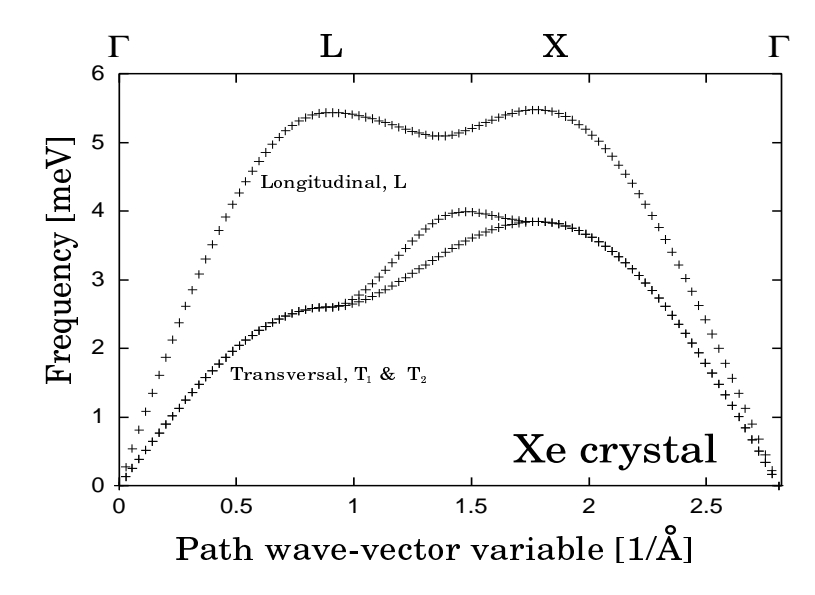


Figure 4.2: Phonons in Xe crystal calculated by lattice dynamics approach.

The situation becomes more complicated when we deal with semiinfinite crystals. Here we cannot exploit the discrete translational invariance in all three directions of space. However, there are still two spatial directions, lying in the surface plane and we can apply the Fourier series approach in these directions. We must leave the direction perpendicular to the surface of the sample in all of the calculations - it will not be adequately represented by a wave vector quantum number. We can imagine the semi-infinite crystal to be represented by a number of two dimensional sheets (the dashed plane in figure 4.3) containing atoms of a particular crystal plane. The phonons in a particular sheet can be represented by a two dimensional wave vector lying in the sheet, but we must additionally specify the "number" of the sheet i.e. how much is a particular sheet separated from the topmost layer of atoms. Therefore, integer "quantum numbers" represent the direction perpendicular to the surface of the crystal. The eigen-frequencies will be seen not to depend on this artificial labeling of the sheets (crystal planes). The method described in the previous section remains more or less unchanged. Actually, if we imagine the crystal of finite thickness, composed of a certain number of crystal planes, the method of the previous section can be applied in a straight-forward fashion. Namely, we can define the unit cell of finite-thickness crystal to be the "column" of 3D crystal unit cells ranging from one to the other "side" of the crystal

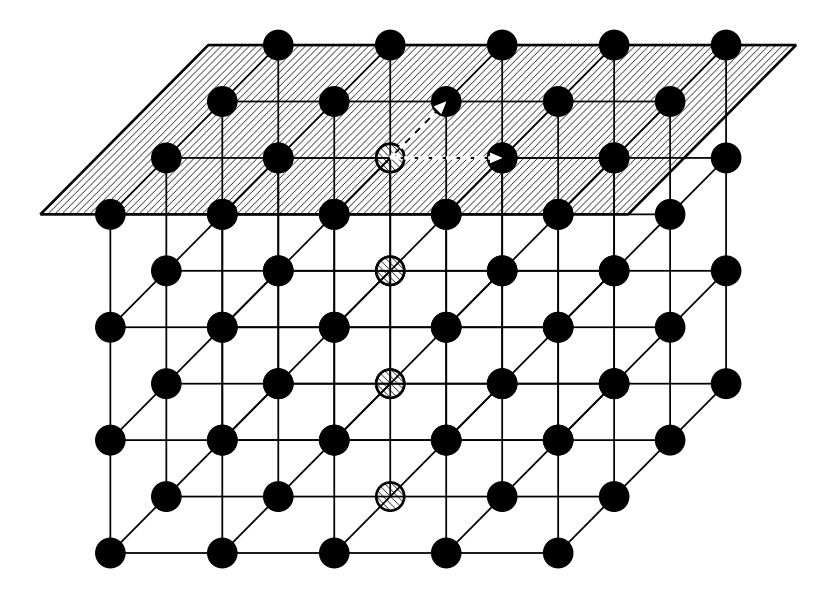


Figure 4.3: The "column" unit cell (dashed atoms) for the simple cubic, 4 layer thick crystal. The whole crystal can be reproduced by applying the translation group (defined by the two dashed arrows in the topmost plane) to the "column" unit cell.

(see fig. 4.3)⁵. In this manner, every atom in the "column" unit cell is to be treated as we treated different atoms in the 3D unit cell (previous section). We will introduce somewhat different notation here, denoting by index κ atoms which belong to different crystal planes ("sheets") of the crystal. Note that this index is completely equivalent to index a(a') from the previous section. The number of modes we obtain by aplying this method to the thin piece of crystal is much larger than in the case od 3D infinite crystal due to the large number of atoms constituting the "column" unit cell of crystal slab. Due to the specific geometry of the crystal employed in the calculation described, the method is usually caled the slab lattice dynamics method ⁶.

There is an additional simplification arising from the two-dimensional character of the phonon wave-vector, \mathbf{Q}^{7} . In the actual application of

⁵The "column" unit cells are more complicated (and more difficult to plot) for FCC and BCC crystals. They are not always perpendicular to the topmost crystal plane.

⁶From Webster's Revised Unabridged Dictionary (1913): Slab /Slab/, n. [OE. slabbe, of uncertain origin; perhaps originally meaning, a smooth piece, and akin to slape, Icel. sleipr, slippery, and E. slip, v.i.] A thin piece of anything, especially of marble or other stone, having plane surfaces. –Gwilt.

⁷We follow the usual convention, denoting the two-dimensional vectors with bold

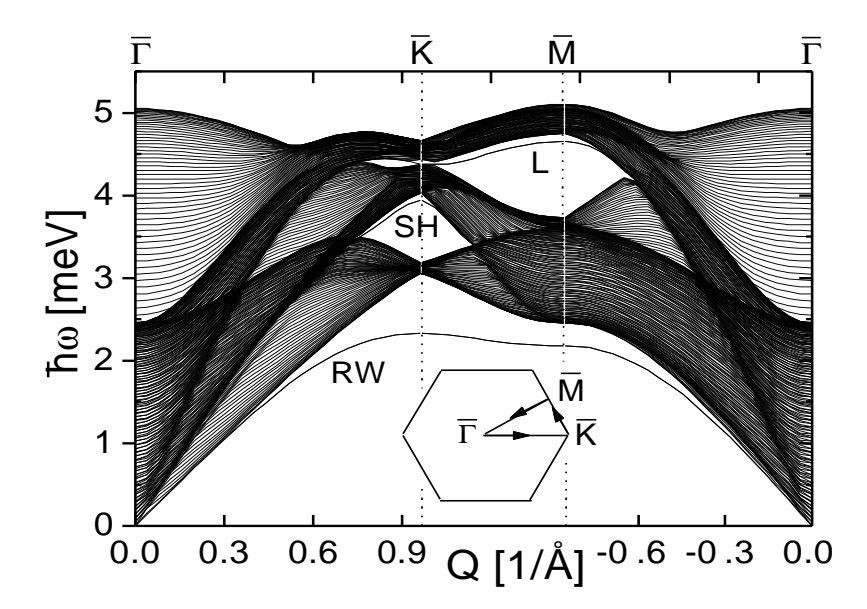


Figure 4.4: Dispersions of phonon modes obtained by applying the slab method to Xe(111) crystal composed of 80 Xe(111) crystal planes.

this method, the case of finite thickness crystal turns out to be more complicated than the 3D infinite crystal due to the fact that one has to numerically generate the "column" unit cell, accounting properly for the symmetry of the crystal in question. The same approach can be used if the atoms in the crystal are not all of the same kind. This will be e.g. the case for ionic and covalent crystals and adlayers on metal surfaces which are of particular interest in this work. The generalization of the above approach in this direction is rather straightforward but the notation becomes even more messy. The details can be found in reference [46]. Additional complication arises when the basic constituents of the crystal arrangement are not atoms but molecules. One must keep track of internal molecular modes which increase the size of the dynamical matrix. Figure 4.4 displays the normal modes of Xe crystal terminated with its (111) surface. The calculation displayed was performed with 80 Xe(111) crystal planes. The most striking feature of figure 4.4 is the appearance of the modes which detach from the quasi-continuum of other modes (the quasi-continuum becomes the true continuum when the number of slabs tends to infinity). These detached modes are localized mainly in the topmost slab of atoms which can be seen by inspecting the mode polarization vectors. They are therefore called the surface phonons. One of these modes is dominantly

capital letters.

z-polarized and called the Rayleigh wave and the two other, higher in energy, are polarized dominantly longitudinally ($\mathbf{e}(\mathbf{Q}, \kappa = 0, s) || \mathbf{Q}$) and transversaly ($\mathbf{e}(\mathbf{Q}, \kappa = 0, s) \perp \mathbf{Q}$) and are called the longitudinal resonance and the shear horizontal mode. $\kappa = 0$ refers to the topmost (surface) Xe(111) crystal plane. The polarization vectors which result from this calculation are summarized in figure 4.5. In the topmost panel of this figure we plot the dispersions of the three surface modes and compare them with the experimental data. In the remaining three panels we plot the quantities related to the phonon density of states, namely

$$\xi_{z} = \sum_{s} |\mathbf{e}(\mathbf{Q}, \kappa = 0, s) \cdot \mathbf{z}_{0}|^{2} \exp(-(\omega - \omega(\mathbf{Q}, s))^{2}/w)$$

$$\xi_{L} = \sum_{s} \frac{|\mathbf{e}(\mathbf{Q}, \kappa = 0, s) \cdot \mathbf{Q}|^{2}}{|\mathbf{Q}|^{2}} \exp(-(\omega - \omega(\mathbf{Q}, s))^{2}/w)$$

$$\xi_{SH} = \sum_{s} \frac{|\mathbf{e}(\mathbf{Q}, \kappa = 0, s) \cdot (\mathbf{Q} \times \mathbf{z}_{0})|^{2}}{|\mathbf{Q}|^{2}} \exp(-(\omega - \omega(\mathbf{Q}, s))^{2}/w),$$

$$(4.28)$$

where w = 0.19 meV.

The actual calculations are always carried out with a finite number of slabs (otherwise the dynamical matrix would be of infinite dimension). One hopes to grasp the properties of a semi-infinite crystal by describing it by a finite number of slabs. The problem of obtaining the derivatives of the potential energy with respect to the motion of crystal sites (equations (4.4),(4.20)) has not been solved in this section. It will be solved in the next section.

4.4 Force constants and the terminology used in the slab lattice dynamical calculations

It is usually assumed in the lattice dynamical slab calculations that the change of the potential energy of a semi-infinite crystal as a result of the displacement of a particular lattice site can be obtained by considering only the local pair (site-site) interactions. Thus, instead of the second derivative of the total potential energy in (4.4), one calculates the second derivative of the sum of the pair potentials with respect to the coordinates actually displaced. The sum can be extended only to nearest neighbors or to second nearest neighbors or even to more distant

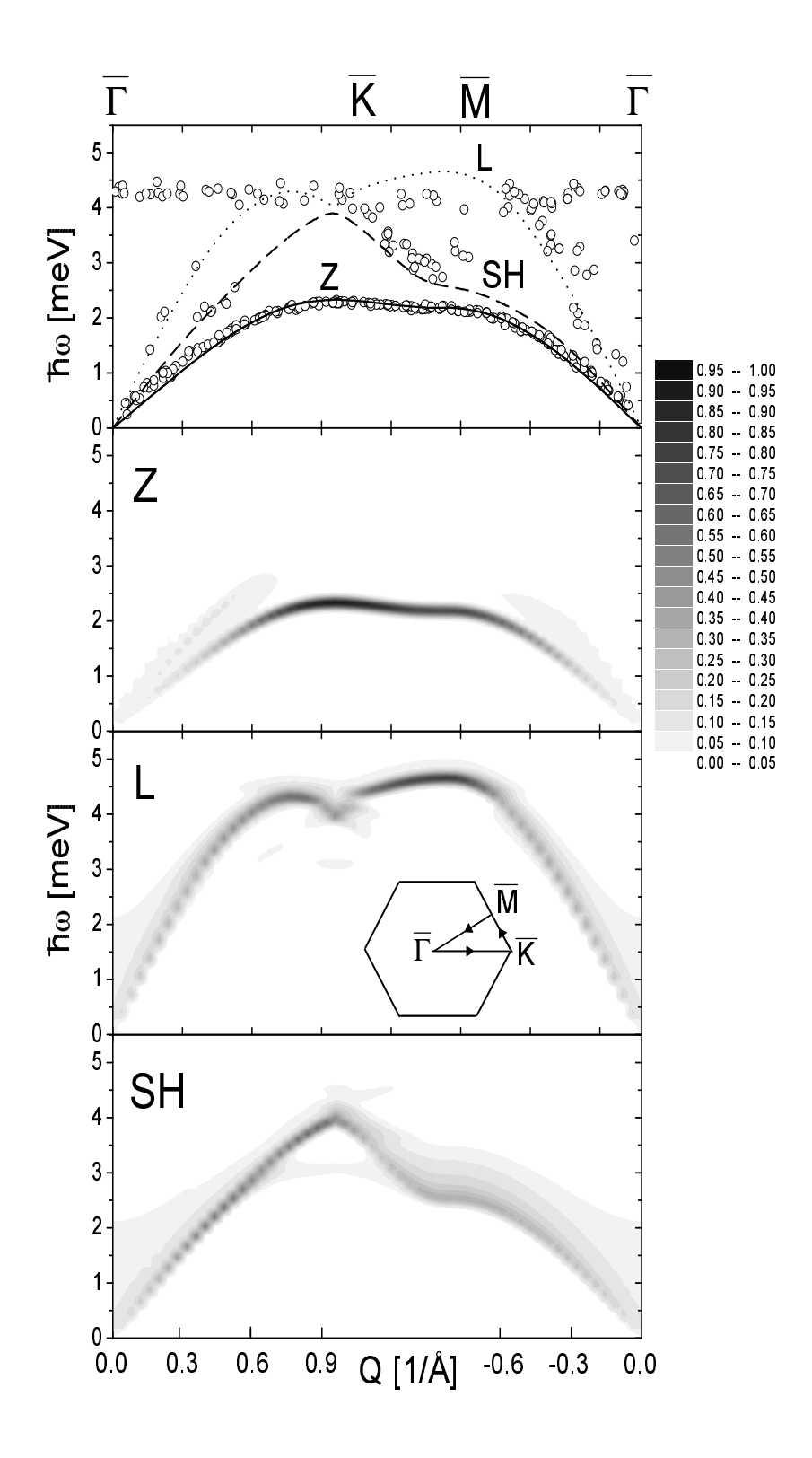


Figure 4.5: A specific representation of the polarization vectors at the Xe atom in the topmost Xe(111) crystal plane

neighbors. This procedure can be expected to work fine if the effective interactions have a range which is short enough (one cannot expect this approximation to hold if the sites interact via e.g. bare Coulomb forces). One usually connects with "springs" a particular site with its nearest and possibly second nearest neighbors (although much more neighbors can be considered, see e.g. [47, 36]) while displacements of other sites do not influence the particular site chosen. The different "springs" have different stiffnesses or, more commonly, force constants. Assuming that the pair interactions are spherically symmetric (i.e. depend only on the relative distance between the sites), it is easy to show that

$$\frac{\partial^{2} V_{rs}}{\partial u_{\alpha}(r) \partial u_{\beta}(s)} = -\frac{(\mathbf{r}_{r} - \mathbf{r}_{s})_{\alpha} (\mathbf{r}_{r} - \mathbf{r}_{s})_{\beta}}{|\mathbf{r}_{r} - \mathbf{r}_{s}|^{2}} \frac{\partial^{2} V}{\partial |\mathbf{r}_{r} - \mathbf{r}_{s}|^{2}}
- \frac{1}{|\mathbf{r}_{r} - \mathbf{r}_{s}|} \frac{\partial V}{\partial |\mathbf{r}_{r} - \mathbf{r}_{s}|} \left\{ \delta_{\alpha,\beta} - \frac{(\mathbf{r}_{r} - \mathbf{r}_{s})_{\alpha} (\mathbf{r}_{r} - \mathbf{r}_{s})_{\beta}}{|\mathbf{r}_{r} - \mathbf{r}_{s}|^{2}} \right\}
\alpha, \beta = x, y, z,$$
(4.29)

where the indices r and s stand for any two sites with the radius vectors \mathbf{r}_r and \mathbf{r}_s and V_{rs} is the pair interaction potential between sites r and s. $(\mathbf{r}_r - \mathbf{r}_s)_{\alpha}$ is α (x, y, z) component of relative radius vector $\mathbf{r}_r - \mathbf{r}_s$. If we chose relative x-axis to point from one site to another and denote $|\mathbf{r}_r - \mathbf{r}_s| = r_{rs}$, then the force constants in equation (4.29) look rather simple,

$$\beta_{rs} = -\frac{\partial^2 V_{rs}}{\partial u_x(r)\partial u_x(s)} = \frac{\partial^2 V_{rs}(r_{rs})}{\partial r_{rs}^2}$$

$$\alpha_{rs} = -\frac{\partial^2 V_{rs}}{\partial u_y(r)\partial u_y(s)} = -\frac{\partial^2 V_{rs}}{\partial u_z(r)\partial u_z(s)} = \frac{1}{r_{rs}} \frac{\partial V_{rs}(r_{rs})}{\partial r_{rs}}, (4.30)$$

where β_{rs} denotes the force constant which corresponds to displacements of r and s sites along the line joining them and α_{rs} denotes the force constant which corresponds to the displacements of r and s sites perpendicular to the line joining them. β_{rs} and α_{rs} are called the ra-dial force constant and the tangential force constant, respectively. One could assume that the pair potential, V_{rs} , is not spherically symmetric to account for inhomogeneities of the electron gas which would yield additional, angular force constant(s) [48].

To successfully model the experimentally determined dispersion relations, it is sometimes necessary [47, 48] to assume that the force constants are not everywhere the same. The standard procedure is to allow the force constants for the atoms close to the surface to differ from the corresponding values in the bulk. Since the force constants at the surface, needed to reproduce the experimental findings are generally smaller than the force constants in the bulk, this "effect" is called the softening of the force constants. This effect can probably be related to the electronic degrees of freedom which can be included only approximately into the lattice-dynamical-force-constants-scheme and to the neglect of the three-body and higher many-body interaction [35, 37, 47].

It is an experimentally established fact that the normal distances between the slabs are not the same throughout the sample. The significant change of the normal distances appears again close to the topmost slab (surface). The normal distances between the slabs can be either larger or smaller than the distance between the two neighboring slabs deep in the bulk of the sample. This effect is called the intralayer relaxation and can be in principle included into a slab dynamics scheme [46, 48].

4.5 Quantization of normal modes

The physics presented so far has been completely classical. We have solved coupled Newton's equations of motion by decoupling them via introduction of new coordinates (normal coordinates). When we turn to quantum mechanical description of the problem, we do not expect a change in the eigenfrequencies and eigenvectors (polarization vectors). This can be made at least plausible by examining the time dependence of a classical and quantum particle in a parabolic potential. Both particles will have the same characteristic time scale $1/\omega$ - the classical particle in the time evolution of its displacement, $u_{class}(t) = u(0) \cdot \cos(\omega t)$ and the quantum particle in the time evolution of its wave function. $\Psi_{quantum}(t) = \Psi(0) \cdot e^{-i\omega t}$. Since the problem of vibration of crystals has been shown to be equivalent to the problem of N independent harmonic oscillators (in the lowest approximation) we can expect the same conclusion to hold here, i.e. we can expect the normal modes to be the same in quantum and classical treatments of the problem. However, one thing surely changes: the occupation of the levels of harmonic oscillator as a function of temperature. Quantum and classical oscillators will follow Planck's (Bose-Einstein) and Boltzman's distributions, respectively.

We can explicitly introduce the quantization of normal modes in the same way as it was introduced for a single harmonic oscillator. This can be done by representing the hamiltonian of the problem in terms of creation and destruction operators, a^{\dagger} and a, respectively. A more detailed description of this procedure can be found in references [44, 8]. The quantization of displacements essentially fixes the phonon amplitude. The freedom of choosing the phonon amplitude is represented by the arbitrary constant u_0 in equation (4.21). The space coordinate x for 1D oscillator with characteristic frequency ω and mass M can be written as [8]

$$x = \sqrt{\frac{\hbar}{2M\omega}} (a^{\dagger} + a). \tag{4.31}$$

We can apply this to the normal, harmonic oscillator coordinates $u_{\mathbf{q}}$ in (4.21) and quantize independently each mode characterized by its wave vector \mathbf{q} (or \mathbf{Q}) and branch s. This yields ⁸ [11, 44, 49]

$$u_{\mathbf{q},a,s} = \sqrt{\frac{\hbar}{2M_a\omega(\mathbf{q},s)}} (a_{\mathbf{q},s}^{\dagger} + a_{-\mathbf{q},s}). \tag{4.32}$$

The operators a^{\dagger} , a satisfy the usual boson commutation relations:

$$[a_{\mathbf{q},s}, a_{\mathbf{q}',s}^{\dagger}]_{-} = \delta_{\mathbf{q},\mathbf{q}'} \delta_{s,s'} \tag{4.33}$$

$$[a_{\mathbf{q},s}, a_{\mathbf{q}',s}]_{-} = [a_{\mathbf{q},s}^{\dagger}, a_{\mathbf{q}',s}^{\dagger}]_{-} = 0.$$
 (4.34)

The hamiltonian of the problem can now be represented in terms of the creation and annihilation (destruction) operators as

$$H = \sum_{\mathbf{q},s} \hbar \omega(\mathbf{q},s) \left\{ a_{\mathbf{q},s}^{\dagger} a_{\mathbf{q},s} + \frac{1}{2} \right\}. \tag{4.35}$$

The displacement in the direct space can be written as

$$\mathbf{u}(p,a) = \sum_{\mathbf{q},s} \sqrt{\frac{\hbar}{2M_a N \omega(\mathbf{q},s)}} \mathbf{e}(\mathbf{q},a,s) (a_{\mathbf{q},s} + a_{-\mathbf{q},s}^{\dagger}) e^{i\mathbf{q} \cdot \mathbf{r}_p}. \tag{4.36}$$

The Bose-Einstein statistics of the excitations (phonons) is now containted in the commutation relations (4.33) and (4.34). The wave function of the system with $n(\mathbf{q}, s)$ phonons in state (\mathbf{q}, s) and no phonons in other states can be written as:

$$|0,0,...,n(\mathbf{q},s),...,0\rangle = \frac{1}{\sqrt{n!}} (a_{\mathbf{q},s}^{\dagger})^n |0,0,...,0,...,0\rangle.$$
 (4.37)

⁸It is sometimes convenient to associate $1/\sqrt{N}$ factor from the Fourier series in equation (4.21) with amplitude $u_{\mathbf{q}}$, and redefine the series.

There can be arbitrary number of phonons in each eigenstate (\mathbf{q}, s) of the system since phonons are boson quasiparticles. The result of action of $a_{\mathbf{q}_a,s_b}^{\dagger}$ and $a_{\mathbf{q}_a,s_b}$ operators on some state with n_{11} phonons in state (\mathbf{q}_1,s_1) , n_{12} phonons in state (\mathbf{q}_1,s_2) , n_{ab} phonons in state (\mathbf{q}_a,s_b) etc. is given by the following relations [8, 11, 44]:

$$\begin{array}{lcl} a_{\mathbf{q}_{a},s_{b}}^{\dagger} | n_{11}, n_{12}...n_{21}...n_{ab}... \rangle & = & \sqrt{n_{ab}+1} | n_{11}, n_{12}...n_{21}...n_{ab}+1... \rangle \\ a_{\mathbf{q}_{a},s_{b}} | n_{11}, n_{12}...n_{21}...n_{ab}... \rangle & = & \sqrt{n_{ab}} | n_{11}, n_{12}...n_{21}...n_{ab}-1... \rangle \end{array}$$

$$(4.38)$$

Here, the vectors $|n_{11}, n_{12}...n_{21}...n_{ab}...\rangle$ completely specify the quantum state of the crystal. By using equations (4.38), it is easy to show that

$$\langle \dots n_{ab} \dots | a_{\mathbf{q}_a, s_b}^{\dagger} a_{\mathbf{q}_a, s_b} | \dots n_{ab} \dots \rangle = n_{ab}$$

$$\langle \dots n_{ab} \dots | a_{\mathbf{q}_a, s_b}^{\dagger} a_{\mathbf{q}_a, s_b} | \dots n_{ab} \dots \rangle = 0$$

$$\langle \dots n_{ab} \dots | a_{\mathbf{q}_a, s_b}^{\dagger} a_{\mathbf{q}_a, s_b}^{\dagger} | \dots n_{ab} \dots \rangle = 0.$$

$$(4.39)$$

This is why $a^{\dagger}a$ combination of operators is called the *number operator*.

Chapter 5

Short survey of atom-surface scattering experiments

The country needs and, unless I mistake its temper, the country demands bold, persistent experimentation.

Franklin Delano Roosevelt

THEORY OF
THERMAL ENERGY
INERT ATOM
SCATTERING FROM
SURFACE VIBRATIONS

Antonio Šiber

In this chapter we shall briefly review the experimental aspects of atom-surface scattering. Hence, it is not our intention to give a comprehensive survey of the experiments in the area of atom-surface scattering, but rather to point out what the experimentalists can measure and how they measure it.

The atoms used as projectiles are in most cases He (helium) atoms. The atomic beam of helium is formed by an irreversible adiabatic expansion of a high pressure gas (≈ 400 bar) contained in the stagnation (or source) chamber through a cylindrical aperture (nozzle) with a diameter of $\approx 10 \mu \text{m}$. This process produces a beam of He atoms with a very small spread in energies, with the mean energy depending on the source temperature. The temperature of the source can be varied continuously, usually in a range from 30 K to 700 K. This corresponds to beam energies in the range of 5 meV to 140 meV ¹. The beam then passes through a conical skimmer and several (≈ 3) vacuum chambers, one of which contains the rotating disc chopper for time-of-flight (TOF) measurements. Thus the beam is chopped before entering the ultrahigh vacuum (UHV) target chamber which houses the target (sample) and additional equipment needed for preparation and characterization of the sample surface (sputter gun, Auger spectrometer, LEED etc.). The scattered atoms are detected by a mass spectrometer which is located at ≈ 1.5 m from the target at a fixed angle $\theta_{SD} \approx 90^{\circ}$ with respect to the line joining the source and the target. The sample is mounted on a manipulator enabling x, y and z translations as well as rotations about three axes. The target holder is provided with an electron bombardment heater and a liquid N₂ or He cooling arrangement which enables the variation of the sample temperatures in the interval 50 K-1200 K.

The detector consists of an electron bombardment ionizer followed by the magnetic sector field mass analyzer. In addition to the three differential pumping stages situated between the source and target chamber, more (≈ 4) pumping stages are located between the target chamber and the detector chamber. A relative resolution of $\Delta E/E=2\%$ can be achieved for energies (E) of He atoms up to 60 meV. A more detailed description of individual parts of the experimental setup follows.

¹Energy of He atoms produced by an irreversible adiabatic expansion through an aperture is very accurately given by $E_k(He) = \frac{5}{2}k_BT_{source}$ [50]. Here k_B is the Boltzman constant and T_{source} is the temperature of the source of He atoms.

He-beam source

The He beam is formed by hydrodynamic expansion from the stagnation chamber into vacuum through a nozzle of 10 μ m in diameter. The pumping system ensures that the ratio of the stagnation pressure inside the nozzle to the background pressure in the expansion chamber is as high as 10^7 , so that no shock structures occur in the expansion region and a smooth transition from continuum to free-molecular flow takes place a few mm downstream from the nozzle. In this jet expansion, random kinetic energy is converted in the course of many collisions into forward kinetic energy. The central part of the free He jet is selected by the skimmer that acts as a collimator and, due to its shape, deviates the non-passing atoms away from the beam path. The final velocity distribution of atoms in the beam is thus sharply peaked with a width $\Delta v/v$ as little as 0.01, which is in contrast with the broad Maxwellian velocity distribution of atoms in the source.

Pumping system

The He apparatus is built with a multishell structure which is necessary to differentially pump the various regions outside the central sample chamber, without increasing largely the apparatus dimensions. The pumping stages are extremely important since they reduce the contamination of both the He beam and the sample. The pressures down to 6×10^{-11} mbar (in the detector chamber) can be achieved by differential pumping [51, 95]. Usually 9 pumping stages are used (as in the apparatus in Göttingen). This causes bulkiness of the experimental setup.

Time-of-flight equipment

The chopping of the beam is needed for the determination of energies of scattered He atoms. Namely, the count rate of scattered particles arriving at the detector is recorded as a function of the time delay from the passage of chopper slit through the helium beam (the effective time in which the chopper is letting the beam pass to the target chamber can be varied between 5 and 110 μ s [95] - the chopper therefore produces pulses of He atoms whose length depends on the He beam energy and the chopping time). Knowing the lengths of the apparatus and the source temperature, one can calculate the energy exchanged in the collision of He-atom with the sample (this requires the scaling of x-axis from

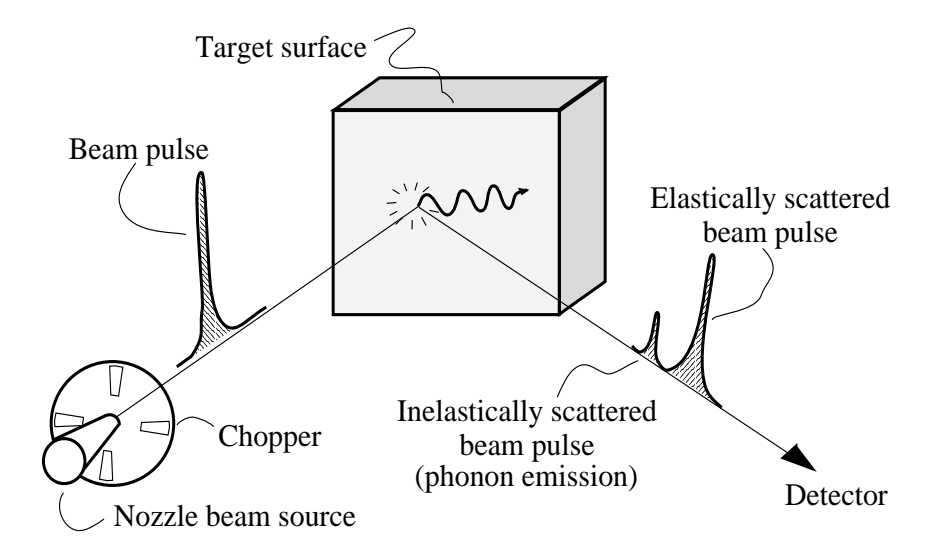


Figure 5.1: Figure displays the basic principle on which the time-of-flight method is founded. For additional explanation see text.

the time of flight to the exchanged energy scale). The basic principle of the time-of-flight technique is illustrated in figure 5.1. The time-of flight spectrum obtained for He \rightarrow Xe/C(111) (diamond) is shown in figure 5.2 both for time-of flight x-axis (right panel) and exchanged energy x-axis (left panel). The equidistant discrete peaks in the spectrum point to dominance of nondispersive vibrational modes (see Chapter 9).

Target chamber

Ion sputter gun, producing usually Ar ions, is used for the preparation of a crystallographically ordered sample [2]. Low energy electron diffraction (LEED) is used (as in many areas of experimental surface physics) for the determination of crystallographic order of the prepared sample. Auger spectroscopy is used to determine the chemical character of the contamination of the sample.

Relative angle of the sample with respect to the incident atomic beam, θ_i can be changed by rotating the sample. It must be born in mind that this also changes the angle between the beam atoms recorded in the detector and the sample, θ_f , since the total angle $\theta_{SD} = \theta_i + \theta_f$ is fixed. Therefore, the experiments always see the scattering spectra for fixed incident and outgoing angle. Atoms which scatter in other outgoing final angles are simply not seen in the experiments since they can not reach the detector due to the geometry of experimental ar-

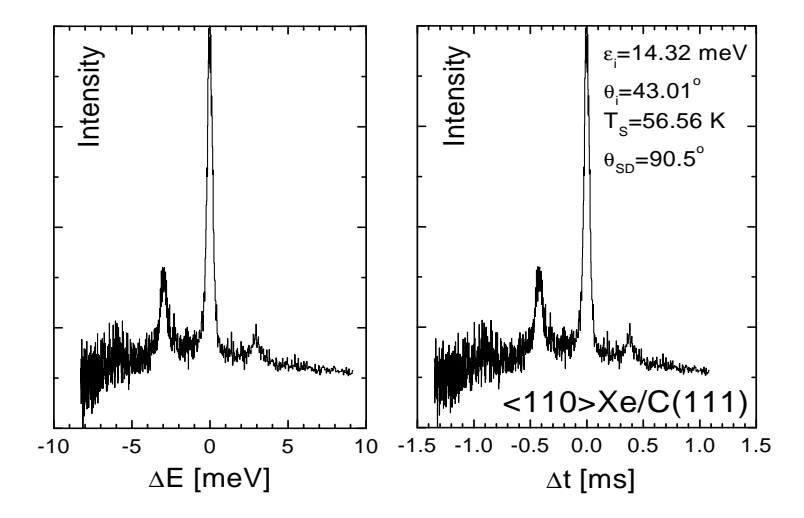


Figure 5.2: A typical TOF spectrum for He \rightarrow Xe/C(111) scattering system taken along < 110 > direction of Xe superstructure. *Left*: Exchanged energy x-axis. *Right*: Time of flight x-axis. The measurements were carried out by D. Fuhrmann, Ruhr-Universität Bochum in 1997.

rangement.

Detector chamber

The ionization of the scattered He atoms is required simply for recording the scattered beam flux. The observation of neutral particles (such as neutrons) requires a much higher degree of experimental sophistication. First, the He beam is ionized by an electron beam intercepting the beam path (efficiency $\approx 10^{-5}$), then it is accelerated ($\approx 3.5 \, \mathrm{kV}$) through the quadrupole mass spectrometer. The quadrupole operates in radio frequency range; the passing beam is then mass selected and focussed on the first plate of a dynode multiplier. A turbo pump is mounted behind the multiplier in an off-axis position, in order to pump away kinetically the neutral He beam. The signal is sent to a pulse-former and then to a counter.

The figures which follow are schemes of the experimental setups used by helium atom scattering groups at Ruhr Universität Bochum (Germany) and Rutgers University (NJ, USA).

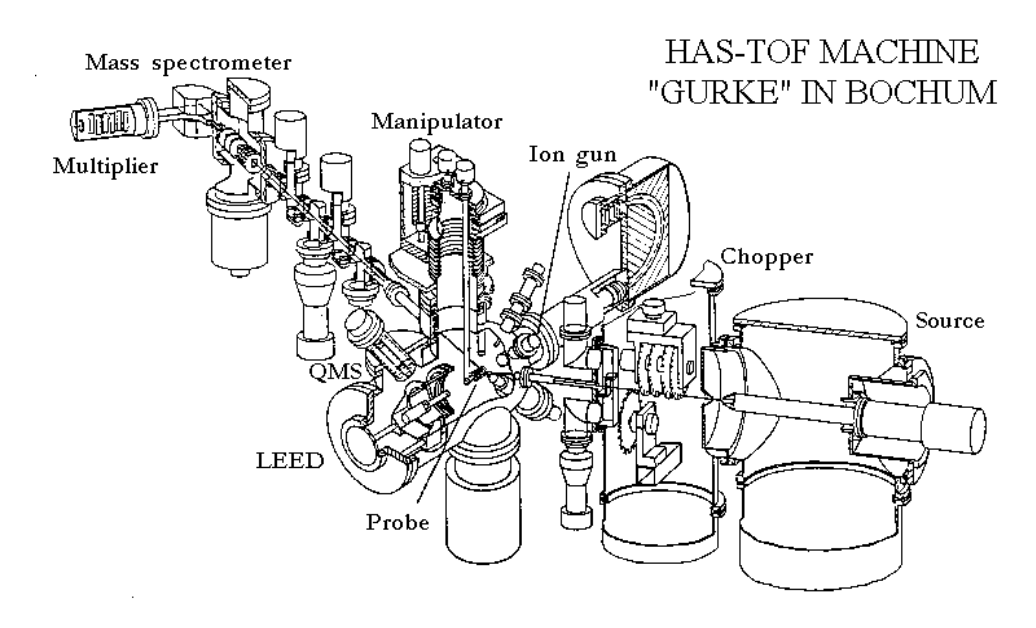


Figure 5.3: Somewhat more detailed scheme of the HAS-TOF experimental setup at Ruhr Universität Bochum. Some parts of the equipment discussed in text are marked.

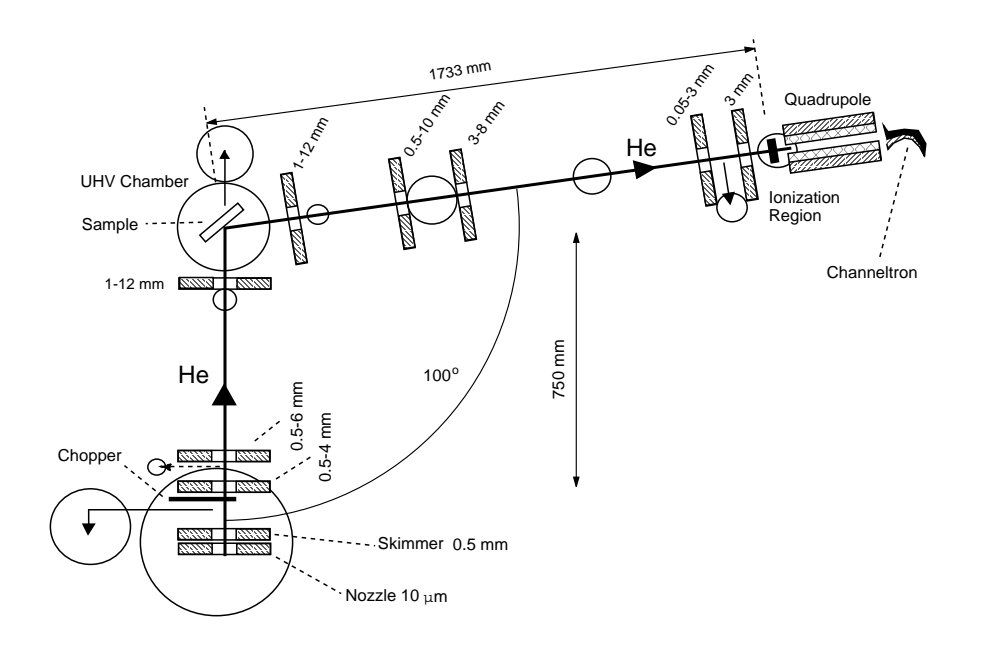


Figure 5.4: A scheme of the HAS-TOF experimental setup at Rutgers University (NJ). Note the geometrical dimensions.

Chapter 6

DWBA: Distorted Wave Born Approximation in the description of atom-surface scattering

Five is a sufficiently close approximation to infinity.

Robert Firth

THEORY OF
THERMAL ENERGY
INERT ATOM
SCATTERING FROM
SURFACE VIBRATIONS

Antonio Šiber

In the atom-surface scattering problems discussed in this thesis both the dynamics of the projectile (e.g. He atom) and the vibrations of the target must be treated quantum-mechanically owing to the scattering conditions typical of this kind of experiments. In other words, the appropriate theoretical description is the one pertaining to two coupled quantum fields.

The Distorted Wave Born Approximation (DWBA) is a first order perturbative approach frequently employed in atom-surface scattering problems under the scattering conditions mentioned. It can appropriately describe the collision processes in which only one phonon is excited. This dominantly happens when the energy and mass of the projectile atom are sufficiently low. The range of validity of the DWBA additionally depends on the "softness" of the target phonons. If the phonons of the target have low frequency (energy), then it is easy to excite them and even atoms with low energy can, on the average, excite more then one quantum (phonon). A more detailed accounts of the DWBA and its use in atom-surface scattering are the subject of this chapter.

6.1 Derivation of the DWBA

We can write the hamiltonian of the atom-target system as:

$$H = \frac{\hbar^2 \mathbf{k}^2}{2m} + V_{atom-target}(\{\mathbf{r}, \mathbf{r}_j\}) + V_{target}(\{\mathbf{r}_j\}) + \sum_j \frac{\mathbf{p}_j^2}{2M}$$
 (6.1)

Here m is the mass of the projectile atom, \mathbf{k} is its wave vector, \mathbf{r} is its radius vector, \mathbf{p}_j is the momentum of the j-th target atom and $\{\mathbf{r}_j\}$ is the set of radius vectors of the atoms in the target. $V_{atom-target}$ is the interaction potential between the projectile atom and the target and $V_{crystal}$ is the potential energy of a particular configuration of target atoms coordinates $\{\mathbf{r}_j\}$. The last two terms in the hamiltonian were quantized in the previous chapter. We shall separate the potential $V_{atom-target}$ in its static and dynamic components as in Chapter 3:

$$V_{atom-target}(\{\mathbf{r}, \mathbf{r}_j\}) = V_{static}(\{\mathbf{r}, \mathbf{r}_j^0\}) + V_{dynamic}(\{\mathbf{u}_j\}, \{\mathbf{r}_j^0\})$$
 (6.2)

We are now going to find the eigenstates of the hamiltonian (6.1) without the dynamic part of the interaction $V_{dynamic}$ in equation (6.2). The idea is to treat this latter part as perturbation to the atom-target system interacting mutually only via static component of $V_{atom-target}$ interaction. The afore mentioned eigenstates can be written as a direct product of the projectile and crystal states:

$$\Psi_{\mathbf{k},\{n(\mathbf{Q},s)\}} = \zeta_{k_z,\mathbf{K}}(\mathbf{r}) \otimes |\{n(\mathbf{Q},s)\}\rangle.$$
(6.3)

Here k_z is the component of the projectile wave vector perpendicular to the target surface and \mathbf{K} is a projection of the projectile wave vector \mathbf{k} onto the target surface. The state $|\{n(\mathbf{Q}, s)\}\rangle$ has the same meaning as in equation (4.38). The projectile wave function ζ was written in coordinate space. If we disregard the corrugation of the potential V_{static} , we can write for $\zeta_{k_z,\mathbf{K}}(\mathbf{r})$ (which is called the distorted wave):

$$\zeta_{k_z, \mathbf{K}}(\mathbf{r}) = \frac{1}{\sqrt{L_S^2 L_z}} \psi_{k_z}(z) e^{i\mathbf{K} \cdot \mathbf{R}}.$$
 (6.4)

Here **R** is the projection of **r** onto the target surface, and L_S is the dimension of the square box used for normalization of plane waves $e^{i\mathbf{K}\cdot\mathbf{R}}$ in the surface plane. These are a free-particle solutions since the potential in the directions parallel to the surface was assumed to be constant for a fixed z coordinate. The wave function $\psi_{k_z}(z)$ is boxnormalized with respect to quantizing box dimension in z direction, L_z . We can find the dependence of ψ_{k_z} on z by solving the 1D Schrödinger equation:

$$\left\{ -\frac{\hbar^2}{2m} \frac{\partial^2}{\partial z^2} + V_0(z) \right\} \psi_{k_z}(z) = \frac{\hbar^2 k_z^2}{2m} \psi_{k_z}(z) = \epsilon(k_z) \psi_{k_z}(z). \tag{6.5}$$

Here V_0 is the laterally averaged static potential as in $Chapter\ 3$ and $\epsilon(k_z)$ is the projectile energy "in z-direction" i.e. $\epsilon(k_z) = \epsilon_i \cos^2(\theta_i)$, where ϵ_i is the projectile total incident energy. The wave functions $\psi_{k_z}(z)$ are called distorted waves since in principle they are plane waves distorted by the presence of a static component of the atom-surface potential. We shall further write ψ_z instead of ψ_{k_z} knowning that the quantum number which uniquely specifies the wave function $\psi(z)$ is the projectile's wave vector in z-direction.

The quantum mechanical state-to-state transition rate characteristic of a scattering event is given by

$$w_{fi} = \frac{2\pi}{\hbar} |T_{fi}|^2 \delta(E_f - E_i), \tag{6.6}$$

where E_i and E_f are total energies of the system consisting of the projectile atom and the crystal prior and after the collision, respectively, and T_{fi} is the transition matrix element. This is the scattering counterpart of the standard "transition probability per unit time" expression

explained in textbooks on quantum mechanics [8, 11]. The index i (initial) stands for the initial wave vector \mathbf{k}_i of the projectile atom and for the initial occupation numbers $n_i(\mathbf{Q}, s)$ of the normal modes (phonons) of the target, and similarly for index f (final). T_{fi} contains the contributions of all the scattering processes possible for a particular set of the atom-target collision parameters (initial energy, angle, temperature ...), therefore also the processes where more than one phonons are excited (multiphonon processes). We are interested here only in the transitions where the occupation number of a particular phonon mode increases or decreases by 1, i.e. $n_f(\mathbf{Q}, s) = n_i(\mathbf{Q}, s) \pm 1$. These are called single phonon or one phonon processes.

The next step is to represent the dynamic component of the potential in (6.2) by exploiting the two dimensional periodicity of the target. Equation (3.14) can now be written in the slab-geometry language introduced in *Chapter 4* as

$$V(\mathbf{r}, \{\mathbf{u}_j\}) = V_{static}(\mathbf{r}) - \sum_{l,\kappa} \mathbf{u}(\mathbf{R}_l, \kappa) \cdot \nabla_{\mathbf{r}} v(\mathbf{r} - \mathbf{R}_l - \mathbf{r}_{\kappa})$$

$$= V_{static} + V_{dynamic}$$
(6.7)

Here \mathbf{r}_{κ} is the radius vector pointing from the point chosen as the origin for projectile radius vector \mathbf{r} to the point chosen as the origin for \mathbf{R}_l vectors in the particular slab κ ($\mathbf{r}_j = \mathbf{R}_l + \mathbf{r}_{\kappa}$, see figure 6.1). Pairwise summation procedure is again used in (6.7). The Distorted Wave Born Approximation consists in replacing T_{fi} with $V_{dynamic}^{fi}$. This is analogous to first order perturbation treatment for stationary discrete states [8, 11]. Here

$$V_{dynamic}^{fi} = \langle f | V_{dynamic}(\{\mathbf{u}(\mathbf{R}_{l}, \kappa)\}, \{\mathbf{r}_{l}^{0}\}) | i \rangle$$

$$= -\sum_{l,\kappa} (\langle \zeta_{f} | \nabla_{\mathbf{r}} v(\mathbf{r} - \mathbf{R}_{l} - \mathbf{r}_{\kappa}) | \zeta_{i} \rangle$$

$$\times \langle \{n_{f}(\mathbf{Q}, s)\} | \mathbf{u}(\mathbf{R}_{l}, \kappa) | \{n_{i}(\mathbf{Q}, s)\} \rangle).$$
 (6.8)

The displacement coordinate $\mathbf{u}(\mathbf{R}_l, \kappa)$ can be expressed via (\mathbf{Q}, κ) coordinates as in equation (4.21). When quantized, the coordinates $u_{\mathbf{Q}}$ contain only one creation and one annihilation operator. Therefore, the phonon part of the matrix element represented by the last line in (6.8) will be different from zero only if there exists a wave vector \mathbf{Q}_a and a branch s_b for which $n_f(\mathbf{Q}_a, s_b) = n_i(\mathbf{Q}_a, s_b) \pm 1$ (see equation (4.38)).

Using equations (4.32) and (4.21) it is possible to write the phonon part of the matrix element (for absorption of one phonon) in equation

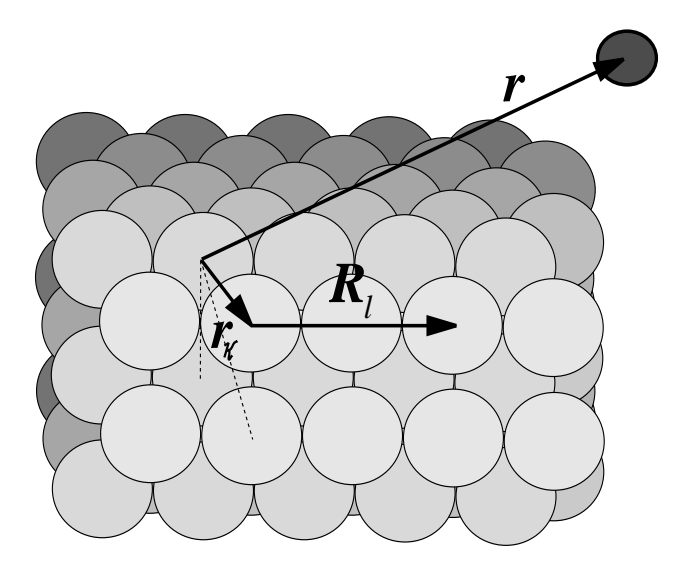


Figure 6.1: The notation adopted in this chapter. Dashed lines represent \mathbf{r}_{κ} vectors for deeper slabs κ . Note that vector \mathbf{r}_{κ} does not necessarily lie in the plane of paper, depending on a particular slab κ .

(6.8) as

$$\langle \{...n_i(\mathbf{Q}_a, s_b) - 1...\} | \mathbf{u}(\mathbf{R}_l, \kappa) | \{...n_i(\mathbf{Q}_a, s_b)...\} \rangle =$$

$$= \sqrt{\frac{\hbar n_i(\mathbf{Q}_a, s_b)}{2MN_{2D} |\omega(\mathbf{Q}_a, s_b)|}} e^{i\mathbf{Q}_a \cdot \mathbf{R}_l} \mathbf{e}(\mathbf{Q}_a, \kappa, s_b). \tag{6.9}$$

Initially the crystal is in thermal equilibrium at temperature T_S and the average value of $n_i(\mathbf{Q}_a, s_b)$ is $\langle n_i(\mathbf{Q}_a, s_b) \rangle = n(|\omega(\mathbf{Q}_a, s_b)|)$ where $n(\omega)$ is the Bose-Einstein distribution:

$$n(\omega) = \frac{1}{\exp\left\{\frac{\hbar\omega}{k_B T_S}\right\} - 1}.$$
 (6.10)

Here k_B is the Boltzmann constant. Now we can write for the transition rate for *all possible* one phonon absorption processes, thermally averaged over *initial* crystal states

$$w_{fi} = \frac{2\pi}{\hbar} \sum_{\mathbf{Q},s} \frac{\hbar n(|\omega(\mathbf{Q},s)|)}{2MN_{2D}|\omega(\mathbf{Q},s)|} |M_{fi}|^2 \delta(\epsilon_f - \epsilon_i - \hbar|\omega(\mathbf{Q},s)|)$$
(6.11)

The summation over \mathbf{Q} and s now collects all possible one phonon processes which conserve energy. Here ϵ 's are the projectile energies

and

$$M_{fi} = \int d^3r \zeta_f(\mathbf{r})^* \left\{ \sum_{l,\kappa} [\mathbf{F}_{l,\kappa}(\mathbf{r}) \cdot \mathbf{e}(\mathbf{Q},\kappa,s)] e^{i\mathbf{Q} \cdot \mathbf{R}_l} \right\} \zeta_i(\mathbf{r})$$
 (6.12)

is the remaining part of the matrix element pertaining to the projectile atom. Here

$$\mathbf{F}_{l,\kappa}(\mathbf{r}) = -\nabla_{\mathbf{r}} v(\mathbf{r} - \mathbf{R}_l - \mathbf{r}_{\kappa}). \tag{6.13}$$

When we repeat the same procedure for one-phonon emission processes we obtain again equation (6.11) with $n(|\omega(\mathbf{Q}, s)|)$ replaced by $n(|\omega(\mathbf{Q}, s)|) + 1$ (since the phonon is created now - see equation (4.38)) and $-\hbar|\omega(\mathbf{Q}, s)|$ replaced by $+\hbar|\omega(\mathbf{Q}, s)|$ in the argument of the energy conserving δ -function. If we let $\omega(\mathbf{Q}, s)$ have either sign (– and + signs representing emission and absorbtion, respectively) we can write the thermally averaged transition rate for all one-phonon processes as

$$w_{fi} = \sum_{\mathbf{Q},s} \left\{ \frac{\pi n(\omega(\mathbf{Q},s))}{M N_{2D} \omega(\mathbf{Q},s)} |M_{fi}|^2 \right\} \delta(\epsilon_f - \epsilon_i - \hbar \omega(\mathbf{Q},s)), \qquad (6.14)$$

where we have used

$$n(|\omega|) + 1 = -n(-|\omega|).$$
 (6.15)

We represent ζ functions as in equation (6.4) i.e., we neglect the corrugation of V_{static} component of the interaction potential. For M_{fi} we have now:

$$M_{fi} = -\frac{1}{L_{z}L_{S}^{2}} \sum_{l,\kappa} \int dz \psi_{f}^{*}(z) \left\{ \int d^{2}R e^{-i\mathbf{K}_{f} \cdot \mathbf{R}} e^{i\mathbf{K}_{i} \cdot \mathbf{R}} \right.$$

$$\times \mathbf{F}_{l,\kappa}(\mathbf{r}) \cdot \mathbf{e}(\mathbf{Q}, \kappa, s) e^{i\mathbf{Q} \cdot \mathbf{R}_{l}} \left\} \psi_{i}(z)$$

$$= -\frac{1}{L_{z}L_{S}^{2}} \int dz \psi_{f}^{*}(z) \psi_{i}(z) \int d^{2}R \sum_{l,\kappa} e^{-i(\mathbf{K}_{f} - \mathbf{K}_{i}) \cdot (\mathbf{R} - \mathbf{R}_{l})} \right.$$

$$\times \mathbf{F}_{l,\kappa}(\mathbf{R} - \mathbf{R}_{l} - \mathbf{R}_{\kappa} + (z - z_{\kappa})\mathbf{z}_{0}) \cdot \mathbf{e}(\mathbf{Q}, \kappa, s) e^{i(\mathbf{K}_{i} - \mathbf{K}_{f} + \mathbf{Q}) \cdot \mathbf{R}_{l}}$$

$$= -\frac{1}{L_{z}L_{S}^{2}} \int dz \psi_{f}^{*}(z) \psi_{i}(z) \sum_{l,\kappa} \int d^{2}(R - R_{l}) e^{-i(\mathbf{K}_{f} - \mathbf{K}_{i}) \cdot (\mathbf{R} - \mathbf{R}_{l})}$$

$$\times \mathbf{F}_{l,\kappa}(\mathbf{R} - \mathbf{R}_{l} - \mathbf{R}_{\kappa} + (z - z_{\kappa})\mathbf{z}_{0}) \cdot \mathbf{e}(\mathbf{Q}, \kappa, s) e^{i(\mathbf{K}_{i} - \mathbf{K}_{f} + \mathbf{Q}) \cdot \mathbf{R}_{l}}$$

$$(6.16)$$

Note now that the part which must remain within the integral over $d^2(R - R_l)$ does not depend on index l. Summation over l has to be performed for the remaining part which yields

$$\sum_{l} e^{i(\mathbf{K}_{i} - \mathbf{K}_{f} + \mathbf{Q}) \cdot \mathbf{R}_{l}} = N_{2D} \sum_{\mathbf{G}} \delta_{\mathbf{K}_{f} - \mathbf{K}_{i} - \mathbf{Q}, \mathbf{G}}.$$
 (6.17)

Using the above identity, we can explicitly write out the part we have to integrate over $d^2(R - R_l) = d^2R'$. We call this part I:

$$I = \int d^{2}R' e^{-i(\mathbf{Q}+\mathbf{G})\cdot\mathbf{R}'} \nabla_{\mathbf{r}'} v(\mathbf{R}' - \mathbf{R}_{\kappa} + (z' - z_{\kappa})\mathbf{z}_{0})$$

$$= \int d^{2}(R' - R_{\kappa}) e^{-i(\mathbf{Q}+\mathbf{G})\cdot(\mathbf{R}'-\mathbf{R}_{\kappa})} \nabla_{\mathbf{r}'} v(\mathbf{R}' - \mathbf{R}_{\kappa} + (z' - z_{\kappa})\mathbf{z}_{0})$$

$$\times e^{-i(\mathbf{Q}+\mathbf{G})\cdot\mathbf{R}_{\kappa}}$$

$$= \int d^{2}R'' e^{-i(\mathbf{Q}+\mathbf{G})\cdot\mathbf{R}''} \left(\frac{\partial}{\partial \mathbf{R}''} \mathbf{R}''_{0} + \frac{\partial}{\partial z'} \mathbf{z}'_{0}\right) v(\mathbf{R}'' + (z' - z_{\kappa})\mathbf{z}_{0})$$

$$\times e^{-i(\mathbf{Q}+\mathbf{G})\cdot\mathbf{R}_{\kappa}}$$

$$= e^{-i(\mathbf{Q}+\mathbf{G})\cdot\mathbf{R}_{\kappa}} \left\{ i(\mathbf{Q}+\mathbf{G}), \frac{\partial}{\partial z} \mathbf{z}_{0} \right\} \int d^{2}R'' v(\mathbf{R}'' + (z - z'_{\kappa})\mathbf{z}'_{0})$$

$$\times e^{-i(\mathbf{Q}+\mathbf{G})\cdot\mathbf{R}''}$$

$$= e^{-i(\mathbf{Q}+\mathbf{G})\cdot\mathbf{R}''}$$

$$= e^{-i(\mathbf{Q}+\mathbf{G})\cdot\mathbf{R}_{\kappa}} \left\{ i(\mathbf{Q}+\mathbf{G}), \frac{\partial}{\partial z} \mathbf{z}_{0} \right\} v_{\mathbf{Q}+\mathbf{G}}(z - z_{\kappa}). \tag{6.18}$$

The fourth equation in the equation array above is obtained by partial integration over d^2R'' . \mathbf{R}''_0 is the unit vector in \mathbf{R}'' direction and $v_{\mathbf{Q}+\mathbf{G}}(z-z_{\kappa})$ is a two dimensional Fourier transform of $v(\mathbf{R}+(z-z_{\kappa})\mathbf{z}_0)$ defined as

$$v_{\mathbf{Q}+\mathbf{G}}(z-z_{\kappa}) = \int d^{2}R e^{-i(\mathbf{Q}+\mathbf{G})\cdot\mathbf{R}} v(\mathbf{R} + (z-z_{\kappa})\mathbf{z}_{0}).$$
 (6.19)

Note that $v_{\mathbf{Q}=0,\mathbf{G}=0}(z-z_{\kappa})/A_c$, where A_c is the area of the surface unit cell, yields the static component of the interaction of the projectile atom with *all* the sites (atoms) in the κ 'th slab of the target crystal.

The precise dependence of $v_{\mathbf{Q}}$ on wave vector \mathbf{Q} can be obtained by performing the integration in equation (6.19). However, this requires additional numerical calculations. In the case when $V_0(z)$ has the Morse functional dependence on z as in equation (3.15), it has proven fruitfull [52, 53, 7] (and quite accurate [40]) to approximate the \mathbf{Q} dependence of $v_{\mathbf{Q}}$ as

$$v_{\mathbf{Q}}(z - z_{\kappa}) = v_{rep,\mathbf{Q}=0}(z - z_{\kappa})e^{-\frac{Q^{2}}{2Q_{c}^{2}}} - v_{att,\mathbf{Q}=0}(z - z_{\kappa})e^{-\frac{Q^{2}}{Q_{c}^{2}}}$$
(6.20)

where

$$Q_c = \sqrt{\frac{2/d}{z_t}} = \sqrt{\frac{\beta}{z_t}}. (6.21)$$

Here z_t is the classical turning point of the projectile atom obtained from $V_0(z_t) = \epsilon_i \cos^2 \theta_i$ and β is the inverse range of the repulsive component of the total static interaction potential. The terms $v_{rep,\mathbf{Q}=0}(z-z_{\kappa})$ and $v_{att,\mathbf{Q}=0}(z-z_{\kappa})$ are the repulsive and attractive parts of the potential $v_{\mathbf{Q}=0}(z-z_{\kappa})$, viz. $v_{\mathbf{Q}=0}(z-z_{\kappa}) = v_{rep,\mathbf{Q}=0}(z-z_{\kappa}) - v_{att,\mathbf{Q}=0}(z-z_{\kappa})^{-1}$. Q_c is usually called the cut-off wave vector (sometimes, the Armand factor [6]) and is typically 1 Å⁻¹ almost irrespective of the actual scattering system studied and of the projectile incident energy [7].

Inserting (6.18) and (6.17) into equation (6.16) for M_{fi} we have

$$M_{fi} = \frac{1}{L_z A_c} \sum_{\kappa, \mathbf{G}} \delta_{\mathbf{K}_f - \mathbf{K}_i, \mathbf{Q} + \mathbf{G}} \times \int dz \psi_f^*(z) \mathbf{e}(\mathbf{Q}, \kappa, s) \cdot \mathbf{F}_{\kappa}(\mathbf{Q} + \mathbf{G}, z) \psi_i(z), \qquad (6.22)$$

where $A_c = L_S^2/N_{2D}$ and

$$\mathbf{F}_{\kappa}(\mathbf{Q} + \mathbf{G}, z) = -\left\{i(\mathbf{Q} + \mathbf{G}), \mathbf{z}_{0} \frac{\partial}{\partial z}\right\} v_{\mathbf{Q} + \mathbf{G}}(z - z_{\kappa}) e^{-i(\mathbf{Q} + \mathbf{G}) \cdot \mathbf{r}_{\kappa}}. \quad (6.23)$$

Note here that $(\mathbf{Q} + \mathbf{G}) \cdot \mathbf{R}_{\kappa} = (\mathbf{Q} + \mathbf{G}) \cdot \mathbf{r}_{\kappa}$ since $(\mathbf{Q} + \mathbf{G}) \cdot \mathbf{z}_0 = 0$. By inspecting the matrix elements of the potential (needed for the modes with the polarization vectors lying in the surface plane) and of the derivative of the potential (needed for z-polarized modes ²) we arrive at the conclusion that the coupling of the projectile to the z-polarized modes is generally much stronger than to the modes polarized in the surface plane [54, 55].

When we divide the transition rate in equation (6.11) with the incident projectile flux $^3 \hbar k_i \cos \theta_i / mL_z$ perpendicular to the surface (here k_i is the length of the three dimensional wave vector of the projectile and θ_i is its incident angle with respect to the surface normal), we obtain a quantity usually called state-to-state reflection coefficient, R_{fi} :

$$R_{fi} = R(\mathbf{k}_f, \mathbf{k}_i) = \frac{\pi m}{L_z A_c^2 \hbar N_{2D} M k_i \cos \theta_i} \sum_{\mathbf{Q}, \mathbf{G}, s} \frac{n(\omega(\mathbf{Q}, s))}{\omega(\mathbf{Q}, s)}$$

$$\times \delta_{\mathbf{K}_f - \mathbf{K}_i, \mathbf{Q} + \mathbf{G}} \delta(\epsilon_f - \epsilon_i - \hbar \omega(\mathbf{Q}, s))$$

$$\times |\sum_{\kappa} \mathbf{e}(\mathbf{Q}, \kappa, s) \cdot \mathbf{F}_{\kappa}(\mathbf{k}_f, \mathbf{k}_i)|^2$$
(6.24)

¹See last section of this chapter

²This follows from the inspection of scalar product $\mathbf{e}(\mathbf{Q}, \kappa, s) \cdot \mathbf{F}_{\kappa}(\mathbf{Q} + \mathbf{G}, z)$.

³This effectively means that we calculate everything with respect to *one incident* atom in the scattering system.

This quantity is averaged over initial phonon states and summed over all one-phonon processes. Here

$$\mathbf{F}_{\kappa}(\mathbf{k}_f, \mathbf{k}_i) = \int \psi_f^*(z) \mathbf{F}_{\kappa}(\mathbf{Q} + \mathbf{G}, z) \psi_i(z) dz.$$
 (6.25)

If we have information on the polarization vectors $\mathbf{e}(\mathbf{Q}, \kappa, s)$ and information on the two-body potential, v, then it is relatively easy to calculate the reflection coefficient from equation (6.24). We only have to pay attention to the energy conserving δ -function and the lateral wave vector conserving Kronecker symbol. For typical in-the-sagittal-plane TOF geometry (see *Chapter 5*) it can easily be shown [6, 47] that processes which satisfy

$$\epsilon_f - \epsilon_i = \epsilon_i \left\{ \frac{(\sin \theta_i + |\mathbf{K}_f - \mathbf{K}_i|/k_i)^2}{\sin^2 \theta_f} - 1 \right\},$$
 (6.26)

conserve both energy and momentum and they will also be seen in the experiment. Other processes either do not satisfy the conservation of momentum or energy or can not be recorded by typical HAS-TOF experimental equipment, because typical TOF experiment can measure only in-the-sagittal-plane scattering processes i.e. processes where $\mathbf{K}_f || \mathbf{K}_i$ and only a fraction of these processes in which the scattered atom ends up in the final angle θ_f . Equation (6.26) is usually called the scan curve equation. One point still remains to be clarified in order to compare the theoretical, DWBA with experimental results (TOF spectra). TOF experiments measure the number of particles of particular energy scattered into a particular region of space (or, equivalently, the phase space). Therefore, the detector gathers all the scattered atoms which after the scattering event move in a direction defined and restricted by the experimental equipment. The scattered beam is collimated 4-5 times before detection and from figure 5.4 we can conclude that all the atoms which scatter into a final angle $\theta_f = \theta_f^0 \pm 0.1^o$ are in fact detected. Here, θ_f^0 is the nominal final angle fixed in a typical scattering experiment. The same holds for polar angle, $\phi_f = 0^o \pm 0.1^o$, which defines the projectile final direction projected onto the surface plane, assuming that the collimators are of rectangular shape. The state-to-state reflection coefficient clearly cannot be directly compared with the experimental TOF spectrum. It is much more convenient to obtain the probability for processes in which the projectile atom exchanges with the target fixed amount of energy, $\Delta \epsilon = \epsilon_f - \epsilon_i$ and fixed amount of lateral wave vector, $\Delta \mathbf{K} = \mathbf{K}_f - \mathbf{K}_i$. This quantity we call energy and lateral momentum resolved state-to-state reflection coefficient and denote by $R_{\mathbf{k}_i}^{res}$. For $R_{\mathbf{k}_i}^{res}$ we can write

$$R_{\mathbf{k}_{i}}^{res} = \sum_{k_{(z,f)}} R_{fi}$$

$$= \sum_{k_{(z,f)}} \frac{\pi m}{L_{z} A_{c}^{2} \hbar N_{2D} M k_{i} \cos \theta_{i}} \sum_{\mathbf{Q},\mathbf{G},s} \frac{n(\omega(\mathbf{Q},s))}{\omega(\mathbf{Q},s)}$$

$$\times \delta_{\mathbf{K}_{f}-\mathbf{K}_{i},\mathbf{Q}+\mathbf{G}} \delta(\epsilon_{f} - \epsilon_{i} - \hbar \omega(\mathbf{Q},s))$$

$$\times |\sum_{\kappa} \mathbf{e}(\mathbf{Q}, \kappa, s) \cdot \mathbf{F}_{\kappa}(\mathbf{k}_{f}, \mathbf{k}_{i})|^{2}$$

$$= \sum_{k_{(z,f)}} \frac{\pi m}{L_{z} A_{c}^{2} \hbar N_{2D} M k_{i} \cos \theta_{i}} \sum_{\mathbf{Q},\mathbf{G},s} \frac{n(\omega(\mathbf{Q},s))}{\omega(\mathbf{Q},s)}$$

$$\times \delta_{\mathbf{K}_{f}-\mathbf{K}_{i},\mathbf{Q}+\mathbf{G}} \frac{m L_{z}}{2\pi \hbar^{2} k_{(z,f)}} \delta_{k_{(z,f)},k_{z}(\pm)}$$

$$\times |\sum_{\kappa} \mathbf{e}(\mathbf{Q}, \kappa, s) \cdot \mathbf{F}_{\kappa}(\mathbf{k}_{f}, \mathbf{k}_{i})|^{2}$$

$$= \frac{m^{2}}{2A_{c}^{2} \hbar^{3} N_{2D} M k_{(z,i)} k_{(z,f)}} \sum_{\mathbf{Q},\mathbf{G},s} \frac{n(\omega(\mathbf{Q},s))}{\omega(\mathbf{Q},s)}$$

$$\times \delta_{\mathbf{K}_{f}-\mathbf{K}_{i},\mathbf{Q}+\mathbf{G}} \delta_{k_{(z,f)},k_{z}(\pm)}$$

$$\times |\sum_{\kappa} \mathbf{e}(\mathbf{Q}, \kappa, s) \cdot \mathbf{F}_{\kappa}(\mathbf{k}_{f}, \mathbf{k}_{i})|^{2}, \qquad (6.27)$$

where $k_{(z,f)}$ ($k_{(z,i)}$) is the final (initial) projectile's wave vector in z-direction. In the derivation above, we have transformed the δ -function of energy into the Kronecker symbol in terms of wave vectors as [56]:

$$\delta(\epsilon_f - \epsilon_i - \hbar\omega(\mathbf{Q}, s)) = \frac{mL_z}{2\pi\hbar^2 k_{(z, f)}} \delta_{k_{(z, f)}, k_z(\pm)} \Theta(k_z(\pm)^2). \tag{6.28}$$

Here,

$$k_z(\pm)^2 = \frac{2M}{\hbar^2} \left\{ \frac{\hbar^2 \mathbf{K}_i \cdot (\mathbf{Q} + \mathbf{G})}{M} - \frac{\hbar^2 (\mathbf{Q} + \mathbf{G})^2}{2M} + \frac{\hbar^2 k_{(z,i)}^2}{2M} \pm \hbar \omega(\mathbf{Q}, s) \right\},$$
(6.29)

and the sign in front of $\hbar\omega$ depends whether the phonon is emitted or absorbed ⁴. It can be seen that $R_{\mathbf{k}_{i}}^{res}$ is a dimensionless quantity. We are

⁴It is assumed here that the projectile's final state is not a bound state of the interaction potential, although a similar relation can also be derived for that case [57]. The Heaviside function, Θ , in equation (6.28) selects only those final projectile states which are *not* the bound states of the interaction potential.

however interested in energy and lateral momentum resolved spectrum of scattered atoms, $N(\Delta\epsilon, \Delta\mathbf{K})$, which only after integration over $\Delta\epsilon$ and $\Delta\mathbf{K}$ yields a dimensionless quantity (number of scattered atoms) and which itself therefore has the dimension of $length^2/energy$. In the one-phonon approximation for the scattering spectrum $N_{1ph.}^{inel.}(\Delta\epsilon, \Delta\mathbf{K})$ we can write [56]

$$N_{1ph.}^{inel.}(\Delta \epsilon, \Delta \mathbf{K}) = \frac{m^2}{2A_c^2 \hbar^3 N_{2D} M k_{(z,i)} k_{(z,f)}} \sum_{\mathbf{Q},\mathbf{G},s} \frac{n(\omega(\mathbf{Q}, s))}{\omega(\mathbf{Q}, s)}$$

$$\times \delta_{\mathbf{K}_f - \mathbf{K}_i, \mathbf{Q} + \mathbf{G}} \delta_{k_{(z,f)}, k_z(\pm)}$$

$$\times |\sum_{\kappa} \mathbf{e}(\mathbf{Q}, \kappa, s) \cdot \mathbf{F}_{\kappa}(\mathbf{k}_f, \mathbf{k}_i)|^2$$

$$\times \delta(\Delta \epsilon - (\epsilon_f - \epsilon_i)) \delta(\Delta \mathbf{K} - \mathbf{Q}), \qquad (6.30)$$

where the δ -functions are used to project out the part of scattered atoms which transfer energy $\Delta \epsilon$ and lateral momentum $\Delta \mathbf{K}$ in a course of a collision with the surface ⁵.

Now we can proceed and calculate the quantity which we can directly compare with TOF spectrum either in the single or even more generally in the multiphonon regime of scattering. In a TOF measurement, the spectra will be recorded in a small element $2\Delta\theta_f$ in the direction of θ_f with respect to surface normal. Hence, for the TOF spectrum, $N_{TOF}(\epsilon, \theta_f)$, we may write

$$N_{TOF}(\Delta\epsilon, \theta_f) = \int_{\theta_f = \theta_f^0 - \Delta\theta_f}^{\theta_f^0 + \Delta\theta_f} \int \int dK_{(x,f)} dK_{(y,f)} N(\Delta\epsilon, \Delta \mathbf{K}) f_{ins}(\mathbf{k}_f).$$
(6.31)

Function $f_{ins}(\mathbf{k}_f)$ is the instrumental function since there is no reason to a priori assume that the detection of the scattered atoms is independent of their final state. In the previous chapter we have seen that the atoms which scatter from the target must be ionized before the detection. The ionization probability, however, depends linearly on the time spent by the scattered atom in the ionization chamber i.e. it depends linearly on inverse final velocity, v_f of the scattered atom. Therefore, for instrumental function, f_{ins} we can write

$$f_{ins}(k_f) = \frac{C_1}{v_f} \delta(K_{(y,f)}),$$
 (6.32)

⁵This, somewhat lengthy, transition from the state-to-state reflection coefficient to the scattering spectrum can be completely avoided in *the scattering spectrum approach* to the atom-surface scattering problem which will be introduced in *Chapter 7* and additionally explained in *Chapter 8*.

where C_1 is a constant containing the information about the flux of electrons used for ionization and the length of the ionization chamber. The δ -function in $K_{(y,f)}$ represents the action of the collimators and effectively selects only those processes in which the scattered atom moves in the sagittal scattering plane. Since for fixed initial and total angle of scattering $(\theta_f + \theta_i = \theta_{SD})$ we have $dK_{(x,f)} = k_f(\epsilon_f) \cos \theta_f$, we can write for the experimental TOF spectrum

$$N_{TOF}(\epsilon, \theta_f) = C_2 \frac{m}{\hbar} \cos(\theta_f) N(\epsilon, \Delta \mathbf{K}(\theta_f)), \tag{6.33}$$

where the proportionality factor, C_2 is a constant in each TOF measurement. The equation above specifies the quantity one should compare with the experimental TOF spectrum.

The generalization of the derivation of the DWBA to the case of corrugated surface is straightforward and can be found in reference [6].

When the scan curve intersects some phonon dispersion branch, a discrete peak in the spectrum occurs (see figure 6.2). This is why the scattering in the low incident energy regime (where the DWBA should work well) is used for experimental determination of the dispersion relations [1]. The multiphonon processes tend to smear the contributions of particular phonon branches to the TOF spectra (see section 9.7), especially when the dispersions of phonon branches are not "flat" i.e. when there is a definitive dependence of frequency of the mode on its wave vector.

We can now proceed to calculate some theoretical "spectra" and directly compare them with the experimental TOF spectra. Figure 6.2 displays the DWBA calculation for $\text{He} \to \text{Xe}(111)$ scattering along Γ -K direction of the surface (Xe) Brillouin zone compared with the experimental data. The potential and the dynamical matrix parameters used in this calculation can be found in section 9.5. The spectrum is dominated by the peaks corresponding to one phonon emission and absorption of the Rayleigh wave phonon of the Xe(111) surface. The full line was calculated by summing up the contributions to the spectrum arising from the coupling of He to first and second slabs of Xe atoms, while the dashed line represents the DWBA calculation with the coupling only to the topmost layer of Xe atoms included.

This calculation suggests that the helium atom scattering technique is not only statically surface sensitive (i.e. surface sensitive with respect to diffraction), but also dynamically surface sensitive (i.e. with respect to the inelastic events), since the contribution of the vibrations localized in the topmost layer of atoms to the scattering spectrum is by far the

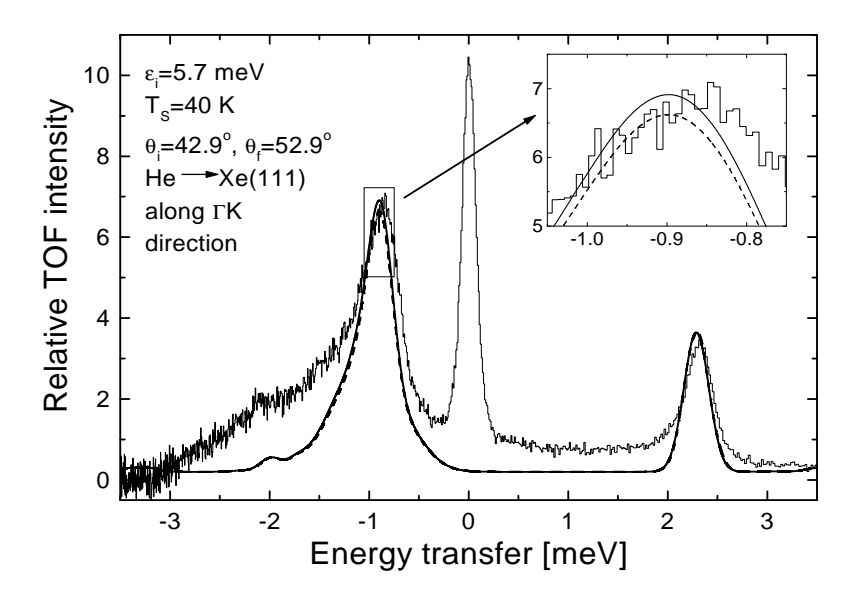


Figure 6.2: DWBA calculation for He \rightarrow Xe(111). Thin full line: Experimental data. Full line: DWBA spectrum for κ =0,1. Dashed line: DWBA spectrum for κ =0. Data taken by A. Graham in 1997.

dominant one, as demonstrated here for the He \rightarrow Xe(111) scattering system (see also figure 6.3).

Although the incident He energy during the aquisition of the data displayed in figure 6.2 is quite low (5.7 meV), the influence of multiphonon processes can be seen as a broad gaussian-like background not accounted for in the DWBA ⁶.

Note also that the DWBA does not reproduce the peak observed at zero energy transfer (the so called *no-loss peak*). This peak is not due to any kind of phononic excitation, but is a consequence of diffuse elastic scattering from defects not accounted for by the form of DWBA presented here.

Figure 6.3 displays a comparison between calculated (DWBA) and measured TOF spectra for the same system (He \rightarrow Xe(111)). The projectile incident energy is 10.43 meV and the sample temperature is 50 K. The incident and final angles are the same as in figure 6.2. The inset shows relative contributions of the vibrations of the second slab of atoms to the DWBA TOF spectrum. Note that this contribution is *not*

 $^{^6}$ Rayleigh wave mode of Xe(111) has a maximum frequency of 2.31 meV along the Γ -K direction, i.e. it is very "soft" and it is easy to multiply excite it even with low incident energy He atoms.

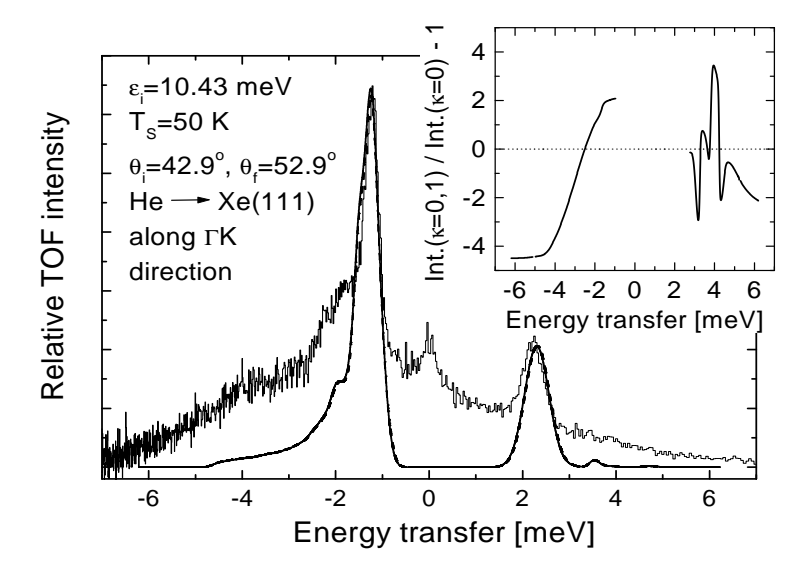


Figure 6.3: DWBA calculation for He \rightarrow Xe(111). Thin full line: Experimental data. Full line: DWBA spectrum for κ =0,1. Dashed line: DWBA spectrum for κ =0. Inset: Relative contribution of κ =1 slab of Xe atoms. Data taken by A. Graham in 1997.

necessarily positive owing to phase factor $\exp(i(\mathbf{Q} + \mathbf{G}) \cdot \mathbf{r}_{\kappa})$ in equation (6.23). The relative contribution of the second slab of Xe atoms to the DWBA spectrum does not exceed 5 % for the scattering parameters studied, irrespective of the energy transfer.

Figure 6.4 displays the character of polarization vectors of the vibrational modes generated by the lattice dynamics calculation and used to obtain the calculated DWBA TOF spectrum displayed in figure 6.3. The absolute values of the polarization vector at the topmost Xe(111) slab are displayed. Although the polarization vector is a function of the lateral wave vector, \mathbf{Q} , it can be represented as a function of the exchanged energy (or the phonon frequency, in the DWBA) since the scan curve imposes a unique relation between the wave vector $\mathbf{Q} = \Delta \mathbf{K}$ and the exchanged energy, $\Delta E = \omega(\mathbf{Q})$.

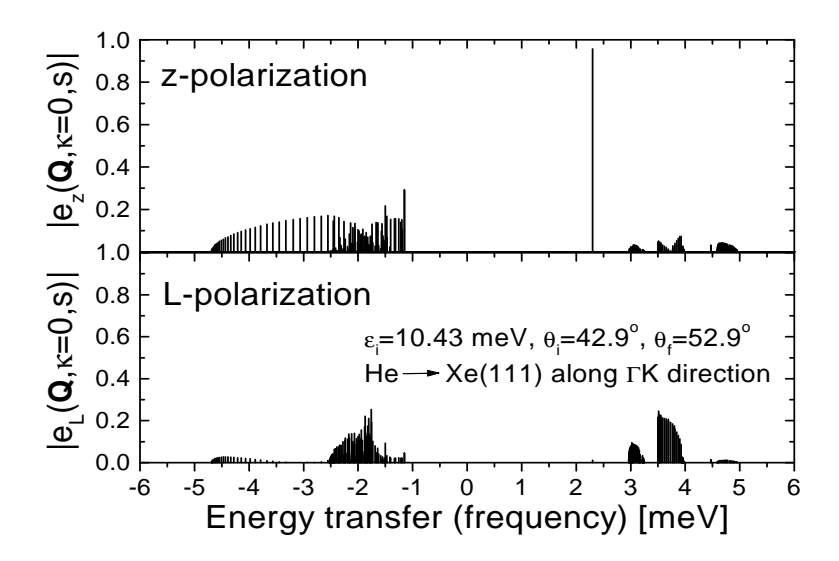


Figure 6.4: Polarizations of the modes used to calculate DWBA TOF spectrum in Fig 6.2. Upper panel: absolute value of the z-component of polarization vector at $\kappa = 0$. Lower panel: absolute value of the longitudinal (L) component of polarization vector at $\kappa = 0$.

6.2 Probability of elastic scattering in the DWBA

If the atom-target scattering is dominated by the single-phonon emission or absorption events, the DWBA will be an adequate approximation to the problem. We naturally ask about a measure which will contain information on the character of scattering - whether it is predominantly single-phonon or multiphonon. A good measure will surely be the average number of phonons excited by the projectile atom. The average number of phonons contained in the wave function of the scattering system after the interaction has terminated can be found by inspecting the matrix element $\langle f^1 | \sum_{\mathbf{Q}} a_{\mathbf{Q}}^{\dagger} a_{\mathbf{Q}} | f^1 \rangle$ at $T_S = 0$, where $|f^1\rangle$ is the wave function of the system calculated in the DWBA (see references [8, 11] for the wave function in first order perturbation approach), and $\sum_{\mathbf{Q},s} a_{\mathbf{Q},s}^{\dagger} a_{\mathbf{Q},s}$ is the phonon number operator. This yields for the average number of phonons in the final wave function,

$$n_{ph} = n_{ph,0} + \sum_{f \neq i} R_{fi}, \tag{6.34}$$

where $n_{ph,0}$ is the number of phonons in the initial wave function, before

the scattering event started. Therefore, the average number of phonons excited (i.e. created, at $T_S = 0$), 2W can be found as

$$2W = \sum_{f \neq i} R_{fi}. \tag{6.35}$$

Note however that 2W in nothing but the probability of inelastic scattering in the DWBA. Assuming that the DWBA is unitary (although it is not, since the DWBA is equivalent to the first term in the Dyson series, see section 8.1), we can write for the probability of elastic scattering in the DWBA,

$$P_{00} = 1 - 2W = 1 - \sum_{f \neq i} R_{fi}.$$
 (6.36)

Here we have assumed that the probabilities of elastic and inelastic scattering events sum up to unity which must hold if the unitary property of the evolution operator of the system is preserved. This is not the case for the DWBA, but we can expect that if 2W << 1 the DWBA probabilities will be approximately correct since the number of excited phonons is small and the DWBA should work fine. Note also that for 2W > 1 equation (6.36) produces senseless results (negative probability). Figure 6.5 displays the DWBA calculation of the elastic scattering probability [19] compared with the experimental data [58] for Ne \rightarrow Cu(111). The scattering system is parametrized as in 9.2. The large disagreement of the DWBA at low sample temperatures is probably due to incoherent scattering of Ne atoms from the defects (disorder) present in Cu(111) surface. Above ≈ 120 K, DWBA gives negative probability of the elastic scattering. For $T_S = 10$ K, 2W(DWBA) = 0.197 << 1.

The probability of elastic scattering obtained in the DWBA can be used to normalize the DWBA scattering spectrum in equation (6.30). We require that the whole spectrum (including both the elastic and inelastic processes) integrates to unity. Thus normalized DWBA spectrum is given by the expression

$$N_{DWBA}^{norm.1ph.}(\Delta\epsilon, \Delta\mathbf{K}) = (1 - 2W)\delta(\Delta\epsilon)\delta(\Delta\mathbf{K}) + 2WN_{1ph}^{inel.}(\Delta\epsilon, \Delta\mathbf{K}),$$
(6.37)

with $N_{1ph.}^{inel.}(\Delta\epsilon, \Delta \mathbf{K})$ given by equation (6.30). It can be seen that

$$\int d(\Delta \epsilon) d(\Delta \mathbf{K}) N_{DWBA}^{norm}(\Delta \epsilon, \Delta \mathbf{K}) = 1 - 2W + 2W = 1.$$
 (6.38)

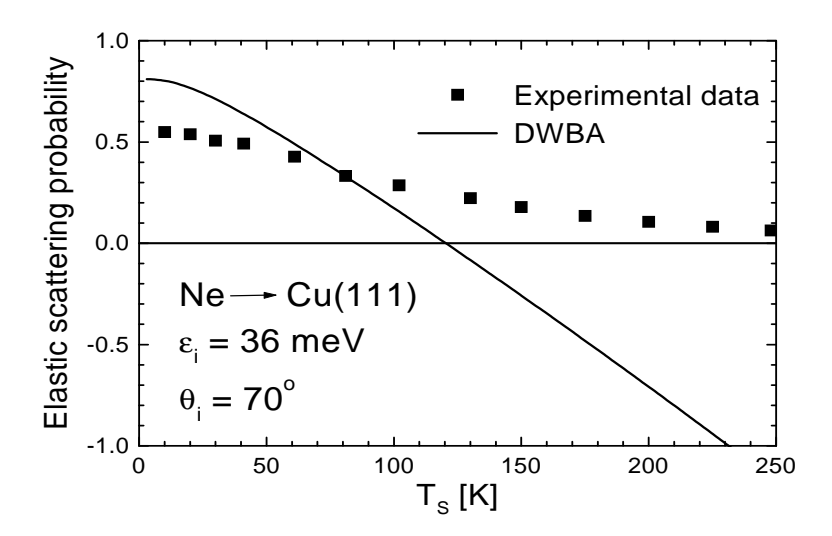


Figure 6.5: The magnitude of the elastic scattering probability calculated in the one phonon (DWBA) approximation for Ne \rightarrow Cu(111) scattering system. Full line: DWBA calculation. Squares: Experimental points.

6.3 Additional comments concerning the application of the DWBA

Note that we have described the inelastic one phonon emission (absorption) scattering events by using the *delocalized* wave functions rather than the wave packets for the description of the projectile atom. It was shown in the previous chapter that the projectile atoms travel about 1 m from their point of injection into the evacuated space to the point where they actually interact with the target. So, even if projectile atoms were fairly localized when they were injected they would quickly become quite delocalized (much before they hit the target). This is a consequence of the *spreading of the wave packet* which happens even if there is no interaction at all (see reference [8], page 63). It can be shown that the width of the wave packet grows in time as

$$\sigma(t) = \sqrt{(\Delta x)^2 + \frac{(\Delta p)^2 t^2}{m^2}},$$
(6.39)

where Δx and Δp are initial uncertainties (at t = 0, this corresponds to the point of injection) in the position and momentum of the projectile

atom, respectively. Assuming that the projectile atom is He with energy of 10 meV, the time needed to reach the target equals to ≈ 1.4 ms (see figure 5.4). The typical uncertainty in the momentum is about $\Delta p/p \approx 0.01$ (see Chapter 5) which yields $\Delta p \approx 5 \cdot 10^{-26}$ kg m/s. Assuming that $\Delta z \Delta p = \hbar/2$, we find $\Delta z \approx 2$ nm. So, even at the time of injection (t=0) the width of the wave packet is about 10 times larger than the typical range of interaction potentials ⁷. The wave packet spreads much more after 1.4 ms, so that the uncertainty in its position is about 4 cm which is a macroscopic length! Therefore, the projectile can safely be described by a completely delocalized, distorted wave ⁸.

Note that for actual calculation we need some matrix elements. But, the matrix elements we need are *not* the matrix elements

$$\langle \psi_f | (i\mathbf{Q}, \mathbf{z}_0 \partial / \partial z) V_0(z) | \psi_i \rangle$$

(see equation (6.5)) which we can find in the literature, but rather

$$\langle \psi_f | (i\mathbf{Q}, \mathbf{z}_0 \partial / \partial z) v_{\mathbf{Q}}(z - z_{\kappa}) | \psi_i \rangle,$$

where $v_{\mathbf{Q}}(z-z_{\kappa})$ is the projectile interaction with the slab κ . The choice of the Morse potential model for V_0 comes convenient again, a little mathematical trick does the job here. The interaction of the projectile atom with the topmost slab of atoms can be represented as the interaction of the projectile with the slabs $\kappa = 0, 1, ... \infty$ minus the interaction of the projectile with slabs $\kappa = 1, 2, ... \infty$ - this is all in the spirit of the approximation of pairwise summation of potentials. Those two interactions are the same, only shifted with respect to each other by a, where a is the normal distance between the slabs (i.e. crystal planes). One can easily show by following this line of reasoning that

$$v_{\mathbf{Q}=0}(z-z_{\kappa}) = A_{c}D\left[e^{-\frac{2}{d}(z-z_{0})}(1-e^{-\frac{2a}{d}})e^{-\frac{2a\kappa}{d}} - 2e^{-\frac{1}{d}(z-z_{0})}(1-e^{-\frac{a}{d}})e^{-\frac{a\kappa}{d}}\right],$$
(6.40)

where D, d and z_0 are the Morse potential parameters of $V_0(z)$. This also gives a precise meaning to quantities $v_{rep,\mathbf{Q}=0}(z-z_{\kappa})$ and $v_{att,\mathbf{Q}=0}(z-z_{\kappa})$ introduced in equation (6.20):

$$v_{rep,\mathbf{Q}=0}(z-z_{\kappa}) = A_c D e^{-\frac{2}{d}(z-z_0)} (1-e^{-\frac{2a}{d}}) e^{-\frac{2a\kappa}{d}}$$
 (6.41)

 $^{^{7}}$ Note that the z-direction is of importance here.

⁸One could consider a so called wave-train which is a convolution of the distorted wave and e.g. gaussian function whose width represents the position uncertainty, but this is clearly not needed here.

and

$$v_{att,\mathbf{Q}=0}(z-z_{\kappa}) = 2A_c D e^{-\frac{1}{d}(z-z_0)} (1-e^{-\frac{a}{d}}) e^{-\frac{a\kappa}{d}}.$$
 (6.42)

This little trick can be done so easily only when $V_0(z)$ is some combination of exponential functions of the coordinate z (as the Morse potential is). Therefore, the matrix elements existing in the literature [38, 39, 59] can be used with slight multiplicative modifications as in equations above in order to account for the interactions with a slab, and not the $whole\ sample$. Of course, the trick was made under the assumption that nothing special happens at the surface of the sample i.e. that the effective potentials in the topmost slab are the same as in all other slabs of the sample. This is clearly a bad assumption for metallic samples where it would be probably better to completely neglect the projectile interaction with all slabs except for the topmost one.

The cut-off wave vector Q_c introduced in equation (6.21) can be shown to be the same for all slabs κ if we chose to represent $V_0(z)$ by the Morse potential [52].

Chapter 7

Forced oscillator model or trajectory approximation in atom-surface scattering

I was not born to be forced. I will breathe after my own fashion. ... If a plant cannot live according to its nature, it dies; and so a man.

Henry David Thoreau

THEORY OF
THERMAL ENERGY
INERT ATOM
SCATTERING FROM
SURFACE VIBRATIONS

Antonio Šiber

The forced oscillator model is a nonperturbative approach of approximately solving the dynamics of atom-surface scattering. It is an exact solution to the approximate hamiltonian of atom-surface scattering. The hamiltonian is simplified by introducing a rather serious approximation to the projectile (atom) dynamics. Namely, the projectile is assumed to be recoilless, classical particle restricted to move on a suitably predefined trajectory.

Before deriving the trajectory approximation for the atom-surface scattering problem, we shall introduce some basic prerequisites, especially the formalism of the time dependent perturbation treatment.

7.1 Essentials of time dependent perturbation approach

(In this section we shall set $\hbar = 1$ except where it needs to be explicitly written.)

Consider a quantum system which can be described by hamiltonian H_0 . The time dependence of the wave function Ψ_S pertaining to this hamiltonian is governed by the Schrödinger equation

$$i\frac{\partial \Psi_S(t)}{\partial t} = H_0 \Psi_S(t). \tag{7.1}$$

The solution to equation (7.1) can be written as

$$\Psi_S(t) = U_0(t, t_0)\Psi_S(t_0) = e^{-iH_0(t - t_0)}\Psi_S(t_0).$$
 (7.2)

Here $U_0(t, t_0)$ is the evolution operator. A subscript S means that the particular quantity (here, the wave function) is to be calculated in the Schrödinger representation of quantum mechanics. Knowing the initial conditions of the system $(\Psi_S(t_0))$ and the evolution operator we can predict the wave function of the system at any future instant. We assume that the evolution operator, $U_0(t,t_0)$, can be found without difficulties. The basic aim is to solve a more complicated hamiltonian $H(t) = H_0 + gV_S(t)$, where $V_S(t)$ is a perturbation to the system. The constant g is introduced here for convenience and will be set equal to 1 in the final results.

We now pass to the *interaction picture* with the interaction and Schrödinger pictures coinciding at t = 0 [8, 11, 44]. Then

$$\Psi_S(t) = e^{-iH_0t} \Psi_I(t), \quad V_I(t) = e^{iH_0t} V_S(t) e^{-iH_0t}, \tag{7.3}$$

where the second identity holds for any operator which we want to express in the interaction picture. We shall further drop the subscripts I and treat the quantities without subscripts in the interaction picture. It follows from the equations above that the time evolution of the operators in the interaction picture is governed by the unperturbed hamiltonian H_0 . It is easy to show that

$$i\frac{\partial \Psi(t)}{\partial t} = gV(t)\Psi(t), \tag{7.4}$$

i.e. the time evolution of the wave function in the interaction picture is governed solely by the perturbation V(t) expressed also in the interaction picture (this means that there is the part H_0 of the total hamiltonian already contained in $V_I(t)$ as in equation (7.3)). We define the evolution operator in the interaction picture as

$$\Psi(t) = U(t, t_0)\Psi(t_0). \tag{7.5}$$

Inserting (7.5) in (7.4) we obtain the following differential equation which must be satisfied by $U(t, t_0)$:

$$i\frac{\partial}{\partial t}U(t,t_0) = gV(t)U(t,t_0). \tag{7.6}$$

The initial condition for this equation is

$$U(t_0, t_0) = 1, (7.7)$$

since, from (7.5)

$$\Psi(t_0) = U(t_0, t_0)\Psi(t_0). \tag{7.8}$$

When two time translations are applied consecutively the following property holds:

$$U(t_2, t_1)U(t_1, t_0) = U(t_2, t_0). (7.9)$$

For the special case $t_2 = t_0$, this gives an expression for the inverse operator

$$U^{-1}(t_0, t_1) = U(t_1, t_0). (7.10)$$

Finally,

$$U^{\dagger}(t_1, t_0) = U^{-1}(t_1, t_0) \tag{7.11}$$

since H_0 is hermitian. From the equation above we conclude that U is a unitary operator which guarantees that the normalization of the state vectors does not depend on time. We define the *scattering matrix*, S, as

$$S = \lim_{t \to \infty, t_0 \to -\infty} U(t, t_0). \tag{7.12}$$

The scattering matrix evolves the scattering system from the initial, noninteracting state (before collision) to the final, also noninteracting state (after collision).

7.2 Derivation of the trajectory approximation or the forced oscillator model in atom-surface scattering

We shall closely follow the derivation of the DWBA from the previous chapter. All the notation in this section is the same as in *Chapter* 6. The dynamical interaction part of the hamiltonian can be written as

$$V_{dynamic}(\mathbf{r}) = -\sum_{l,\kappa} \mathbf{u}(\mathbf{R}_{l},\kappa) \cdot \nabla_{\mathbf{r}} v(\mathbf{r} - \mathbf{R}_{l} - \mathbf{r}_{\kappa})$$
$$= \sum_{l,\kappa} \mathbf{u}(\mathbf{R}_{l},\kappa) \cdot \mathbf{F}_{l,\kappa}(\mathbf{r}), \tag{7.13}$$

where \mathbf{r} represents the coordinates of the projectile atom and $\mathbf{F}_{l,\kappa}(\mathbf{r})$ is given by equation (6.13). Expressing the displacement coordinate $\mathbf{u}(\mathbf{R}_l,\kappa)$ as in equations (4.21) and (4.32), we obtain

$$V_{dynamic}(\mathbf{r}) = -\sum_{l,\kappa,\mathbf{Q},s} \sqrt{\frac{\hbar}{2M N_{2D} \omega(\mathbf{Q},s)}} \mathbf{e}(\mathbf{Q},\kappa,s) \cdot \mathbf{F}_{l,\kappa}(\mathbf{r}) e^{i\mathbf{Q}\cdot\mathbf{R}_{l}}$$

$$\times (a_{\mathbf{Q},s}^{\dagger} + a_{-\mathbf{Q},s}). \tag{7.14}$$

We introduce a lateral Fourier transform of $\mathbf{F}_{l,\kappa}(\mathbf{r})$ as

$$\mathbf{F}_{l,\kappa}(\mathbf{r}) = \frac{1}{(2\pi)^2} \int d^2K e^{i\mathbf{K}\cdot(\mathbf{R} - \mathbf{R}_l - \mathbf{R}_\kappa)} \mathbf{F}_{\kappa}(\mathbf{K}, z), \tag{7.15}$$

where

$$\mathbf{F}_{\kappa}(\mathbf{K}, z) = \int d^{2}R e^{-i\mathbf{K}\cdot(\mathbf{R} - \mathbf{R}_{l} - \mathbf{R}_{\kappa})} \mathbf{F}_{l,\kappa}(\mathbf{r}). \tag{7.16}$$

Substituting equation (7.15) into (7.14) and performing the summation over index l as in (6.17), we obtain

$$V_{dynamic}(\mathbf{r}) = \frac{1}{A_c} \sum_{\kappa, \mathbf{Q}, s, \mathbf{G}} \sqrt{\frac{\hbar}{2MN_{2D}\omega(\mathbf{Q}, s)}} \mathbf{F}_{\kappa}(\mathbf{Q} + \mathbf{G}, z) \cdot \mathbf{e}(\mathbf{Q}, \kappa, s)$$

$$\times e^{i(\mathbf{Q} + \mathbf{G}) \cdot (\mathbf{R} - \mathbf{R}_{\kappa})} (a_{\mathbf{Q}, s}^{\dagger} + a_{-\mathbf{Q}, s}). \tag{7.17}$$

We have transformed the Kronecker symbol from equation (6.17) into a δ -function according to

$$\delta_{\mathbf{K},\mathbf{Q}+\mathbf{G}} = \frac{(2\pi)^2}{L_S^2} \delta(\mathbf{K} - \mathbf{Q} - \mathbf{G}). \tag{7.18}$$

Performing exactly the same procedure as in equation (6.18), for $\mathbf{F}_{\kappa}(\mathbf{Q} + \mathbf{G}, z)$ we obtain

$$\mathbf{F}_{\kappa}(\mathbf{Q} + \mathbf{G}, z) = \left\{ i(\mathbf{Q} + \mathbf{G}), \frac{\partial}{\partial z} \mathbf{z}_{0} \right\} v_{\mathbf{Q} + \mathbf{G}}(z - z_{\kappa}), \tag{7.19}$$

where $v_{\mathbf{Q}+\mathbf{G}}(z-z_{\kappa})$ is given by equation (6.19). We rewrite the dynamical interaction potential for later convenience as

$$V_{dynamic}(\mathbf{r}) = \sum_{\mathbf{Q},s} W_{\mathbf{Q},s}(\mathbf{r}) (a_{\mathbf{Q},s}^{\dagger} + a_{-\mathbf{Q},s}), \qquad (7.20)$$

where

$$W_{\mathbf{Q},s}(\mathbf{r}) = \frac{1}{A_c} \sum_{\kappa,\mathbf{G}} \sqrt{\frac{\hbar}{2MN_{2D}\omega(\mathbf{Q},s)}} \mathbf{F}_{\kappa}(\mathbf{Q} + \mathbf{G}, z) \cdot \mathbf{e}(\mathbf{Q}, \kappa, s)$$

$$\times e^{i(\mathbf{Q} + \mathbf{G}) \cdot (\mathbf{R} - \mathbf{R}_{\kappa})}. \tag{7.21}$$

The total hamiltonian of the system can be written as

$$H = \frac{\mathbf{p}^{2}}{2m} + V_{static}(\mathbf{r})$$

$$+ \sum_{\mathbf{Q},s} \hbar \omega(\mathbf{Q}, s) \left\{ a_{\mathbf{Q},s}^{\dagger} a_{\mathbf{Q},s} + \frac{1}{2} \right\}$$

$$+ \sum_{\mathbf{Q},s} W_{\mathbf{Q},s}(\mathbf{r}) (a_{\mathbf{Q},s}^{\dagger} + a_{-\mathbf{Q},s}), \qquad (7.22)$$

where $V_{static}(\mathbf{r})$ is the static part of the interaction potential as in equation (3.14). Note that the convention we have chosen for writing this hamiltonian is a mixed one; we used a notation of second quantization for representing the vibrations of the target, while the part of the hamiltonian pertaining to the projectile was written in a "classical fashion", i.e. in \mathbf{p} and \mathbf{r} coordinates which are not quantized. This is exactly what suits us now, since we are going to make a trajectory approximation, i.e. we shall treat the projectile as a source of time-dependent perturbation acting on the phonons of the target. We shall classically solve the projectile part of the hamiltonian represented by

the first two terms on the RHS of equation (7.22) (all target atoms are fixed in their equilibrium positions). Neglecting the corrugation of the static interaction potential in the directions parallel to the surface, we have

$$\mathbf{r}(t) = (\mathbf{R}, z) \to (\mathbf{V}t, z_{cl}(t)), \tag{7.23}$$

where t is the time variable, **V** is the projectile velocity in the surface plane and $z_{cl}(t)$ is the projectile classical trajectory projected onto the z-axis. Now we approximate the hamiltonian in (7.22) by

$$H_{TA} = \sum_{\mathbf{Q},s} \hbar \omega(\mathbf{Q}, s) \left\{ a_{\mathbf{Q},s}^{\dagger} a_{\mathbf{Q},s} + \frac{1}{2} \right\} + \sum_{\mathbf{Q},s} W_{\mathbf{Q},s}(\mathbf{r}(t)) (a_{\mathbf{Q},s}^{\dagger} + a_{-\mathbf{Q},s})$$

$$= \sum_{\mathbf{Q},s} \hbar \omega(\mathbf{Q}, s) \left\{ a_{\mathbf{Q},s}^{\dagger} a_{\mathbf{Q},s} + \frac{1}{2} \right\} + \sum_{\mathbf{Q},s} W_{\mathbf{Q},s}(t) (a_{\mathbf{Q},s}^{\dagger} + a_{-\mathbf{Q},s})$$

$$= H_0 + H_I(t), \qquad (7.24)$$

where we have inserted the classical solution in equation (7.23) into the dynamical interaction part of the hamiltonian and dropped out the uncoupled part of the hamiltonian corresponding to the projectile (first two terms on the RHS of equation (7.22) which we already solved in a classical manner as in equation (7.23). The time dependent function $W_{\mathbf{Q},s}(t)$ is given by

$$W_{\mathbf{Q},s}(t) = \frac{1}{A_c} \sum_{\kappa,\mathbf{G}} \sqrt{\frac{\hbar}{2MN_{2D}\omega(\mathbf{Q},s)}} \mathbf{F}_{\kappa}(\mathbf{Q} + \mathbf{G}, z_{cl}(t)) \cdot \mathbf{e}(\mathbf{Q}, \kappa, s)$$

$$\times e^{i(\mathbf{Q} + \mathbf{G}) \cdot (\mathbf{V}t - \mathbf{R}_{\kappa})}. \tag{7.25}$$

The time dependent hamiltonian in equation (7.24) can be exactly solved [12, 13, 60]. Clearly, the projectile appears in (7.24) as a time dependent perturbation $H_I(t)$ acting on the target phonons described by H_0 and the quantum nature of the system is reflected only through the wave function describing the phonons of the target. This explains the name "forced oscillator model". It is obvious that if the scattering is very far from elastic, the hamiltonian in (7.24) can be expected to produce wrong evolution of the target state vector, since the time dependent force was obtained by assuming elastic collision. Strictly speaking, the validity of the trajectory approximation can be proved for weakly inelastic, quasiadiabatic scattering, although one can expect that qualitative conclusions obtained by the use of the trajectory approximation remain valid also for strongly inelastic scattering [18].

The phonon state vector in the interaction representation ¹

$$|\Pi^{I}(t)\rangle = e^{\frac{i}{\hbar}H_{0}t}|\Pi^{S}(t)\rangle \tag{7.26}$$

satisfies equation

$$i\hbar \frac{d}{dt}|\Pi^I(t)\rangle = V_I(t)|\Pi^I(t)\rangle,$$
 (7.27)

where

$$V_{I}(t) = e^{\frac{i}{\hbar}H_{0}t}H_{I}e^{-\frac{i}{\hbar}H_{0}t}$$

$$= \sum_{\mathbf{Q},s}W_{\mathbf{Q},s}(t)(a_{\mathbf{Q},s}^{\dagger}e^{i\omega(\mathbf{Q},s)t} + a_{-\mathbf{Q},s}e^{-i\omega(\mathbf{Q},s)t}). \quad (7.28)$$

The last line of the equation above was obtained by noting that the operator

$$a_{-\mathbf{Q},s}(t) = e^{\frac{i}{\hbar}H_0t}a_{-\mathbf{Q},s}e^{-\frac{i}{\hbar}H_0t},$$
 (7.29)

satisfies equation

$$\frac{\partial a_{-\mathbf{Q},s}(t)}{\partial t} = i \left[H_0, a_{-\mathbf{Q},s}(t) \right], \tag{7.30}$$

and by using the boson commutation relations for a-operators as in equations (4.33) and (4.34). The solution to equation (7.27) is given by [13]

$$|\Pi^{I}(t)\rangle = \exp\left(i\sum_{\mathbf{Q},s}\Phi_{\mathbf{Q},s}(t,t_{0})\right)$$

$$\times \exp\left(-\frac{i}{\hbar}\sum_{\mathbf{Q},s}(I_{\mathbf{Q},s}(t,t_{0})a_{-\mathbf{Q},s}+I_{\mathbf{Q},s}^{*}(t,t_{0})a_{\mathbf{Q},s}^{\dagger})\right)$$

$$\times |\Pi^{I}(t_{0})\rangle, \tag{7.31}$$

where

$$I_{\mathbf{Q},s}(t,t_0) = \int_{t_0}^t dt' W_{\mathbf{Q},s}(t') e^{-i\omega(\mathbf{Q},s)t'}$$

$$(7.32)$$

and

$$\Phi_{\mathbf{Q},s}(t,t_0) = \frac{1}{\hbar^2} \int_{t_0}^t dt' \int_{t_0}^{t'} dt'' W_{\mathbf{Q},s}(t') W_{\mathbf{Q},s}(t'') \sin\left(\omega(\mathbf{Q},s)(t'-t'')\right).$$
(7.33)

 $^{^{1}}I$ and S denote the interaction and Schrödinger representation, respectively, as in the previous section.

This can be checked by direct substitution of (7.31) into (7.27) ². The target state vector in the Schrödinger representation is therefore given by

$$|\Pi^{S}(t,t_{0})\rangle = \exp\left(-\frac{i}{\hbar}H_{0}t\right)$$

$$\times \exp\left(i\sum_{\mathbf{Q},s}\Phi_{\mathbf{Q},s}(t,t_{0})\right)$$

$$\times \exp\left(-\frac{i}{\hbar}\sum_{\mathbf{Q},s}(I_{\mathbf{Q},s}(t,t_{0})a_{-\mathbf{Q},s}+I_{\mathbf{Q},s}^{*}(t,t_{0})a_{\mathbf{Q},s}^{\dagger})\right)$$

$$\times \exp\left(-\frac{i}{\hbar}H_{0}t_{0}\right)|\Pi^{S}(t_{0})\rangle$$

$$= U_{H_{0}}(t)U_{V_{I}}(t,t_{0})\exp\left(-\frac{i}{\hbar}H_{0}t_{0}\right)|\Pi^{S}(t_{0})\rangle, \quad (7.34)$$

where

$$U_{H_0}(t) = \exp\left(-\frac{i}{\hbar}H_0t\right) \tag{7.35}$$

and

$$U_{V_I}(t, t_0) = \exp\left(-\frac{i}{\hbar} \sum_{\mathbf{Q}, s} (I_{\mathbf{Q}, s}(t, t_0) a_{-\mathbf{Q}, s} + I_{\mathbf{Q}, s}^*(t, t_0) a_{\mathbf{Q}, s}^{\dagger})\right).$$
(7.36)

Since we are dealing with a scattering problem, we let $t \to \infty$ and $t_0 \to -\infty$, as in equation (7.12).

The energy and lateral momentum resolved spectrum of the outgoing projectile atoms will be described by the function $N(\varepsilon, \Delta \mathbf{K})$ giving the intensity of atoms which have suffered a loss of energy ε and of lateral momentum $\Delta \mathbf{K}$ which are absorbed by the target phonon bath. $N(\varepsilon, \Delta \mathbf{K})$ is therefore defined as the probability that at time $t \to \infty$ the target is found in any of the states $|\{f\}\rangle$ of the free hamiltonian H_0 with a total energy $E_{\{f\}} = E_0 + \varepsilon$ and total momentum $\mathbf{Q}_{\{f\}} = \Delta \mathbf{K}^3$, where E_0 is the energy of the target at $t_0 \to -\infty$. Thus, in order to find $N(\varepsilon, \Delta \mathbf{K})$, we should project the final $(t \to \infty)$ wave function of the target onto the $|\{f\}\rangle$ set of states choosing only those states $|\{f\}\rangle$ which differ from the initial target state in energy and momentum by ε and $\Delta \mathbf{K}$, respectively. Therefore, we have

$$N(\varepsilon, \Delta \mathbf{K}) = \lim_{t \to \infty, t_0 \to -\infty} \sum_{\{f\}} |\langle \Pi^S(t, t_0) | \{f\} \rangle|^2$$

 $^{^{2}\}mathrm{A}$ general solution of equation (7.27) will be illustrated in the next chapter.

³The total phonon momentum of the target before the interaction has been "switched on" was clearly zero.

$$\times \delta(\varepsilon - (E_{\{f\}} - E_0))\delta(\Delta \mathbf{K} - \mathbf{Q}_{\{f\}}), \qquad (7.37)$$

where we have used δ -functions to project out the states of interest. Equation (7.37) can be also written as

$$N(\varepsilon, \Delta \mathbf{K}) = \lim_{t \to \infty, t_0 \to -\infty} \frac{1}{(2\pi\hbar)^3} \int_{-\infty}^{\infty} d\tau e^{\frac{i}{\hbar}\varepsilon\tau} \int_{\mathcal{R}} d^2 \mathcal{R} e^{i\Delta \mathbf{K} \cdot \mathcal{R}}$$
$$\times \langle \Pi^S(t, t_0) | e^{-\frac{i}{\hbar}(H_0 - E_0)\tau} e^{-\frac{i}{\hbar}\hat{\mathbf{P}} \cdot \mathcal{R}} | \Pi^S(t, t_0) \rangle, \qquad (7.38)$$

where τ and \mathcal{R} are integration variables in time and two-dimensional space domains, respectively. $\hat{\mathbf{P}}$ is the operator of the *total momentum* of the phonon bath, i.e.

$$\hat{\mathbf{P}}|\{f\}\rangle = \hbar \mathbf{Q}_{\{f\}}|\{f\}\rangle. \tag{7.39}$$

The equivalence of equations (7.37) and (7.38) can be seen by inserting the projecting operator

$$\hat{1} = \sum_{\{f\}} |\{f\}\rangle\langle\{f\}| \tag{7.40}$$

between $e^{\frac{i}{\hbar}H_0\tau}$ and $e^{\frac{i}{\hbar}\hat{\mathbf{P}}\cdot\mathcal{R}}$ operators in the second line of equation (7.38) and using the fact that states $|\{f\}\rangle$ are the eigenstates of both H_0 and $\hat{\mathbf{P}}$ operators, i.e.

$$e^{\frac{i}{\hbar}H_0\tau}|\{f\}\rangle = e^{\frac{i}{\hbar}E_{\{f\}}\tau}|\{f\}\rangle$$

$$e^{\frac{i}{\hbar}\hat{\mathbf{P}}\cdot\mathcal{R}}|\{f\}\rangle = e^{\frac{i}{\hbar}\mathbf{Q}_{\{f\}}\cdot\mathcal{R}}|\{f\}\rangle. \tag{7.41}$$

Inserting equation (7.34) into (7.38) we have

$$N(\varepsilon, \Delta \mathbf{K}) = \lim_{t \to \infty, t_0 \to -\infty} \frac{1}{(2\pi\hbar)^3} \int_{-\infty}^{\infty} d\tau e^{\frac{i}{\hbar}\varepsilon\tau} \int_{\mathcal{R}} d^2 \mathcal{R} e^{i\Delta \mathbf{K} \cdot \mathcal{R}} \times \langle \Pi^S(t, t_0) | A^{\dagger}(\tau, \mathcal{R}) A | \Pi^S(t, t_0) \rangle,$$
(7.42)

where

$$A = U_{V_I}(t, t_0) (7.43)$$

and

$$A(\tau, \mathcal{R}) = e^{\frac{i}{\hbar}\hat{\mathbf{P}}\cdot\mathcal{R}} e^{\frac{i}{\hbar}H_0\tau} U_{V_t}(t, t_0) e^{-\frac{i}{\hbar}H_0\tau} e^{-\frac{i}{\hbar}\hat{\mathbf{P}}\cdot\mathcal{R}}.$$
 (7.44)

In deriving equation (7.42) we have used the fact that the operators H_0 and $\hat{\mathbf{P}}$ commute, i.e.

$$\left[H_0, \hat{\mathbf{P}}\right] = 0. \tag{7.45}$$

By using equation (7.34) for the explicit forms of $U_{H_0}(t)$ and $U_{V_I}(t, t_0)$, for $A(\tau, \mathcal{R})$ we have

$$A(\tau, \mathcal{R}) = \exp\left(-\frac{i}{\hbar} \sum_{\mathbf{Q}, s} (I_{\mathbf{Q}, s}(t, t_0) a_{-\mathbf{Q}, s} e^{-i\omega(\mathbf{Q}, s)\tau} e^{-i\mathbf{Q}\cdot\mathcal{R}} + I_{\mathbf{Q}, s}^*(t, t_0) a_{\mathbf{Q}, s}^{\dagger} e^{i\omega(\mathbf{Q}, s)\tau} e^{i\mathbf{Q}\cdot\mathcal{R}})\right).$$
(7.46)

To evaluate $A(\tau, \mathcal{R})A$ we use

$$e^{\hat{C}}e^{\hat{D}} = e^{\hat{C}+\hat{D}+(1/2)[\hat{C},\hat{D}]},$$
 (7.47)

which holds when $[\hat{C}, \hat{D}]$ is a c-number. The ground state average is finally obtained by using relation [12]

$$\langle \Pi^{S}(t,t_0)|e^{\hat{L}(a,a^{\dagger})}|\Pi^{S}(t,t_0)\rangle = \exp\left\{\frac{1}{2}\langle \Pi^{S}(t,t_0)|\hat{L}^{2}(a,a^{\dagger})|\Pi^{S}(t,t_0)\rangle\right\},\tag{7.48}$$

where \hat{L} is any operator containing only linear combinations of boson operators a and a^{\dagger} . The application of equation (7.48) to $A(\tau, \mathcal{R})A$ combination of operators produces expectation values of a type

$$\langle \Pi^S(t, t_0) | a_{\mathbf{Q},s} a_{\mathbf{Q},s}^{\dagger} + a_{\mathbf{Q},s}^{\dagger} a_{\mathbf{Q},s} | \Pi^S(t, t_0) \rangle,$$
 (7.49)

which are to be understood as thermal averages, since the wave function of the phonon bath at $t_0 \to -\infty$ depends on the temperature of the target. These averages can be calculated by using equation (4.39), so that we finally obtain the expression for the scattering spectrum,

$$N(\varepsilon, \Delta \mathbf{K}) = \frac{1}{(2\pi\hbar)^3} \int d\tau \int d^2 \mathcal{R} N(\tau, \mathcal{R}) e^{\frac{i}{\hbar}\varepsilon\tau + i\Delta \mathbf{K}\cdot\mathcal{R}}, \qquad (7.50)$$

where

$$N(\tau, \mathcal{R}) = e^{-2W} \exp \left\{ \sum_{\mathbf{Q}, s} |I_{\mathbf{Q}, s}|^2 \left[e^{-i(\omega(\mathbf{Q}, s)\tau - \mathbf{Q} \cdot \mathcal{R})} [n(\omega(\mathbf{Q}, s)) + 1] + e^{i(\omega(\mathbf{Q}, s)\tau - \mathbf{Q} \cdot \mathcal{R})} n(\omega(\mathbf{Q}, s)) \right] \right\},$$

$$(7.51)$$

and

$$I_{\mathbf{Q},s} = \lim_{t \to \infty, t_0 \to -\infty} I_{\mathbf{Q},s}(t, t_0)$$

=
$$\int_{-\infty}^{\infty} dt' W_{\mathbf{Q},s}(t') e^{-i\omega(\mathbf{Q},s)t'}.$$
 (7.52)

The Bose-Einstein distribution $n(\omega(\mathbf{Q}, s))$ is given by equation (6.10). The term independent of τ and \mathcal{R} in equation (7.51) gives a contribution to the spectrum proportional to $\delta(\varepsilon)\delta(\Delta\mathbf{K})$, i.e. it gives the elastic line of the spectrum. For the probability of elastic scattering (or the *Debye-Waller factor*), P_{00} , we can write

$$P_{00} = e^{-2W}, (7.53)$$

where

$$2W = \sum_{\mathbf{Q},s} |I_{\mathbf{Q},s}|^2 \left[2n \left(\omega(\mathbf{Q},s) \right) + 1 \right]$$
$$= \sum_{\mathbf{Q},s} |I_{\mathbf{Q},s}|^2 \left[\coth \left(\frac{\omega(\mathbf{Q},s)}{2k_B T_S} \right) \right]. \tag{7.54}$$

The quantity in equation (7.54) is called the *Debye-Waller exponent*.

7.3 Temporal dependence of the force in the trajectory approximation

To evaluate equations (7.51) and (7.54) we must know the temporal dependence of $W_{\mathbf{Q},s}(t)$ in equation (7.25). Therefore, we have to evaluate the projectile classical trajectory projected onto the z-axis, i.e. $z_{cl}(t)$. This can be done by solving the Newton equation

$$m\frac{d^2}{dt^2}\mathbf{r} = -\nabla V_{static}(\mathbf{r}) \tag{7.55}$$

subject to initial conditions

$$\frac{d}{dt}z(t\to -\infty) = \frac{\sqrt{2\epsilon_i}}{m}\cos\theta_i = v_z \tag{7.56}$$

and

$$\frac{d}{dt}\mathbf{R}(t \to -\infty) = \frac{\sqrt{2\epsilon_i}}{m}\sin\theta_i \mathbf{V}_0 = \mathbf{V}$$
 (7.57)

where ϵ_i is the projectile initial kinetic energy, \mathbf{V}_0 is the unit vector in \mathbf{V} direction and θ_i is the projectile incident angle with respect to the z-axis (surface normal). Neglecting now the static corrugation of the potential $V_{static}(\mathbf{r})$, i.e. dropping out all terms with $\mathbf{G} \neq 0$ in equation (3.4), we have

$$\mathbf{R}(t) = \mathbf{V}t + \mathbf{R}(t \to -\infty) \tag{7.58}$$

and

$$\frac{d^2}{dt^2}z = -\frac{1}{m}\frac{d}{dz}V_0(z). {(7.59)}$$

To proceed further analytically, we make necessary approximations. First, we neglect both static and dynamic interaction between the projectile and slabs with $\kappa > 0$. Second, we make the same approximation to \mathbf{Q} dependence of $v_{\mathbf{Q}+\mathbf{G}}(z)$ as in equation (6.20). We could in principle proceed with the calculation, but we make an additional approximation which will enable us to write the final result for the spectrum and the probability of elastic scattering in a simple and appealing way [18]. We take

$$Q_c \to \infty$$
 (7.60)

which is sometimes called the vibrating soft wall approximation [61]. This approximation effectively neglects the fact that the projectile interacts simultaneously with several lattice atoms (sites), so that very short wavelength oscillations cannot be excited (Armand effect, see also equation (6.21) and the discussion following it). We also keep only $\mathbf{G} = 0$ term from the sum in equation (7.21), consistently neglecting all the effects arising from the static corrugation of the interaction potential. This yields

$$I_{\mathbf{Q},s} = \sqrt{\frac{\hbar}{2MN_{2D}\omega(\mathbf{Q},s)}}$$

$$\times \left\{ \mathbf{Q} \cdot \mathbf{e}(\mathbf{Q},s) \left[\int dt V_0(z(t)) e^{i(\omega(\mathbf{Q},s)+\mathbf{Q}\cdot\mathbf{V})t} \right] + \mathbf{z}_0 \cdot \mathbf{e}(\mathbf{Q},s) \left[\int dt \frac{dV_0(z(t))}{dz} e^{i(\omega(\mathbf{Q},s)+\mathbf{Q}\cdot\mathbf{V})t} \right] \right\}, \quad (7.61)$$

where the integrals in square brackets 4 can be calculated analytically when $V_0(z)$ is given by the Morse potential as in equation (3.15) [14, 18].

⁴Note that these integrals have the role of the matrix elements of the interaction potential with respect to the projectile states - see e.g. equation (6.16). Clearly, when the quantum nature of the projectile can be neglected, the matrix elements should become identical to the Fourier transform integrals in the square brackets.

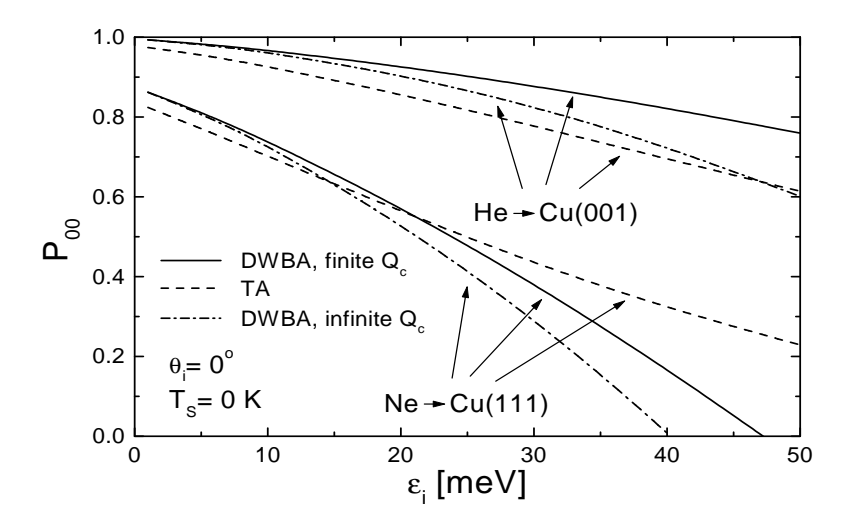


Figure 7.1: Elastic scattering probability for He \rightarrow Cu(001) and Ne \rightarrow Cu(111) scattering systems. Full line: DWBA with Q_c from equation (6.21). Dashed-dotted line: DWBA with $Q_c \rightarrow \infty$. Dashed line: TA equivalent to the one in reference [18].

7.4 Comparison of the elastic scattering probabilities in the DWBA and the trajectory approximation

Note that the elastic scattering probability, P_{00} , in equation (7.53), is always greater than zero and less than one owing to $0 < e^{-2W} < 1$ when 2W > 0. Therefore, the trajectory approximation does not have the unitarity defect which was inherent in the DWBA approach (see figure 6.5 and the related discussion). In this section we compare the results for P_{00} in the trajectory approximation and in the DWBA for He \rightarrow Cu(001) and Ne \rightarrow Cu(111) scattering systems. The DWBA calculation is based on equations (6.36) and (6.24), where we have also included transitions into the bound states of the static interaction potential. This was approximately done as in equation (9.1) in *Chapter 9*. The interaction potential parameters and target phonon density of states used can be found in section 9.1 ⁵. Figure 7.1 displays the calculation of P_{00} as a function of the projectile incident energy, ϵ_i . The surface temperature is $T_S = 0$ K and normal projectile incidence

⁵A simple "surface Debye model" is used.

is assumed ⁶. After all the approximations made in this calculation, one can show that the trajectory approximation calculation displayed here is completely equivalent to the one elaborated in reference [18]. The only difference is in the integral in equation (22) of reference [18] whose upper limit is the Debye frequency of the target rather than infinity as in [18]. The figure also displays the influence of the Armand factor (cut-off wave vector Q_c) on the DWBA calculation of the elastic scattering probability. Note that

$$\lim_{\epsilon_i \to \infty} P_{00}(TA) = 0, \tag{7.62}$$

while

$$\lim_{\epsilon_i \to \infty} P_{00}(DWBA) = -\infty, \tag{7.63}$$

which is again a consequence of the nonunitarity of the DWBA. The comparison of the TA and the DWBA results can be used to evaluate an upper incident energy limit on the validity of the DWBA approach. Note here that we expect the DWBA to work better than the TA in the low incident energy regime, while we expect the TA to provide a good description of the scattering dynamics in the high incident energy regime where one can expect that the truly quantum nature of the projectile fades out. It would be of interest to construct the approximation to the scattering problem which somehow "interpolates" between the DWBA and the TA, reducing to one or to another in the appropriate scattering regime and which treats both the target phonons and the projectile quantum mechanically (as DWBA approximately does). The construction of such an approximation is exactly the aim of the following chapter.

⁶This additionally simplifies Fourier transforms in square brackets in equation (7.61).

Chapter 8

Exponentiated Born Approximation in atom-surface scattering

Laundry increases exponentially in the number of children.

Miriam Robbins

THEORY OF
THERMAL ENERGY
INERT ATOM
SCATTERING FROM
SURFACE VIBRATIONS

Antonio Šiber

To obtain the quantum scattering probabilities w_{fi} to higher order in the coupling constant, one could in principle calculate the contribution to transition amplitude (described in Chapter 6) arising from twophonon processes, then from three-phonon processes and so on. This procedure is called *Dyson expansion* of the scattering matrix and is a common approach to many-body problems in solid state physics. It is not too difficult to see that this calculation would be rather complicated since one should integrate over all possible intermediate phonon wave vectors and frequencies which satisfy the requirement of conservation of energy. For two-phonon processes, this would imply two dimensional summation over \mathbf{Q}_1 and \mathbf{Q}_2 phonon wave vectors with additional requirement that $(\mathbf{Q}_1 + \mathbf{Q}_2)||\mathbf{K}_i||$ since, then $\mathbf{K}_f||\mathbf{K}_i||$ i.e. the projectile atom after the two-phonon process emerges in plane defined by \mathbf{K}_i and surface normal so that it can be observed by the experimental equipment (in sagittal plane scattering). Additional condition is needed the projectile atom must continue to move in direction θ_f after the collision, otherwise it will not reach the detector.

In this chapter, I shall specify an alternative procedure of finding the solution to the T matrix (or S - the scattering matrix, or U - the time evolution operator) of the problem. This procedure is usually called the *exponential resummation of perturbation series* and its specific approximation in the context of atom-surface scattering - called the *exponentiated Born approximation*.

The application of the procedure to three dimensions seems somewhat complicated due to the quantum numbers characteristic of the system which is not translationally invariant in all three spatial dimensions.

8.1 Dyson form as the iteration solution for the evolution operator

The standard perturbation analysis starts from the integral equation equivalent to equation (7.6) with the initial condition as in equation (7.7):

$$U(t, t_0) = 1 - ig \int_{t_0}^t V(t')U(t', t_0)dt'.$$
(8.1)

The iteration solution is

$$U(t,t_0) = \sum_{n=0}^{\infty} (-i)^n g^n \int_{t_0}^t dt_1 \int_{t_0}^{t_1} dt_2 \dots \int_{t_0}^{t_{n-1}} dt_n V(t_1) V(t_2) \dots V(t_n),$$

(8.2)

with

$$t > t_1 > t_2 > \dots > t_{n-1}.$$
 (8.3)

Introducing the time ordering (or chronological) operator T defined as

$$T\{V(t_1)V(t_2)\} = V(t_1)V(t_2), t_1 > t_2$$

= $V(t_2)V(t_1), t_1 < t_2,$ (8.4)

equation (8.2) can be written as

$$U(t, t_0) = \sum_{n=0}^{\infty} \frac{1}{n!} (-i)^n g^n \int_{t_0}^t \int_{t_0}^t \dots \int_{t_0}^t T\{V(t_1) \dots V(t_n)\} dt_1 \dots dt_n.$$
(8.5)

The factor 1/n! comes from n! permutations in the set $\{t_1, t_2, ...t_n\}$ which all contribute equally to $U(t, t_0)$ and they must not be overcounted (see reference [11], page 391). We can symbolically write

$$U(t, t_0) = T \left\{ \exp[-ig \int_{t_0}^t V(t')dt'] \right\}, \tag{8.6}$$

having, of course equation (8.2) in mind.

Equation (8.5) is called the Dyson form of the evolution operator. Although it formally solves the problem of finding the evolution operator, the series on the right hand side of equation (8.2) has infinitely many terms. One usually calculates the first few terms and discards the others. This makes the evolution operator nonunitary which violates the norm and current conservation in applications of such approximate solutions to the scattering problems.

8.2 Alternative approach to the evolution operator - the time dependent exponential transform

We may also seek the solution of equation (7.4) by introducing the time dependent unitary transform of the wave function as ¹

$$\Psi(t) = W(t)\Phi(t),
W(t) = e^{-iG(t)}.$$
(8.7)

Inserting the equation above into (7.4) we obtain

$$i\frac{\partial\Phi}{\partial t} = (W^{-1}(t)gV(t)W(t) - iW(t)\frac{\partial W(t)}{\partial t})\Phi(t). \tag{8.8}$$

Since $W(t) = \exp(-iG(t))$ we have

$$W^{-1}gVW = gV + i[G, gV] + \frac{i^2}{2!}[G, [G, gV]] + \dots$$
 (8.9)

and

$$iW^{-1}\frac{\partial W}{\partial t} = \frac{\partial G}{\partial t} + \frac{i}{2!}[G, \frac{\partial G}{\partial t}] + \frac{i^2}{3!}[G, [G, \frac{\partial G}{\partial t}]] + \dots$$
 (8.10)

Here, [A, B] = AB - BA. The relations above can be obtained by straightforward expansion of the exponential $\exp(-iG(t))^2$ [62, 44] as follows:

$$e^{L}Ae^{-L} = (1 + L + \frac{1}{2}L^{2} + ...)A(1 - L + \frac{1}{2}L^{2} - ...)$$

$$= A + (LA - AL) + \frac{1}{2}(L^{2}A - 2LAL + AL^{2}) + ...$$

$$= A + [L, A] + \frac{1}{2}[L, [L, A]] + ...$$
(8.11)

Another relation which will prove to be of use is ³

$$e^{A}e^{B} = \exp\left\{A + B + \frac{1}{2!}[A, B] + \frac{1}{3!}(\frac{1}{2}[[A, B], B] + \frac{1}{2}[A, [A, B]]) + \ldots\right\}.$$
 (8.12)

¹The following procedure also specifies the way to solve the trajectory approximation equation (7.27).

²One has to pay some attention here not to confuse the functions of the operators with the functions of simple number variables.

³We already used the specific form of this equation in (7.47).

The relations above (called *Baker-Hausdorff lemmas*) can be obtained by more elegant means than the brute inspection of the Taylor series [44].

The whole idea, which is probably obscured by now, is to find W(t) (or, equivalently G(t)) which makes the right hand side of equation (8.8) vanish. Then we have $\partial \Phi/\partial t = 0$ or $\Phi = const = \Phi_0$. We start our quest for G(t) by writing

$$G = g \int_{t_0}^{t} V(t')dt' + \dots$$

$$\frac{\partial G}{\partial t} = gV(t) + \dots$$
(8.13)

Let us suppose for the moment that V(t) has such operator structure that

$$[V(t), V(t')] = C(t, t') \cdot 1. \tag{8.14}$$

Here, C(t,t') is c-number, i.e. not an operator. Then, the double commutator [V(t), [V(t'), V(t'')]] = 0 and all higher order commutators also vanish! Thus, the infinite series in equation (8.9) and (8.10) stops after only two terms and, from equation (8.8) we have

$$i\frac{\partial\Phi}{\partial t} = \left\{\frac{i}{2}g^2 \int_{t_0}^t C(t', t)dt'\right\}\Phi(t) \tag{8.15}$$

so that the problem is solved (equations (8.7) and (8.15)) by

$$\Psi(t) = \exp\left\{-ig \int_{t_0}^t V(t')dt'\right\} \exp\left\{\frac{1}{2}g^2 \int_{t_0}^t dt' \int_{t_0}^{t'} C(t'', t')dt''\right\} \Psi(t_0).$$
(8.16)

It is easy to generalize this to the case when some higher order commutator vanishes, e.g. when $[V(t), [V(t_1), V(t_2)]] = D(t, t_1, t_2) \cdot 1$ [62].

The procedure sketched above enables one to solve the forced harmonic oscillator mentioned in Chapter 2 and elaborated in a realistic application to atom-surface scattering in Chapter 7 in a closed analytic fashion. In the one dimensional problem from Chapter 2, the interaction potential is $V(t) = F^*(t)a^{\dagger}e^{i\omega t} + F(t)ae^{-i\omega t}$ where F(t) is time dependent external force and a^{\dagger} is the phonon creation operator. It is easy to see that the second order commutator does not contain operators since

$$C(t, t') = [V(t), V(t')] = F(t)F^*(t')e^{i\omega(t'-t)} + F^*(t)F(t')e^{-i\omega(t'-t)}.$$
(8.17)

Thus, this simple problem can be solved exactly since the infinite series in (8.9) and (8.10) can be evaluated due to its termination after a finite number of terms ⁴. Note that the Dyson expansion in (8.5) must be summed to an infinite order for this problem.

The closed form solution for the G operator can be found by writing it as a power series in the coupling constant g (that is why we have been dragging g from the beginning - to inspect the power series in g).

$$G = \sum_{n=1}^{\infty} g^n G_n \tag{8.18}$$

Inserting this form in equation (8.8) and using (8.9) and (8.10) and demanding that $\partial \Phi/\partial t = 0$ we obtain

$$gZ_1 + g^2Z_2 + \dots + g^mZ_m + \dots = \sum_{n=1}^{\infty} Z_n g^n = 0,$$
 (8.19)

where

$$Z_{1} = V(t) - \frac{\partial G_{1}}{\partial t}$$

$$Z_{2} = i[G_{1}, V(t)] - \frac{\partial G_{2}}{\partial t} - \frac{i}{2!}[G_{1}, \frac{\partial G_{1}}{\partial t}]$$

$$Z_{3} = i[G_{2}, V(t)] + \frac{i^{2}}{2!}[G_{1}, [G_{1}, V(t)]] - \frac{i}{2!}[G_{1}, \frac{\partial G_{2}}{\partial t}] - \frac{\partial G_{3}}{\partial t}$$
...
$$(8.20)$$

It is seen from the equations above that every G_n depends only on a set of G_i where i = 1, ..., n - 1. Therefore, the equations can be easily solved and we conclude after equating all Z_m 's with zero that

$$G_{1}(t, t_{0}) = \int_{t_{0}}^{t} dt_{1} V(t_{1})$$

$$G_{2}(t, t_{0}) = \frac{i}{2} \int_{t_{0}}^{t} dt_{1} \int_{t_{0}}^{t_{1}} dt_{2} [V(t_{2}), V(t_{1})]$$
...
(8.21)

It is one's hope that even if the series in (8.9) and (8.10) do not terminate after finite number of steps, the series in (8.21) will converge much more rapidly than the Dyson expansion (8.5). If this is the case,

⁴Note here that C(t, t') is completely analogous to the subintegral function of $\Phi_{\mathbf{Q},s}(t,t_0)$ in equation (7.33).

one can approximate better the exact solution by using the displayed alternative approach rather than the Dyson expansion and by calculating the same number of terms in both expansions. This happens to be the case e.g. for the polaron [63] and the atom-surface scattering problem [64, 56]. Of course, one has to have an assurance that the contribution of G's (to the evolution operator $U(t, t_0)$) of order higher than the calculated one can be safely neglected. The inspection of the relative contribution of different G's was performed in references [64, 65].

8.3 The alternative approach applied to the problem of atom-surface scattering: The scattering spectrum

In the case of atom surface scattering we can explicitly write the unperturbed part of the hamiltonian, H_0 , which governs the time evolution of the operators, and the interaction (perturbation) part of the hamiltonian, V_I , which governs the time evolution of the wave function in the interaction representation of quantum mechanics. In order to emphasize the quantum character of the field of projectile particles and the vibrations of the target, and to treat them on equivalent quantum mechanical footing 5 , both fields can be represented in the second quantization form, i.e. expressed through the "fundamental" or basic phonon and projectile atom creation and destruction (annihilation) operators [44, 11, 66]. For H_0 we write

$$H_{0} = H_{0}^{a} + H_{0}^{ph}$$

$$= \sum_{\mathbf{K}_{i}, k_{(z,i)}} \epsilon_{\mathbf{K}_{i}, k_{(z,i)}} c_{\mathbf{K}_{f}, k_{(z,f)}}^{\dagger} c_{\mathbf{K}_{i}, k_{(z,i)}} + \sum_{\mathbf{Q}, s} \hbar \omega(\mathbf{Q}, s) a_{\mathbf{Q}, s}^{\dagger} a_{\mathbf{Q}, s},$$

$$(8.22)$$

and for the interaction V

$$V = g \sum_{\mathbf{K}_{i},\mathbf{K}_{f},k_{(z,i)},k_{(z,f)}} \sum_{\mathbf{Q},s} V_{k_{(z,f)},k_{(z,i)},s}^{\mathbf{K}_{f},\mathbf{K}_{i},\mathbf{Q}} \delta_{\mathbf{K}_{f},\mathbf{K}_{i}+\mathbf{Q}}$$

$$\times c_{\mathbf{K}_{f},k_{(z,f)}}^{\dagger} c_{\mathbf{K}_{i},k_{(z,i)}} a_{\mathbf{Q},s} + h.c.$$
(8.23)

Here H_0^a is the part of the unperturbed hamiltonian corresponding to the projectile atom and H_0^{ph} corresponds to the unperturbed hamiltonian of the target phonon field (this part was already written in this way

⁵This is where this approach goes beyond the trajectory approximation.

in Chapter 4 - note that the zero point motion is neglected here since there is no 1/2 factor as in equation (4.35)). The notation used in writing this hamiltonian is consistent with the notation used in Chapter 6. The part of the interaction explicitly written in equation (8.23) which derives from the dynamic component of the interaction corresponds to absorption (destruction) of a phonon by the projectile atom and the hermitian conjugate part, h.c. corresponds to emission (creation) of a phonon by the projectile atom 6 .

In the description of a scattering event we are interested in the spectrum of the scattered particles $N_{\mathbf{k_i}}(\varepsilon, \Delta \mathbf{K})$, i.e. in the fraction of scattered atoms which have exchanged certain amount of energy ε and lateral (in the surface plane) momentum $\Delta \mathbf{K}$ with the target ⁷. We can find this fraction of atoms by projecting it out of the wave function of the system after the completion of the scattering event with the help of δ -function operators as ⁸:

$$N_{\mathbf{k}_{i}}(\varepsilon, \Delta \mathbf{K}) = \langle \Psi_{e} \mid \delta[\varepsilon - (H_{0}^{ph} - \varepsilon_{i})] \delta(\hbar \Delta \mathbf{K} - \hat{\mathbf{P}}) \mid \Psi_{e} \rangle.$$
 (8.24)

Here

$$|\Psi_{e}\rangle = \lim_{t \to \infty, t_{0} \to -\infty} |\Psi(t, t_{0})\rangle = \lim_{t \to \infty, t_{0} \to -\infty} U(t, t_{0}) |\Psi_{0}\rangle$$
$$= S|\Psi_{0}\rangle = S|i\rangle$$
(8.25)

is the wave function of the system evolved from the initial noninteracting state of the system $|i\rangle$ to the final, also noninteracting state of the system as in (7.12), $\Delta \mathbf{K} = \mathbf{K_i} - \mathbf{K_f}$ and $\hat{\mathbf{P}}$ is the lateral momentum operator of the phonon field

$$\hat{\mathbf{P}} = \sum_{\mathbf{Q},s} \hbar \mathbf{Q} n_{\mathbf{Q},s},\tag{8.26}$$

with $n_{\mathbf{Q},s}$ standing for the phonon number operator of the mode (\mathbf{Q},s) . ε_i is the initial energy of the target phonons. Note that we project out of the target part of the wave function only those "events" for which $\varepsilon_f - \varepsilon_i = \varepsilon$. Note also that the scattering spectrum is unitary, since integration of the spectrum over all $\Delta \mathbf{K}$'s and ε 's yields unity assuming

The explicit form of $V_{k_{(z,f)},k_{(z,i)},s}^{\mathbf{K}_{f},\mathbf{K}_{i},\mathbf{Q}}$ can be inferred from the derivation in *Chapter* 6.

 $^{^7}$ Note here that we do not ask about the fraction of atoms which lost certain momentum in z-direction. This can be uniquely determined from the conservation of energy and lateral momentum requirements (8.24).

⁸From now on, we shall follow the notation and the formalism of reference [56].

the unitarity of the S-matrix (which must be unitary if one does not degrade its properties by nonunitary approximations). By expressing the energy and lateral momentum conserving δ -functions in (8.24) as Fourier transforms of exponentials of the operators H_0^{ph} and $\hat{\mathbf{P}}$, we obtain ⁹:

$$N_{\mathbf{k_{i}}}(\varepsilon, \Delta \mathbf{K}) = \int_{-\infty}^{\infty} \frac{d\tau}{2\pi\hbar} \int \frac{d^{2}\mathbf{R}}{(2\pi\hbar)^{2}} e^{\frac{i}{\hbar}[\varepsilon\tau - \hbar(\Delta \mathbf{K})\mathbf{R}]}$$

$$\times \langle \Psi(\infty) \mid e^{-\frac{i}{\hbar}(H_{0}^{ph}\tau - \hat{\mathbf{P}}\mathbf{R})} \mid \Psi(\infty) \rangle =$$

$$= \int_{-\infty}^{\infty} \frac{d\tau}{2\pi\hbar} \int \frac{d^{2}\mathbf{R}}{(2\pi\hbar)^{2}} e^{\frac{i}{\hbar}[\varepsilon\tau - \hbar(\Delta \mathbf{K})\mathbf{R}]}$$

$$\times \langle i \mid S^{\dagger} e^{-\frac{i}{\hbar}(H_{0}^{ph}\tau - \hat{P}_{x}X - \hat{P}_{y}Y)} S \mid i \rangle =$$

$$= \int_{-\infty}^{\infty} \frac{d\tau}{2\pi\hbar} \int \frac{d^{2}\mathbf{R}}{(2\pi\hbar)^{2}} e^{\frac{i}{\hbar}[\varepsilon\tau - \hbar(\Delta \mathbf{K})\mathbf{R}]}$$

$$\times \langle i \mid e^{-\frac{i}{\hbar}(H_{0}^{ph}\tau - \mathcal{P}_{x}X - \mathcal{P}_{y}Y)} \mid i \rangle. \tag{8.27}$$

Here $\mathbf{R} = (X, Y)$ is a two dimensional radius vector parallel to the surface plane, and τ has the dimension of time, although it is not the physical evolution time of the system. The canonically transformed operators appearing in the last line of equation (8.27) are defined by:

$$\mathcal{H}_{0}^{ph} = S^{\dagger} H_{0}^{ph} S,$$

$$\mathcal{P}_{x} = S^{\dagger} \hat{P}_{x} S,$$

$$\mathcal{P}_{y} = S^{\dagger} \hat{P}_{y} S.$$
(8.28)

We know from the previous section that for the S-matrix we can write

$$S = \lim_{t \to \infty, t_0 \to -\infty} e^{-iG(t, t_0)} = e^{-iG(\infty, -\infty)} = e^{-iG}.$$
 (8.29)

The formal solution of equation (8.27) can be presented somewhat more clearly by introducing a unified vector notation for the variables and exponentiated operators:

$$(\tau, X, Y) \rightarrow (\xi_0, \xi_1, \xi_2) = \boldsymbol{\xi},$$

$$(\frac{\varepsilon}{\hbar}, -\Delta K_x, -\Delta K_y) \rightarrow (\varepsilon_0, \varepsilon_1, \varepsilon_2) = \boldsymbol{\varepsilon},$$

$$(\omega_{\mathbf{Q},j}, -Q_x, -Q_y) \rightarrow (\nu_0, \nu_1, \nu_2) = \boldsymbol{\nu},$$

$$(\frac{H_0^{ph}}{\hbar}, -\frac{\hat{P}_x}{\hbar}, -\frac{\hat{P}_y}{\hbar}) \rightarrow (\mathcal{H}_0, \mathcal{H}_1, \mathcal{H}_2) = \boldsymbol{\mathcal{H}},$$

$$(8.30)$$

⁹Note the similarity with the procedure used to derive the trajectory approximation.

where due to the property that H_0^{ph} and $\hat{\mathbf{P}}$ commute, also the components of the operator \mathcal{H} commute with each other, i.e.

$$[\mathcal{H}_l, \mathcal{H}_{l'}] = 0. \tag{8.31}$$

Using the notation of equation (8.30) we can write

$$\frac{\varepsilon}{\hbar}\tau - (\Delta \mathbf{K})\mathbf{R} = \sum_{l=0}^{2} \varepsilon_{l} \xi_{l} = \varepsilon \boldsymbol{\xi},$$

$$\frac{H_{0}^{ph}}{\hbar}\tau - \frac{\hat{P}_{x}}{\hbar}X - \frac{\hat{P}_{y}}{\hbar}Y = \sum_{l=0}^{2} \mathcal{H}_{l} \xi_{l} = \mathcal{H}\boldsymbol{\xi},$$

$$\mathcal{L} = (\mathcal{L}_{0}, \mathcal{L}_{1}, \mathcal{L}_{2}) = S^{\dagger}\mathcal{H}S,$$
(8.32)

which enables us to express equation (8.27) in a compact form:

$$N_{\mathbf{k_i}}(\varepsilon, \Delta \mathbf{K}) = N_{\mathbf{k_i}}(\varepsilon) = \int_{-\infty}^{\infty} \int_{-\infty}^{\infty} \int_{-\infty}^{\infty} \frac{d^3 \boldsymbol{\xi}}{(2\pi\hbar)^3} \exp(i\varepsilon \boldsymbol{\xi})$$

$$\times \langle i \mid \exp(-i\boldsymbol{\mathcal{L}}\boldsymbol{\xi}) \mid i \rangle. \tag{8.33}$$

To obtain a perturbative solution to equation (8.33) we proceed by making use of the operator identity which was demonstrated in the previous section:

$$\mathcal{L} = S^{\dagger} \mathcal{H} S = e^{iG} \mathcal{H} e^{-iG} = \sum_{n=0}^{\infty} \frac{i^n}{n!} G^n[\mathcal{H}], \tag{8.34}$$

where $G^n[\Lambda] = [G, [G, ..., [G, \Lambda]]$ is the n-th order repeated commutator of G with arbitrary operator Λ . Using this we find

$$N_{\mathbf{k_i}}(\varepsilon, \Delta \mathbf{K}) = N_{\mathbf{k_i}}(\varepsilon) = \int_{-\infty}^{\infty} \int_{-\infty}^{\infty} \int_{-\infty}^{\infty} \frac{d^3 \boldsymbol{\xi}}{(2\pi\hbar)^3} \exp(i\varepsilon \boldsymbol{\xi}) \times \langle i \mid \exp[-i(\boldsymbol{\mathcal{H}} + \boldsymbol{\mathcal{W}})\boldsymbol{\xi}] \mid i \rangle.$$
(8.35)

where

$$\mathcal{W} = \sum_{n=1}^{\infty} \frac{i^n}{n!} G^n[\mathcal{H}]$$
$$= e^{iG} \mathcal{H} e^{-iG} - \mathcal{H}. \tag{8.36}$$

We have here explicitly written the n=0 part of \mathcal{W} as \mathcal{H} . The equations in this section appear rather complicated, but this is a consequence of many symbols involved rather than difficult mathematics.

The only thing we had actually to do in this section was to transform the δ -operators into integrals over τ and \mathbf{R} coordinates and carry out the canonical transformation (8.34). All the rest was known from previous sections. However, the problem is far from being actually solved. Fortunately, there exists a procedure to treat the diagonal matrix elements of operators which can be represented as exponential functions of some other operators. This procedure is called the generalized cumulant expansion method [67]. The basic idea is to "move" the "averaging" (here, the diagonal matrix element $\langle i|...|i\rangle$) into the argument of the exponential function ¹⁰. According to reference [67], once \mathcal{W} has been found, $N_{\mathbf{k_i}}(\varepsilon)$ may be expressed as a cumulant expansion,

$$\ln N_{\mathbf{k}_{i}}(\boldsymbol{\varepsilon}) = \gamma_{1}(\boldsymbol{\varepsilon}) + \gamma_{2}(\boldsymbol{\varepsilon}) + ..., \tag{8.37}$$

where

$$\gamma_{1}(\boldsymbol{\varepsilon}) = -i \int_{0}^{\boldsymbol{\varepsilon}} d\boldsymbol{\varepsilon}' < \boldsymbol{\mathcal{W}}(\boldsymbol{\varepsilon}') >_{c},$$

$$\gamma_{2}(\boldsymbol{\varepsilon}) = -\int_{0}^{\boldsymbol{\varepsilon}} d\boldsymbol{\varepsilon}' \int_{0}^{\boldsymbol{\varepsilon}'} d\boldsymbol{\varepsilon}'' < \boldsymbol{\mathcal{W}}(\boldsymbol{\varepsilon}') \boldsymbol{\mathcal{W}}(\boldsymbol{\varepsilon}'') >_{c}, \qquad (8.38)$$

and so forth. The cumulants $< ... >_c$ are evaluated on the initial state $|i\rangle$ and the ε dependence of $\mathcal{W}(\varepsilon)$ is generated by \mathcal{H} alone, i.e. $\mathcal{W}(\varepsilon) = e^{i\mathcal{H}\varepsilon}We^{-i\mathcal{H}\varepsilon}$. The cumulants involve expectation values with means subtracted (in our case $\langle i|...|i\rangle$). Explicitly,

$$\langle \mathcal{W}(\varepsilon) \rangle_{c} = \langle \mathcal{W}(\varepsilon) \rangle$$

 $\langle \mathcal{W}(\varepsilon) \mathcal{W}(\varepsilon') \rangle_{c} = \langle \mathcal{W}(\varepsilon) \mathcal{W}(\varepsilon') \rangle - \langle \mathcal{W}(\varepsilon) \rangle \langle \mathcal{W}(\varepsilon') \rangle$
... (8.39)

All the relations presented so far are exact. Of course, one has to calculate all the terms in the sums (8.18), (8.36) and (8.37).

8.4 EBA: Exponentiated Born Approximation to the scattering spectrum

The EBA approximation consists of retaining *only* the full G_1 and the diagonal components of G_2 in the series (8.18) for the operator G.

¹⁰This is exactly what we have already done in equation (7.48), albeit for much simpler "argument" of the exponential function.

The diagonal means here that we are considering only processes where $\mathbf{k}_i = \mathbf{k}_f$ in G_2 i.e. there is no exchange of energy in these processes [65, 64] (this will all soon become clearer when we explicitly write down the expressions for G_1 and G_2). Physically, this approximation means the neglect of correlated multiphonon processes in the spectrum relative to the effects brought about by the multiple emission or absorption of uncorrelated phonons [63, 56]. By uncorrelated processes we mean that successive emissions (absorptions) of phonons are independent. The correlations between successive emissions (absorptions) of phonons are contained in higher terms of the G-series. Properly calculated G_2 term contains the correlations between pairs of phonons emissions (absorptions), G_3 term contains the correlations between trios of phonons emissions (absorptions) and so on [12, 63].

We can now proceed to calculate G_1 and G_2 contributions to the G series. We shall temporarily abandon the specific notation developed so far in order to clearly explain what will be done next. The G_1 part is easy - it just requires the integration of the interaction over time.

The time dependence of the perturbing, dynamical part of the interaction potential can be explicitly written since the time dependence of the projectile and phonon Heisenberg operators is quite simple:

$$V = \sum_{\mathbf{K}_{i}, \mathbf{K}_{f}, k_{(z,i)}, k_{(z,f)}, s} V(\mathbf{K}_{i}, \mathbf{K}_{f}, k_{(z,i)}, k_{(z,f)}, s)$$

$$\times c_{\mathbf{k}_{f}}^{\dagger} e^{i\epsilon(\mathbf{k}_{f})t} c_{\mathbf{k}_{i}} e^{-i\epsilon(\mathbf{k}_{i})t} a_{\Delta \mathbf{K}, s} e^{-i\omega(\Delta \mathbf{K}, s)t} + h.c., \qquad (8.40)$$

where we have explicitly written the quantum numbers \mathbf{K} and k_z only where convenient. It will prove usefull to transform one of the sums above into integration over the transferred energy $\omega = \epsilon(\mathbf{k}_i) - \epsilon(\mathbf{k}_f)$. This yields

$$V = \sum_{\Delta \mathbf{K}, \mathbf{k}_{i}, s} \int_{-\infty}^{\infty} d\omega \bar{V}(\mathbf{K}_{i}, \mathbf{K}_{i} + \Delta \mathbf{K}, k_{(z,i)}, k_{(z,f)}, s)$$

$$\times c_{\mathbf{k}_{f}}^{\dagger} c_{\mathbf{k}_{i}} e^{-i\omega t} a_{\Delta \mathbf{K}, s} e^{-i\omega(\Delta \mathbf{K}, s)t} + h.c., \qquad (8.41)$$

where \bar{V} differs from V only by a multiplicative factor which is a product of $L_z/2\pi$ arising from a transformation of a discrete sum over k_z' into an integral over k_z' and a Jacobian factor m/k_z' arising from a transformation of integral over k_z' into an integral over ω (this is all very similar to what has already been done in *Chapter 6*) and $\Delta \mathbf{K} = \mathbf{K}_f - \mathbf{K}_i$.

Now we can calculate G_1 by integrating (8.41) over t. This yields

$$G_1 = \sum_{\Delta \mathbf{K}, \mathbf{k}_i, s} \mathcal{V}(\mathbf{K}_i, \epsilon(\mathbf{k}_i); \Delta \mathbf{K}, \omega(\Delta \mathbf{K}, s)) c_{\mathbf{k}_f}^{\dagger} c_{\mathbf{k}_i} a_{\Delta \mathbf{K}, s} + h.c.$$
(8.42)

The δ -function which appears as a result of integration of the term

$$e^{-i(\omega-\omega(\Delta\mathbf{K},s))t}$$

over time, t, can be transformed into a Kronecker symbol (at least for continuum-continuum transitions) as in equation (6.28) which can be inserted into "new" on-the-energy-shell matrix elements \mathcal{V} , accounting also for the integration over ω .

Note that the first and second two arguments of the matrix element \mathcal{V} correspond to projectile's initial state and the lateral wave vector and energy exchanged with the target in a single-phonon emission (absorption) event.

For the evaluation of G_2 term we have to calculate some commutators. c and a operators commute, a' and a operators satisfy the bosonic commutation relations (4.33) and 4.34) while c' and c operators can be also assumed to satisfy the bosonic commutation relations - it is of no importance since there is only one projectile atom in the system. The G_2 term can be shown to take the form [65]

$$G_{2} = \sum_{\Delta \mathbf{K}, \Delta \mathbf{K}', \mathbf{k}_{i}, s, s'} \int_{-\infty}^{\infty} \frac{d\omega}{2\pi} \int_{-\infty}^{\infty} \frac{d\omega'}{2\pi} \bar{C}(\mathbf{K}_{i}, \epsilon(\mathbf{k}_{i}); \Delta \mathbf{K}, \omega, s; \Delta \mathbf{K}', \omega', s')$$

$$\times \rho(\mathbf{K}_{i}, \epsilon(\mathbf{k}_{i}); \Delta \mathbf{K} + \Delta \mathbf{K}', \omega + \omega') \bar{A}(\Delta \mathbf{K}, \omega, s; \Delta \mathbf{K}', \omega', s')$$

$$+ G_{2}^{diag}$$
(8.43)

where

$$\bar{A}(\Delta \mathbf{K}, \omega, s; \Delta \mathbf{K}', \omega', s') = \int_{-\infty}^{\infty} dt \int_{-\infty}^{\infty} dt' [a_{\Delta \mathbf{K}, s}(t) + a_{-\Delta \mathbf{K}, s}^{\dagger}(t)] \times [a_{\Delta \mathbf{K}', s'}(t') + a_{-\Delta \mathbf{K}', s'}^{\dagger}(t')] e^{i\omega t' + i\omega' t'},$$
(8.44)

$$\bar{C}(\mathbf{K}_{i}, \epsilon(\mathbf{k}_{i}); \Delta \mathbf{K}, \omega, s; \Delta \mathbf{K}', \omega', s') =
= \mathcal{V}(\mathbf{K}_{i} + \Delta \mathbf{K}', \epsilon(\mathbf{k}_{i}) + \omega'; \Delta \mathbf{K}, \omega, s)
\times \mathcal{V}(\mathbf{K}_{i}, \epsilon(\mathbf{k}_{i}); \Delta \mathbf{K}', \omega', s')
- \mathcal{V}(\mathbf{K}_{i} + \Delta \mathbf{K}, \epsilon(\mathbf{k}_{i}) + \omega; \Delta \mathbf{K}', \omega', s')
\times \mathcal{V}(\mathbf{K}_{i}, \epsilon(\mathbf{k}_{i}); \Delta \mathbf{K}, \omega, s),$$
(8.45)

$$\rho(\mathbf{K}_{i}, \epsilon(\mathbf{k}_{i}); \Delta \mathbf{K}, \omega) = c_{\mathbf{k}_{f}}^{\dagger} c_{\mathbf{k}_{i}}$$

$$\mathbf{K}_{f} = \mathbf{K}_{i} + \Delta \mathbf{K}$$

$$\epsilon_{f} = \epsilon_{i} + \omega, \qquad (8.46)$$

and

$$G_2^{diag} = \lim_{t_0 \to -\infty, t \to \infty} \sum_{\mathbf{k}_i} [V(\mathbf{K}_i, \epsilon(\mathbf{k}_i); 0; 0)]^2 c_{\mathbf{k}_i}^{\dagger} c_{\mathbf{k}_i} f(t, t_0).$$
(8.47)

Here, $f(t,t_0)$ is a real function ¹¹. The diagonal part of G_2 is seen to be equal to G_2^{diag} . If the interaction matrix elements, \bar{V} were independent of the initial state of the particle, which is not the case in atom-surface scattering, the whole G_2 would reduce to G_2^{diag} . However, for quasielastic scattering (i.e. very close to elastic scattering [64]), we expect the dominant states occurring in the integrals to be close in \mathbf{k} space to the initial state. The EBA is recovered by replacing $\mathcal{V}(\mathbf{K}_i + \Delta \mathbf{K}', \epsilon(\mathbf{k}_i) + \omega'; \Delta \mathbf{K}, \omega)$ with $\mathcal{V}(\mathbf{K}_i, \epsilon(\mathbf{k}_i); \Delta \mathbf{K}, \omega)$ which makes the nondiagonal terms of G_2 (and all nondiagonal terms of G_m , m > 1) to vanish. Since G_2^{diag} is a real function, we have:

$$e^{iG_2^{diag}} \mathcal{H} e^{-iG_2^{diag}} = e^{iG_2^{diag}} e^{-iG_2^{diag}} \mathcal{H} = \mathcal{H},$$
 (8.48)

which cancels the $-\mathcal{H}$ term in equation (8.36). Since G_1 part contains only one phonon operator, only $[G_1, \mathcal{H}]$ and $[G_1, [G_1, \mathcal{H}]]$ commutators are different from zero and we are left with only two terms for \mathcal{W} in (8.36). Returning now to the specific notation introduced earlier we have that

$$\mathcal{W}_l = \mathcal{W}_l^{(1)} + \mathcal{W}_l^{(2)}, \tag{8.49}$$

in which

$$\mathcal{W}_{l}^{(1)} = i[G_{1}, \mathcal{H}_{l}]
= \sum_{\mathbf{K}_{i}, \Delta \mathbf{K}, k_{(z,i)}, k_{(z,f)}, s} \left[i\hbar \nu_{l} \mathcal{V}_{k_{(z,i)}, k_{(z,f)}, s}^{\mathbf{K}_{i}, \Delta \mathbf{K}}(-) c_{\mathbf{K}_{i} + \Delta \mathbf{K}, k_{(z,f)}}^{\dagger} c_{\mathbf{K}_{i}, k_{(z,i)}} a_{\mathbf{Q}, s} \right]
+ h.c. \right] \propto g,$$

$$\mathcal{W}_{l}^{(2)} = -\frac{1}{2} [G_{1}, [G_{1}, \mathcal{H}_{l}]]
\approx \sum_{\mathbf{K}_{i}, k_{(z,i)}, k_{(z,f)}} c_{\mathbf{K}_{i}, k_{(z,i)}} c_{\mathbf{K}_{i}, k_{(z,f)}}
\times \sum_{\Delta \mathbf{K}, k'_{(z,f)}, s} \hbar \nu_{l} [\mathcal{V}_{k_{(z,i)}, k'_{(z,f)}, s}^{\mathbf{K}_{i}, \Delta \mathbf{K}}(+)]^{*} \mathcal{V}_{k'_{(z,f)}, k_{(z,f)}, s}^{\mathbf{K}_{i}, \Delta \mathbf{K}}(+) \propto g^{2},$$
(8.51)

where, for continuum-continuum transitions

$$\mathcal{V}_{k_{(z,i)},k_{(z,f)},s}^{\mathbf{K}_{i},\Delta\mathbf{K}}(\mp) = \frac{gV_{k_{(z,i)},k_{(z,f)},s}^{\mathbf{K}_{i},\mathbf{K}_{f},\mathbf{Q}}\delta_{\mathbf{K}_{f},\mathbf{K}_{i}+\mathbf{Q}+\mathbf{G}}}{\hbar}$$

 $^{^{11}}G_2^{diag}$ is obviously closely related to $\Phi_{\mathbf{Q},s}(t,t_0)$ in equation (7.33).

$$\times \int_{-\infty}^{\infty} dt_1 e^{\pm \frac{i}{\hbar} (\epsilon(\mathbf{K}_f, k_{(z,f)}) - \epsilon(\mathbf{K}_i, k_{(z,i)}) \mp \hbar \omega_{\mathbf{Q},s}) t_1} \\
= \frac{\tilde{V}_{k_{(z,i)}, k_{(z,f)},s}^{\mathbf{K}_i, \mathbf{K}_i + \mathbf{Q} + \mathbf{G}} \delta_{k_{(z,f)}, k_z(\pm)} \Theta(k_z(\pm)^2)}{\hbar} \tag{8.52}$$

as in equation (6.28). Here, the tilded matrix element, V, is calculated with projectile atom wave functions normalized with respect to the unit current in the z-direction, and is box-normalized in the two lateral directions i.e. the wave functions bear a multiplicative factor $1/\sqrt{L_S^2 v_z}$ (see *Chapter 6*).

We can now proceed and calculate the cumulants $\langle \mathcal{W}(\varepsilon) \rangle$, ..., needed for the energy and lateral momentum resolved spectrum $N_{\mathbf{k_i}}(\varepsilon)$ in equation (8.37). Since the time dependence of $\mathcal{W}(\varepsilon)$ is governed by the unperturbed part of the hamiltonian \mathcal{H} corresponding to target phonons, the transformation $e^{i\mathcal{H}\varepsilon}(...)e^{-i\mathcal{H}\varepsilon}$ acting on $c_{\mathbf{k'}}^{\dagger}c_{\mathbf{k}}a_{\mathbf{Q},s}$ combination of operators produces

$$c_{\mathbf{k}'}^{\dagger} c_{\mathbf{k}} a_{\mathbf{Q},s} \exp(-i[\omega(\mathbf{Q},s)\tau - \mathbf{Q} \cdot \mathbf{R}]).$$

After some mathematics [65], we conclude that only the first two cumulants need be taken into account in the EBA and we arrive at the expression

$$N_{\mathbf{k}_{i},T_{s}}^{EBA}(\varepsilon,\Delta\mathbf{K}) = \int_{-\infty}^{\infty} \frac{d\tau d^{2}\mathbf{R}}{(2\pi\hbar)^{3}} e^{\frac{i}{\hbar}(\varepsilon\tau-\hbar(\Delta\mathbf{K})\mathbf{R})} \times \exp[2W^{EBA}(\mathbf{R},\tau) - 2W^{EBA}(0,0)], \quad (8.53)$$

where

$$2W^{EBA}(\mathbf{R},\tau) = \sum_{\mathbf{G},\mathbf{Q},s,k_{(z,i)}} \left[|\mathcal{V}_{k_{(z,i)},k_{(z,f)},s}^{\mathbf{K}_{i},\mathbf{Q}+\mathbf{G}}(+)|^{2} \left[\bar{n}(\hbar\omega(\mathbf{Q},s)) + 1 \right] \right] \times e^{-i(\omega(\mathbf{Q},s)\tau - (\mathbf{Q}+\mathbf{G})\cdot\mathbf{R})} + |\mathcal{V}_{k_{(z,i)},k_{(z,f)},s}^{\mathbf{K}_{i},\mathbf{Q}+\mathbf{G}}(-)|^{2} \bar{n}(\hbar\omega_{\mathbf{Q},s})e^{i(\omega(\mathbf{Q},s)\tau - (\mathbf{Q}+\mathbf{G})\cdot\mathbf{R})} \right],$$

$$(8.54)$$

is the so-called driving function which is generally complex and whose zero point value $2W^{EBA}(0,0) = 2W_{T_S}^{EBA}$ gives the *Debye-Waller exponent* in the EBA. Here $\omega(\mathbf{Q}, s)$ is restricted only to positive values and \bar{n}_{ph} is the Bose function describing the initial distribution of phonons thermally excited in the substrate kept at finite temperature T_S . Equations (8.53) and (8.54) describe the scattering spectrum containing all uncorrelated real multiphonon processes.

The EBA expression for the *Debye-Waller factor* which describes specular elastic scattering is then given by the $\delta(\varepsilon)\delta(\Delta \mathbf{K})$ component of the scattering spectrum. For substrates at finite temperatures T_S this reads:

$$e^{-2W^{EBA}} = \exp\left\{-\sum_{\mathbf{G},\mathbf{Q},s,k_{(z,i)}} \left[|\mathcal{V}_{k_{(z,i)},k_{(z,f)},s}^{\mathbf{K}_{i},\mathbf{Q}+\mathbf{G}}(+)|^{2} \left[\bar{n}_{ph}(\hbar\omega(\mathbf{Q},s)) + 1 \right] \right] + |\mathcal{V}_{k_{(z,i)},k_{(z,f)},s}^{\mathbf{K}_{i},\mathbf{Q}+\mathbf{G}}(-)|^{2} \bar{n}_{ph}(\hbar\omega(\mathbf{Q},s)) \right]$$

$$= e^{-\sum_{f\neq i} R_{fi}^{DWBA}}, \tag{8.55}$$

where R_{fi}^{DWBA} is the reflection coefficient introduced in Chapter 6.

The mean energy transferred in the course of a collision can be found in the EBA as

$$\mu_1^{EBA}(\mathbf{k}_i, T_S) = \int_{-\infty}^{\infty} \varepsilon d\varepsilon \int_{-\infty}^{\infty} d(\Delta \mathbf{K}) N_{\mathbf{k}_i, T_s}^{EBA}(\varepsilon, \Delta \mathbf{K})$$
(8.56)

which can be easily shown to reduce to

$$\mu_1^{EBA}(\mathbf{k}_i, T_S) = i \frac{\partial}{\partial \tau} 2W^{EBA}(\tau = 0, \mathbf{R} = 0). \tag{8.57}$$

8.5 Additional comments concerning the use of the EBA in atom-surface scattering

After all the mathematics in the previous section, it is still not quite clear what kind of physical approximations have been introduced. In this section, I will try to give at least a partial answer to this question.

First, due to all the approximations introduced, only the uncorrelated multiphonon processes are included in the EBA. The subsequent emissions (absorptions) of phonons in the EBA are assumed to be statistically independent [67]. This means that the emission (absorption) of a phonon does not depend on what has happened to the projectile atom "in the past" i.e. whether it already emitted (absorbed) some other (or the same) phonon. We could also say, that the projectile atom emits (absorbs) phonons with the same probability amplitude during its motion through the phase space. If this were really the choice of Nature, then only G_1 and the diagonal component of G_2 (G_2^{diag}) would survive in (8.18).

Second, note that the EBA is quite similar to the forced oscillator model. The EBA was in fact inspired by the forced oscillator model, as I hoped to show by introducing numerous footnotes pointing to this fact. The only difference is that in the forced oscillator model, $\mathcal{W}^{(1)}$ and $\mathcal{W}^{(2)}$ are operators composed of only phonon operators (a, a^{\dagger}) , while in the EBA, they contain also the projectile operators (c, c^{\dagger}) . If we write in EBA everywhere where the $c_{\mathbf{k}'}^{\dagger}c_{\mathbf{k}}$ combination of operators occurs, the $c_{\mathbf{k}_i}^{\dagger}c_{\mathbf{k}_i}$ instead (diagonal, recoilless term), the projectile atom becomes represented by a c-number, rather than by an operator and we recover the forced oscillator model - the projectile atom becomes the time dependent force. Where the EBA goes beyond the forced oscillator model is the effect of recoil because the interaction matrix elements in (8.52) depend on both the initial and final projectile states.

Third, the EBA is a unitary approximation: it conserves the particle current during the collision. However, the EBA does not conserve total energy in the collision event. Although the EBA conserves energy in each one-phonon emission (absorption) event (as the DWBA also does), there is a finite probability in the EBA that projectile loses more energy than it has initially carried (even when one includes the sticking processes). In the region of parameters where the EBA should work, these probabilities are vanishingly small (although not zero).

Fourth, if we expand the exponential of the driving function (8.54) around the point ($\mathbf{R} = 0, \tau = 0$) up to the first order, and substitute it in (8.53), we obtain the DWBA approximation. Thus, for low Debye-Waller exponents, where this expansion is allowed, the EBA reduces to the DWBA. On the other hand, if we deal with the situation where the scattering is quasielastic regarding the projectile motion i.e. the projectile atom final state is quite close to its initial state which happens for heavy atoms (Kr,Xe) which recoil negligibly, we obtain the trajectory approximation (forced oscillator model) result [19]. Therefore, the EBA smoothly interpolates between the single-phonon regime (DWBA) and quasielastic multiphonon regime (forced oscillator model). Figure 8.1 illustrates the EBA and the FOM-TA (forced oscillator model-trajectory approximation) calculation of the Debye-Waller exponent for the scattering system Ar \rightarrow Cu(111) [19, 58]. The potential parameters were fixed in this calculation (as in section 9.2 - see also the approximations to the phonon spectrum of Cu(111) surface) but the projectile mass was varied in steps of 1 amu (atomic mass unit). The projectile incident energy is $\epsilon_i = 36$ meV and the incident angle is $\theta_i = 70^{\circ}$. The results for the Debye-Waller exponent (DWE) are plotted as a function of the projectile mass, both for $T_S \to 0$ and $T_S = 300$ K. It can be seen that

 $^{^{12}\}mathcal{W}^{(2)}$ becomes a c-number [64] for the forced oscillator model.

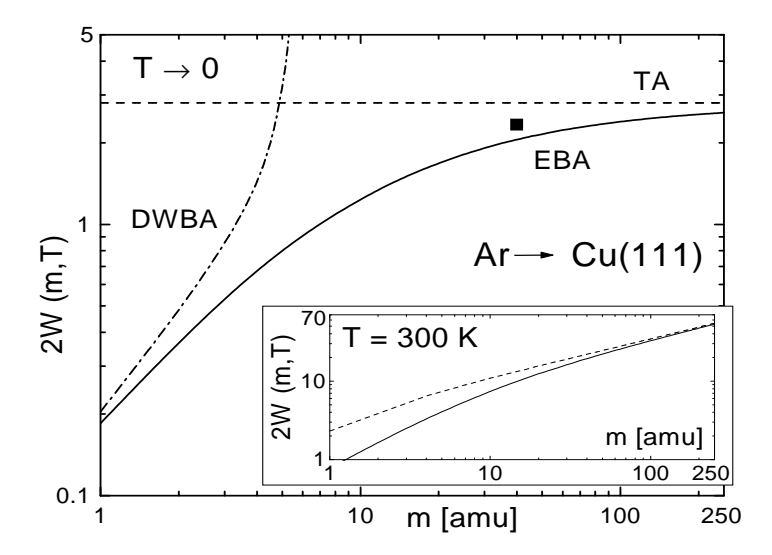


Figure 8.1: 2W(0,0) (DWE) for "Ar" \rightarrow Cu(111) scattering as a function of the projectile mass. Full line: EBA calculation. Dashed line: Trajectory approximation. Dash-dotted line: DWBA calculation. Square: Experimental point.

 $2W(T_S \to 0)$ does not depend on projectile mass in FOM-TA (dashed lines), but it does in EBA (full lines). The FOM-TA values are seen to be the limiting values of EBA when the projectile mass, m tends to infinity, i.e. when the scattering is truly quasielastic. Negative logarithm of the DWBA elastic scattering probability (this is DWBA counterpart of the Debye-Waller exponent) is also plotted in this figure (dash-dotted line). As promised at the end of previous chapter, the EBA smoothly interpolates between the DWBA and the TA values, reducing to the DWBA (TA) in the low (high) projectile mass limit. The experimental point in this graph was taken from reference [58]. The version of the forced oscillator model chosen for the calculations displayed here [18] 13 does not include recoil effect. There are ways to approximately include the recoil effect in the FOM-TA calculations [16, 21] which makes the FOM-TA model to agree better with the EBA [68].

¹³We have used the FOM-TA version of reference [18] and applied it to the scattering system studied as it was applied in reference [58].

Chapter 9

Comparison of theoretical and experimental results for selected scattering systems

The computer can't tell you the emotional story. It can give you the exact mathematical design, but what's missing is the eyebrows.

Frank Zappa

THEORY OF
THERMAL ENERGY
INERT ATOM
SCATTERING FROM
SURFACE VIBRATIONS

Antonio Šiber

In this chapter I shall present the examples of application of the EBA scattering formalism developed in *Chapter 8* to selected scattering systems studied experimentally. The chapter is divided in several sections. First five sections specify the models of interaction potentials and vibrational dynamics of the systems studied and the remaining sections are concerned with the calculated scattering spectra and related quantities pertaining to these systems.

* Scattering systems

$9.1 \quad ext{He} ightarrow ext{Cu}(001)$

This system was studied using the EBA formalism in references [7, 69, 54]. The phonons of the Cu(001) surface were modeled by a single phonon branch corresponding to the Rayleigh wave (RW) of Cu(001) surface. The dispersion of this mode was taken to be linear and independent of the direction of the wave vector **Q** with a maximum frequency of $\omega_D = 25$ meV at the edge of the surface Brillouin zone which was approximated by a circle (reference [7]). The polarization vector of the mode was taken to be in z-direction, localized at the surface according to $|\mathbf{e}(\mathbf{Q})|^2 = 3\omega(|\mathbf{Q}|)/2\omega_D$. This relation is correct for long wavelength phonons, but is surely incorrect for larger values of $|\mathbf{Q}|$ where it produces unphysical localization larger than 1. However, the density of states of such a model is exactly the same as in the well known Deby model of phonons. More sophisticated model was used in reference [54], where the dispersion of the RW(Cu(001)) mode was taken to be sinusoidal with a maximum frequency of 17.5 meV at the K point of the surface Brillouin zone ¹. The polarization vectors were again taken to be in the z-direction, with a localization modeled according to lattice dynamical calculations (this produces the correct long wavelength behavior). The static interaction potential was approximated by the uncorrugated Morse potential (see equation (3.15)) with parameters specified in the table below.

¹The Cu crystal has the FCC structure with the lattice parameter a(Cu) = 3.61 Å.

	Morse potential parameters		
System	D [meV]	d [Å]	$z_0 [A]$
$\text{He} \to \text{Cu}(001)$	7.0	0.926	3.64

This model interaction potential is in a good agreement with the one calculated in reference [31]. The simplified model of the vibrational dynamics of Cu(001) surface allows one to calculate the coupling of He atoms only to the topmost layer of the target atoms.

9.2 Ne, Ar, Kr \rightarrow Cu(111)

These scattering systems were studied by means of the EBA formalism in reference [19]. The isotropic Debye model for RW mode of Cu(111) was again used with a maximum frequency of $\omega_D = 23$ meV ². The Brillouin zone was taken to be circular in shape. For Ne, Ar, Kr \rightarrow Cu(111) scattering systems the Morse potential parameters are specified in the table below.

•••	Morse potential parameters		
System	D [meV]	d [Å]	$z_0 [A]$
$Ne \rightarrow Cu(111)$	15.8	0.778	3.33
$Ar \rightarrow Cu(111)$	58.2	0.799	3.33
$Kr \rightarrow Cu(111)$	89.5	0.826	3.28

The D and d parameters were taken from calculations in reference [71] (see also reference [58]). These potentials support $\approx 10, 26$ and 48 bound states for Ne, Ar and Kr, respectively, so that the prompt sticking effects (the projectile atom after the collision event may remain in one of the bound states of the interaction potential) dominate in these systems at low projectile incident energies. The effects of sticking were calculated in references [19, 57].

Figure 9.1 displays the static interaction potential used in the EBA calculations (to be presented) for the scattering systems described in this section.

9.3 He \rightarrow Xe/Cu(111)

This system was studied within a framework of the EBA in references [55, 54, 72]. The phonons of this system were studied in references [55]

²The experimental phonon spectrum of Cu(111) can be found in ref. [51]

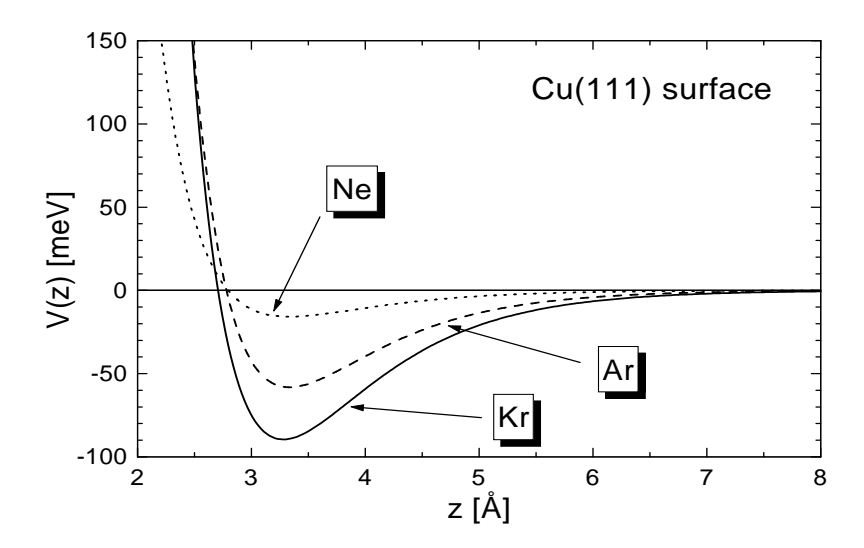


Figure 9.1: The Morse static interaction potentials for Ne, Ar, Kr \rightarrow Cu(111) scattering.

and [54] by setting up the full dynamical matrix in the slab approach described in *Chapter 4*. This was possible due to the fact that Xe atoms on Cu(111) substrate form a commensurate overlayer structure [55], so that the periodicity in the directions parallel to the surface exists. Namely, the Xe overlayer forms a hexagonal $(\sqrt{3} \times \sqrt{3})R30^{\circ}$ close packed (HCP) two dimensional structure commensurate with the substrate [73] (see figure 3.2). The parameters needed for the calculation of the dynamical matrix are specified in the following table:

Force constant	Value [N/m]
β_1^{Cu-Cu}	28.0
β_1^{Xe-Cu}	3.7
α_1^{Xe-Cu}	0.086
β_1^{Xe-Xe}	0.5
α_1^{Xe-Xe}	0

The nearest neighbor Xe-Xe distance is $d^{Xe-Xe} = 4.42 \text{ Å}[73]$. All other force constants were set equal to zero. Subscript 1 denotes the coupling to the nearest neighbor atom. Superscripts denote the atoms which are connected via a particular force constant. α 's and β 's are the tangential and radial force constants, respectively (see *Chapter* 4). Note here that the force constant β_1^{Xe-Xe} needed to reproduce the dispersion

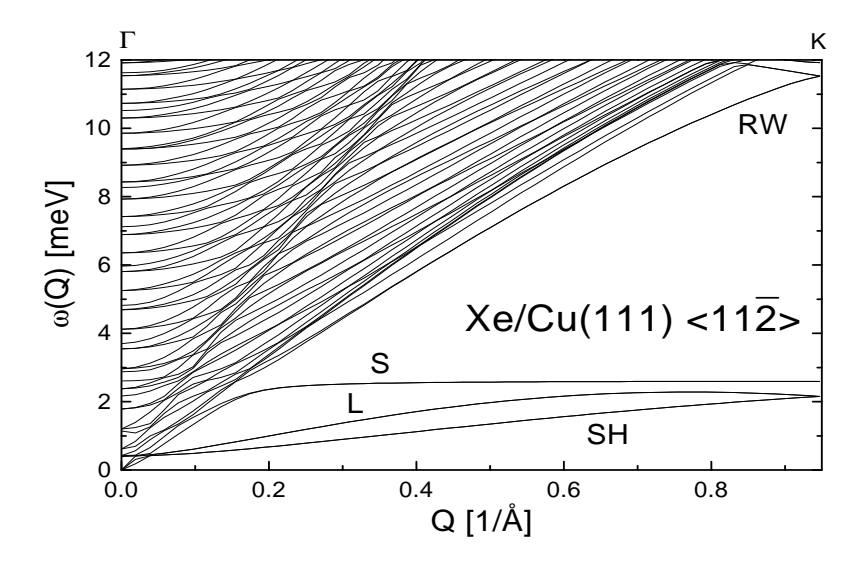


Figure 9.2: The dispersion curves for phonons of the Xe/Cu(111) system along Γ -K direction of the surface Brillouin zone. Xe overlayer induced modes are denoted by SH, L and S. Rayleigh wave mode of Cu(111) surface is denoted by RW.

relations is 3 times smaller than the value one would expect from Xe-Xe gas phase interaction potential. The reason for this extreme force constant softening is at present unclear and may be indicative of some peculiarity of the Cu substrate [55, 74, 75, 76]. The attempt to interpret the peaks observed in TOF spectra for this system as pertaining to shear horizontal mode has failed, because the probability of exciting the shear horizontal mode along the high symmetry direction of the surface Brillouin zone is vanishingly small and exactly zero in the DWBA [55, 75, 76]. The dispersion of vibrational modes obtained from the present dynamical matrix calculation are displayed in figure 9.2.

There are three modes (denoted by SL, L and S in figure 9.2) in this system which are almost exclusively localized in the Xe overlayer and with mutually perpendicular polarization vectors (except for small interval in \mathbf{Q}). The SH mode is polarized dominantly in the surface plane with the polarization vector perpendicular to the wave vector \mathbf{Q} (shear horizontal mode), the L mode is polarized dominantly in the surface plane with the polarization vector parallel to the wave vector \mathbf{Q} (longitudinal mode) and the S mode is polarized dominantly in z-direction (shear vertical or transverse mode). Note that the S mode

is almost dispersionless with a constant frequency of 2.62 meV. The L mode exhibits a zone-center frequency gap i.e. $\omega(Q=0,L)=0.4$ meV $\neq 0$ which is a consequence of the commensurability of Xe monolayer with the Cu(111) substrate [77]. The magnitude of this gap is directly related to the tangential Xe-Cu force constant, α_1^{Xe-Cu} . It is interesting to note here that from the magnitude of the L-phonon zone center gap one can extract the information on the corrugation of the adsorbate (Xe) - substrate (Cu) interaction potential [55, 77] which is of great importance for the theory of sliding friction and structural phase transitions [2, 78, 79].

More detailed characteristics of the polarization vectors of these modes are displayed in figure 9.3. Note that the S mode becomes surface delocalized in the wave vector region where it meets the RW phonon of the Cu substrate (the region of avoided crossing). The same happens to the L mode (only at a different value of the wave vector, since the L mode meets the RW mode of Cu(111) surface for smaller Q) and the L mode becomes additionally elliptically polarized i.e. its polarization vector, $\mathbf{e}(\mathbf{Q}, s = L)$, exhibits a small z-component (max. $\approx 14\%$).

A more detailed discussion of phonons in this system can be found in reference [55]. The surface averaged ($\mathbf{G}=0$ component) of the He \rightarrow Xe/Cu(111) interaction potential was modeled with the Morse potential with the parameters specified in the table below.

	Morse potential parameters		
System	D [meV]	d [Å]	z ₀ [Å]
$\mathrm{He} \to \mathrm{Xe/Cu}(111)$	6.6	0.82	3.49

This potential supports three bound states with energies $E_0 = -4.53$ meV, $E_1 = -1.55$ meV and $E_2 = -0.13$ meV. The parameters of the potential are quite close to those obtained using the pairwise summation of He-Xe gas-phase potentials [22, 29, 55, 80].

$9.4~{ m He} ightarrow { m Xe/Cu}(001)$

This system was studied both experimentally and theoretically in references [74, 73, 55, 72]. Xe monolayer forms again the HCP structure which is, however, incommensurate with the Cu(001) substrate, so that the full dynamical matrix cannot be set up for this system. It is possible [81], however, to treat the Cu(001) substrate as a rigid and homogeneous supporting medium for the Xe overlayer. The diagonalization

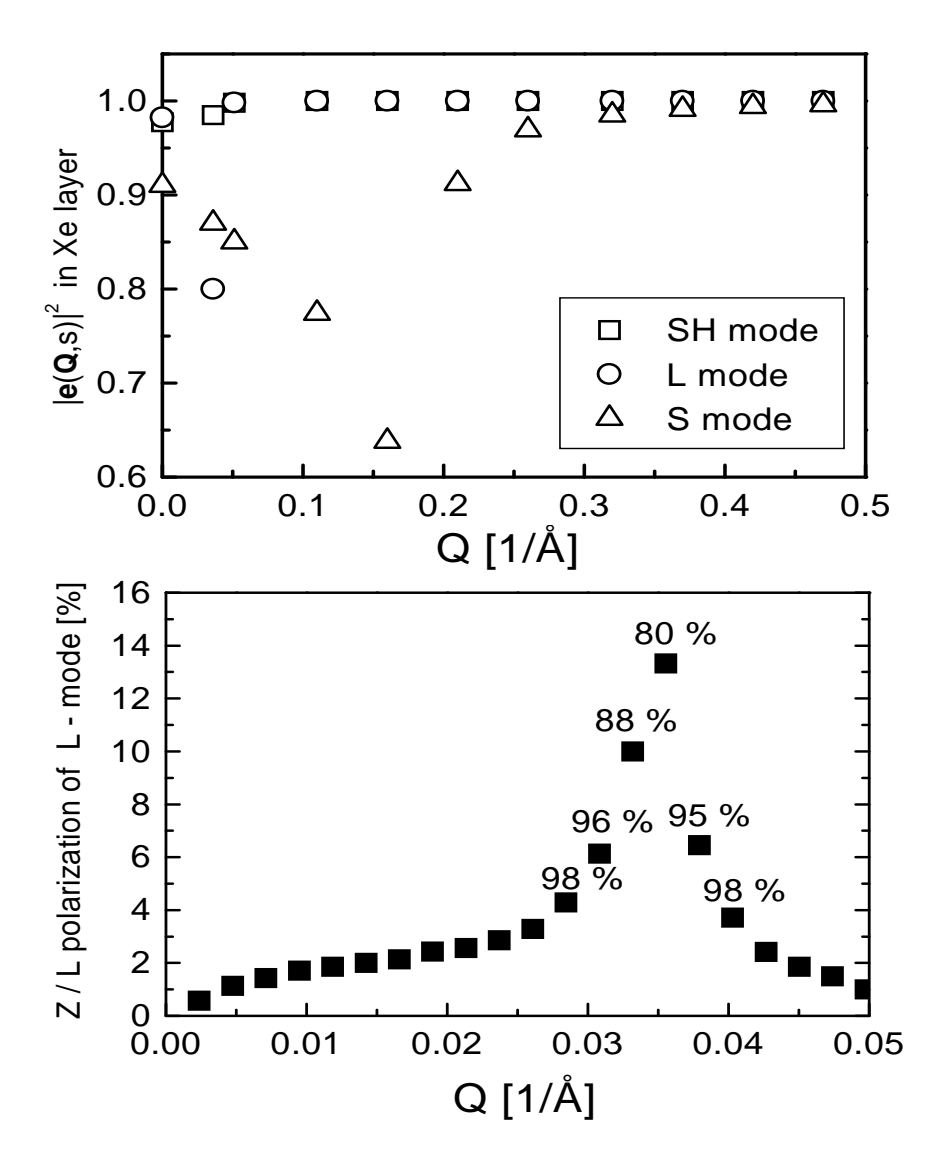


Figure 9.3: The polarization vectors of SH, L and S phonons of Xe/Cu(111). Upper panel displays the localization of the modes, while the lower panel displays the portion of the z- polarized component of the polarization vector of the L-phonon. The percentage above the full squares in lower panel denotes the localization of the L-mode in the adlayer.

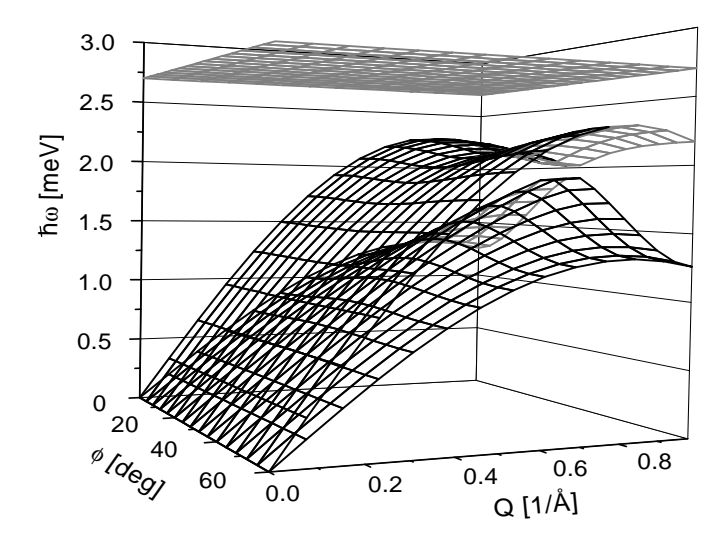


Figure 9.4: The dispersion curves of SH,L and S modes of Xe monolayer on Cu(001) surface as a function of the direction (angle ϕ) in the Brillouin zone of the Xe superstructure. $\phi = 0^o$ corresponds to $(\Gamma-M)_{Xe}$ direction.

of the one-layer dynamical matrix then produces dispersion curves and polarization vectors of SH, L and S modes which are of completely pure character (either z, longitudinal or shear horizontal for all values of \mathbf{Q}) and 100 % localized in the Xe monolayer. The parameters needed for setting up the dynamical matrix are specified in the table:

Force constant	Value [N/m]
$\beta_1^{Xe-Cu(001)}$	3.8
β_1^{Xe-Xe}	0.42
α_1^{Xe-Xe}	0.012

The nearest neighbor Xe-Xe distance is $d^{Xe-Xe}=4.40$ Å for this system [74, 55]. $\beta_1^{Xe-Cu(001)}$ force constant is again much softer than one would expect from Xe-Xe gas phase interaction potential. Due to the incommensurability of the Xe adlayer with the Cu(001) substrate, the L mode does not exhibit a zone center gap in this system , which is also confirmed experimentally [74]. Figure 9.4 displays the dispersion curves of SH, L and S modes of Xe/Cu(001) obtained from the dynamical matrix with the parameters specified above. The parameters of the He \rightarrow Xe/Cu(001) Morse interaction potential are specified in the table below.

	Morse potential parameters		
System	D [meV]	d [Å]	z ₀ [Å]
$\mathrm{He} \to \mathrm{Xe/Cu}(001)$	6.4	1.03	3.60

$9.5 \quad ext{He} ightarrow ext{Xe}(111)$

The vibrational dynamics of Xe(111) can be quite successfully described by the use of a slab lattice dynamics formalism. It turns out that the force constants needed to reproduce the experimentally determined dispersion curves are quite close to those obtained from Xe-Xe gas phase potential [82]. Unlike in the previous models, we have here connected the first and second neighboring Xe atoms. The parameters used for setting up the dynamical matrix for this system are:

Force constant	Value [N/m]
β_1^{Xe-Xe}	1.58
β_2^{Xe-Xe}	-0.075
$\frac{\alpha_1^{Xe-Xe}}{\alpha_1^{Xe-Xe}}$	0.004
α_2^{Xe-Xe}	0.015

All other force constants were set equal to zero. The subscripts 1 and 2 correspond to nearest and second nearest neighbor force constants. The nearest neighbor Xe-Xe distance is $d^{Xe-Xe} = 4.37$ Å[83] and the Xe crystal grows in the FCC crystallographic arrangement. One should compare β_1^{Xe-Xe} force constants for this system with those for Xe/Cu(111) and Xe/Cu(001) systems. The dispersion curves obtained from the dynamical matrix with 50 Xe(111) slabs are shown in figure 9.5. The parameters of He \rightarrow Xe(111) Morse interaction potential were obtained from the pairwise summation of He-Xe gas phase potential [80] which yields the parameters specified in the table below.

	Morse potential parameters		
System	D [meV]	d [Å]	z ₀ [Å]
$\mathrm{He} \to \mathrm{Xe}(111)$	7.2	0.76	3.44

* Measurable quantities

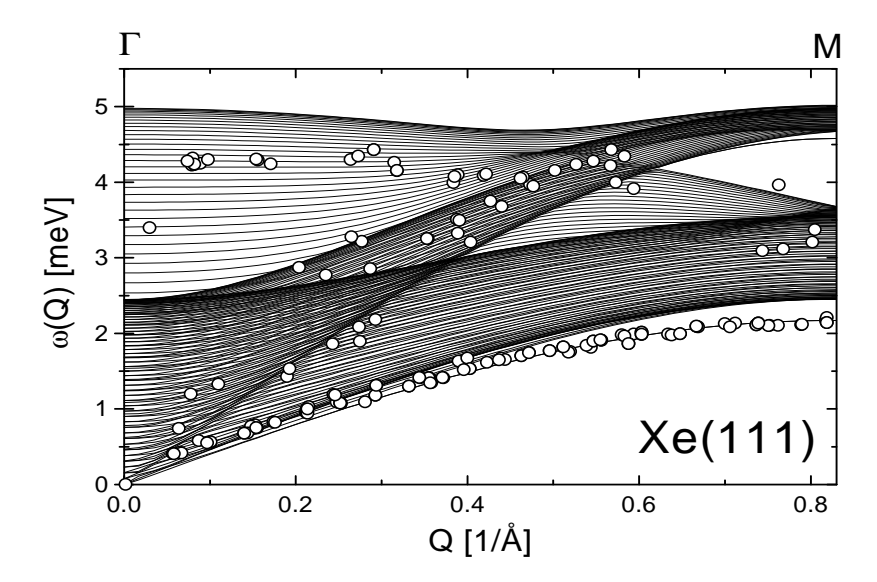


Figure 9.5: Phonon dispersion curves of Xe(111) along the Γ -M direction of the surface Brillouin zone. *Lines*: Lattice dynamics calculation. *Circles*: Experimentally determined peak positions.

9.6 Debye-Waller factor and exponent

The Debye-Waller factor in the EBA formalism is obtained from equation (8.55). Note that the depletion of the specular, elastic peak in the EBA arises as a consequence of inelastic processes: the projectile atom has a finite probability to emit (absorb) a phonon resulting in the change of its wave vector and energy. This is quite different from the Glauber - van Hove concept of the Debye-Waller factor [84, 85] in which there is no link through the energy or momentum conservation between the values of the lateral momentum change and lattice displacements appearing in the expression for the Debye-Waller exponent [49]. The Glauber - van Hove Debye-Waller factor can be interpreted as a consequence of renormalization of the interaction vertices by multiple vacuum fluctuations of the phonon field ("quantum noise"). On the other hand, the Debye-Waller factor in the EBA arises as a consequence of real on-the-energy-shell phonon excitation processes, which act so as to reduce the probability of detecting the projectile in the elastic channel.

A thorough discussion concerning the different concepts of the Debye-Waller factor can be found in references [86, 87].

In this section I shall present the evaluations of equation (8.55) for some of the scattering systems parametrized in the previous sections.

9.6.1 Ne, Ar, $Kr \rightarrow Cu(111)$

Figure 9.6 represents the comparison of the Debye-Waller exponent calculated in the EBA [19] with the measured probabilities of elastic scattering [58, 88] for the scattering systems Ne, Ar, Kr \rightarrow Cu(111). The well depths of the interaction potentials are larger than the "component of energy in z-direction" (this is the incident energy multiplied by the square of the cosine of the incident angle) which amounts to 4.21 meV, so that the effects of transitions into the bound states of the atom-surface potential cannot be neglected. To simplify the summation over the transitions into a large number of final bound states, $|b\rangle$, we have replaced the latter by a quasi-continuum and made use of the relation

$$\sum_{n_b} \to \int dn_b = \int d\epsilon_b \frac{1}{\left\{\frac{\partial \epsilon_b}{\partial n_b}\right\}},\tag{9.1}$$

where n_b is the quantum number of the bound state and ϵ_b is the energy of the state n_b . Equation (9.1) holds in the case of Ne, Ar and Kr atom-surface potentials ³. Calculations with the discrete spectrum of bound states have produced the values which for these systems are indistinguishable from those obtained from the quasi-continuum approximation for the bound states. However, when there are only few bound states, as is the case when the projectile is a He atom, the quasi-continuum approximation for bound states spectrum breaks down.

The agreement between the theoretical and the experimental results for the DWF in figure 9.6 is seen to be excellent. The trajectory approximation results of reference [18], applied as in reference [58], are seen to be inferior to the EBA although the trajectory approximation is generally assumed to correctly describe the scattering of heavy projectile atoms from surfaces. It was shown in reference [19] that the trajectory approximation cannot be safely applied in the regime of scattering studied here, and that e.g. Ar atom is not "heavy enough" for the trajectory approximation to hold ⁴.

³For the Morse potential, the derivative $\partial \epsilon_b/\partial n_b$ can be found in [89].

⁴It should be added here that more advanced schemes of trajectory approximation which approximately include the projectile recoil effect yield better results [68].

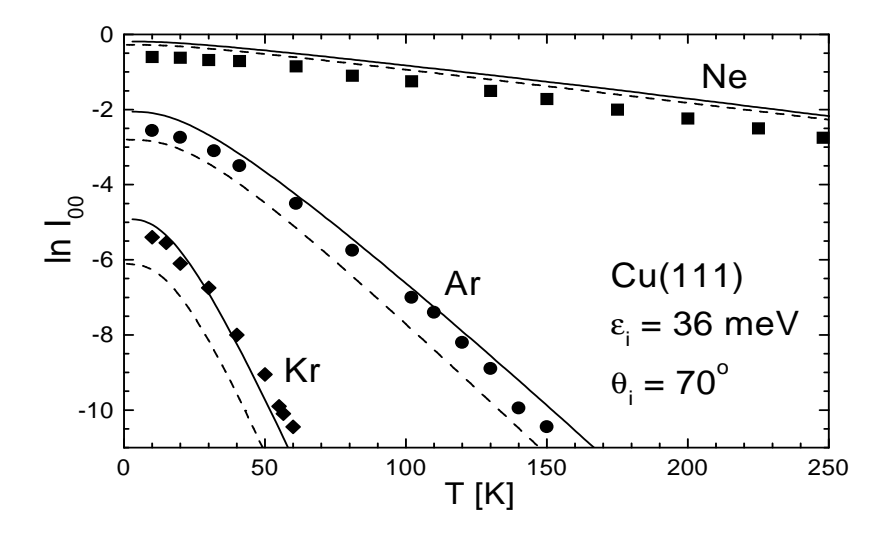


Figure 9.6: The Debye-Waller exponent for Ne, Ar, Kr \rightarrow Cu(111) scattering system. Full lines: EBA calculations. Dashed lines: Trajectory approximation. Symbols: Experimental data.

$9.6.2 \quad \mathrm{He} ightarrow \mathrm{Cu}(001)$

Figure 9.7 displays the calculation of the elastic part of the scattered intensity for He \rightarrow Cu(001) collision system [7]. The experimental results are taken from reference [90]. It is seen that the agreement is quite satisfactory, although an extremely simple model of vibrational dynamics of Cu(001) was used (the Debye model of the RW phonon of Cu(001) with a circular approximation for the surface Brillouin zone shape). The nonlinearity of surface vibrations of Cu(001) at higher target temperatures had to be included in the calculations. This was done by using a simple model as in reference [91].

$9.6.3 \quad \text{He} \rightarrow \text{Xe}(111)$

Figure 9.8 displays the calculation of the Debye-Waller exponent, 2W as a function of the projectile incident energy for the He \rightarrow Xe(111) collision system. Note the effects of transitions into the bound states for low incident energies of He. Since the final density of states for these transitions is discrete, a characteristic resonance behavior occurs when kinematic conditions favor the transition of He atom into a particular bound state of the He \rightarrow Xe(111) interaction potential by emission of

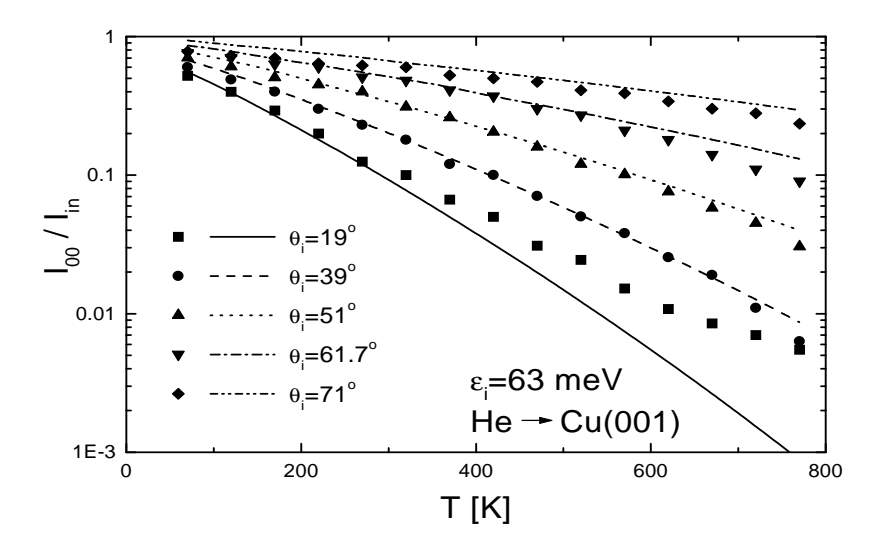


Figure 9.7: The probability of elastic scattering (Debye-Waller factor) for He \rightarrow Cu(001) scattering system as a function of the sample temperature. Lines: EBA calculation. Symbols: Experimental data.

a phonon. This effect is reminiscent of kinematic focusing [6, 92] and a similar resonance behavior was apparently found in reference [93] for H_2 and D_2 scattering from Cu(100) surface.

It should be added at the end of this section that comparisons of the calculated and measured values of the Debye-Waller factor can serve as a relatively straightforward measure of the reliability of the various atom-surface potentials [58, 19, 88, 7].

9.7 Angular resolved TOF spectra

The angular resolved TOF spectra can be obtained in the EBA formalism by using equation (8.53). The evaluations of this equation involve the use of direct and inverse Fast Fourier Transforms (FFT).

We have already presented two angular resolved TOF spectra in figures 5.2 and 6.2 recorded in the dominantly single-phonon regime of scattering. In this section we shall concentrate on multiphonon regime of scattering and the influence of multiphonon processes on the angular resolved TOF spectra.

There are basically two distinct types of multiphonon TOF spectra depending on the vibrational characteristics of the target. If the

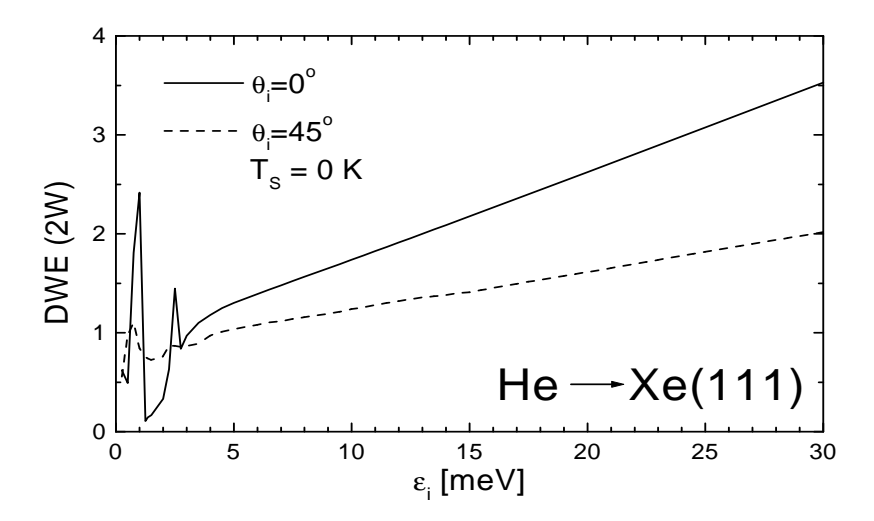


Figure 9.8: The Debye-Waller exponent (DWE) for He \rightarrow Xe(111) scattering system. Full line: $\theta_i = 0^o$. Dashed line: $\theta_i = 45^o$.

frequencies of dominantly z-polarized surface phonons do not exhibit dispersion (variation of phonon frequency with the phonon wave vector), as is the case for Xe/Cu(001) and Xe/Cu(111) systems, the TOF spectrum is dominated by a series of approximately equidistant peaks (on the scale of exchanged energy). On the other hand, if the frequencies of dominantly z-polarized surface phonons do show significant dependence on the phonon wave vector, the TOF spectrum has usually a continuous, gaussian-like appearance. This can be easily understood. The coupling of projectile atoms to the target vibrations is strongest for z-polarized modes and they dominate the TOF spectra, especially in the multiphonon scattering regime [54]. A particular multiphonon event consists of n_e emissions and n_a absorptions of phonons (n_a and n_e being integers). But, for the dispersionless z-polarized modes, this event leaves "a mark" (peak) in the TOF spectrum at exchanged energy equal to $\Delta E = \hbar \omega_S (n_a - n_e)$, where ω_S is the frequency of the mode. Therefore, the multiphonon spectrum pertaining to a surface sustaining dispersionless, dominantly z-polarized surface phonons, consists of discrete peaks separated by $\hbar\omega_S$. On the other hand, for surfaces supporting z-polarized surface phonons showing significant dispersion, we obtain a continuos TOF spectrum since the spectral intensity of multiphonon processes can be traced at any exchanged energy ΔE .

A direct numerical evaluation of equation (8.53) for dispersionless

modes is not feasible. However, it is possible to analytically simplify equation (8.53) to yield a more convenient form for numerical evaluation. It can be shown [57] that the TOF spectrum calculated for projectile scattering from dispersionless (i.e. Einstein) modes can be represented it the EBA as

$$N_{Einst.}^{EBA}(\Delta E, \Delta \mathbf{K}) = e^{-2W_S} \sum_{l=-\infty}^{\infty} N_l(\Delta \mathbf{K}) \delta(\Delta E - l\hbar\omega_S), \qquad (9.2)$$

where

$$N_l(\Delta \mathbf{K}) = \int \frac{d^2 R}{2\pi^2} e^{-i\Delta \mathbf{K} \cdot \mathbf{R}} P_l(\mathbf{R}), \qquad (9.3)$$

and

$$P_{l}(\mathbf{R}) = \left\{ \left[\sqrt{\frac{(n(\omega_{S}) + 1)\mathcal{V}_{S}^{2}(\mathbf{R}, +)}{n(\omega_{S})\mathcal{V}_{S}^{2}(\mathbf{R}, -)}} \right]^{l} \times I_{l}(\sqrt{4n(\omega_{S})(n(\omega_{S}) + 1)\mathcal{V}_{S}^{2}(\mathbf{R}, +)\mathcal{V}_{S}^{2}(\mathbf{R}, -))} \right\}, \quad (9.4)$$

with

$$\mathcal{V}_{S}^{2}(\mathbf{R}, \pm) = \sum_{\mathbf{Q}, k_{(z,f)}, \mathbf{G}} |\mathcal{V}_{k_{(z,f)}, k_{(z,i)}}^{\mathbf{K}_{i}, \mathbf{Q} + \mathbf{G}, S}(\pm)|^{2} e^{\pm i\mathbf{Q} \cdot \mathbf{R}}, \tag{9.5}$$

where the notation is the same as in Chapter 8 ($2W_S$ is the Debye-Waller exponent calculated for the dispersionless mode). Index S denotes here the particular dispersionless mode we are interested in.

Note that after the calculation of the TOF spectrum, N_{TOF}^{EBA} in the EBA, we must again select only those processes (i.e. combinations of ΔE and $\Delta \mathbf{K}$) which are seen by the detector (and which satisfy the lateral momentum and total energy conservation requirement). Therefore, we use the scan curve, as in the DWBA, equation (6.26) to select those processes.

9.7.1 He \rightarrow Xe/Cu(111)

Figure 9.9 shows the results of calculation of the EBA scattering spectrum based on equation (9.2) for the He \rightarrow Xe/Cu(111) collision system. Only S modes of Xe/Cu(111) were included in the calculation. The contribution of other modes can be safely neglected in the multiphonon regime due to their much weaker coupling to He atoms (see Chapter 4 and references [54, 57, 55]). The frequency of the flat mode

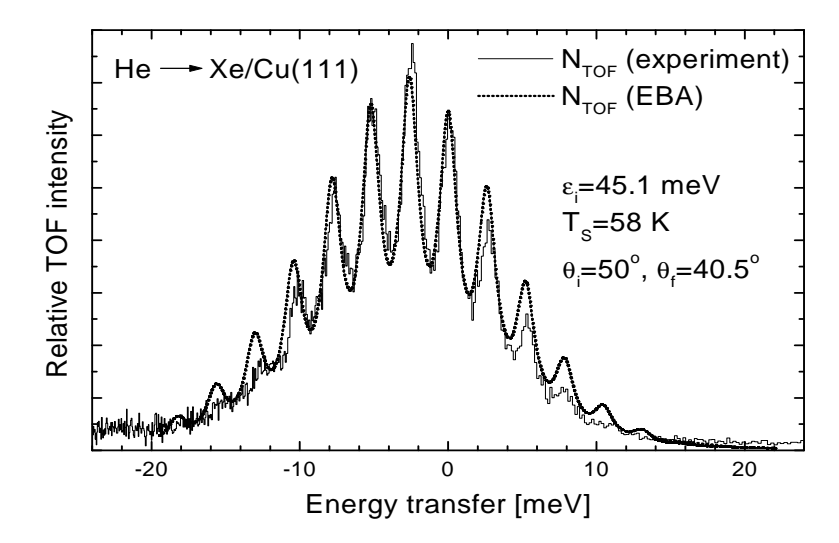


Figure 9.9: Comparison of experimental and EBA TOF spectrum for $He \to Xe/Cu(111)$ collision system. Full line: Experimental TOF spectrum. Dotted line: TOF spectrum in the EBA.

was set to $\omega_S = 2.62$ meV in accordance with the lattice dynamics calculations. The delta functions in (9.2) were broadened into lorentzians ⁵ to account for finite S-phonon lifetime and experimental resolution.

$9.7.2 \quad \mathrm{He} \rightarrow \mathrm{Xe/Cu}(001)$

A similar calculation was performed for the He \rightarrow Xe/Cu(001) collision system with the frequency of the S mode $\omega_S = 2.71$ meV. The results are displayed in figure 9.10. The agreement with the experimental data is somewhat less satisfactory, possibly due to a more disordered Xe overlayer than in the case of the Xe/Cu(111) system which is seen by the magnitude of the no-loss peak ($\Delta E = 0$). The small peak at $\Delta E = 1.5$ meV in the experimental TOF spectrum is due to the excitation of the Cu(001) Rayleigh wave mode. The theoretical peak at $\Delta E = -2.71$ meV was broadened more than the other peaks to account for smaller lifetime of S phonon in the region where its dispersion curve meets the

 $^{^{5}}$ The peaks should actually be of the so called Voigt profile which is a convolution of gaussian (experimental resolution) and lorentzian (lifetime) function.

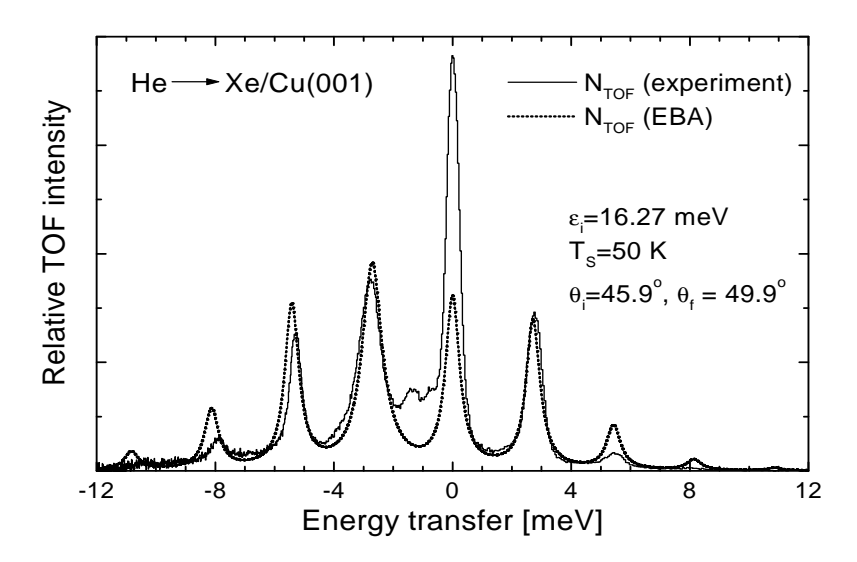


Figure 9.10: Comparison of experimental and EBA TOF spectrum for He \rightarrow Xe/Cu(001) collision system. *Full line*: Experimental TOF spectrum. *Dotted line*: TOF spectrum in the EBA.

dispersion curve of the Cu(001) Rayleigh wave phonon ⁶. Note also that the multiphonon spectrum in the EBA has a peak at $\Delta E = 0$ meV. This peak corresponds to the scattering events in which equal number of S phonons is emitted and absorbed. These multiphonon events are seen at zero energy transfer. There are no observable anharmonic shifts in the experimental TOF spectra in figures 9.9 and 9.10 which means that all S derived peaks are equally separated within the experimental uncertainty. If all phonons were excited on one Xe atom, then the anharmonic shifts deriving from the Xe-Cu interaction potential should be visible [55]. The fact that they are not visible, points to a particular physical picture of the phonon excitation mechanism. Namely, the phonons are excited in the surface as a whole and not on a particular surface atom. Therefore, the multiphonon scattering event with e.g. 5 phonons emitted does not correspond to one Xe atom being excited from e.g. n=0 to n=5 level of the harmonic oscillator, but more likely to five Xe atoms being excited from n = 0 to n = 1 levels.

 $^{^6\}mathrm{This}$ feature cannot be reproduced from the simple lattice dynamical model of the incommensurate Xe adlayers on $\mathrm{Cu}(001)$ surface because the $\mathrm{Cu}(001)$ substrate was assumed to be completely rigid in this model, but the RW is clearly observed in the experimental TOF spectrum

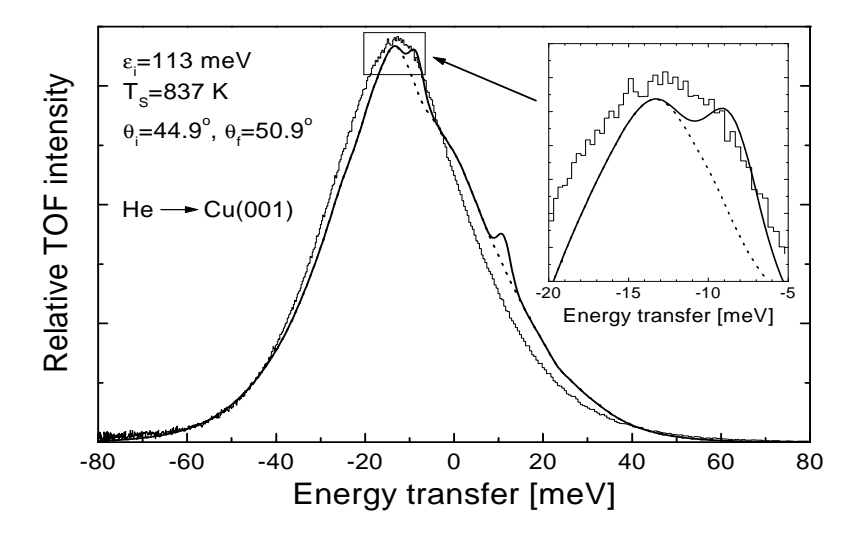


Figure 9.11: TOF spectra for He \rightarrow Cu(001) collision system along $\langle 110 \rangle$ -azimuth. Thin full line: Experimental TOF spectrum. Thick full line: TOF spectrum in the EBA. Thick dotted line: TOF spectrum in the EBA without the DWBA contributions.

This a posteriori justifies the assumption of linear coupling to atomic displacements which was introduced in all atom-target hamiltonians discussed in the previous chapters.

$9.7.3 \quad \mathrm{He} ightarrow \mathrm{Cu}(001)$

Figure 9.11 displays the multiphonon calculation for He \rightarrow Cu(001) collision system.

This calculation is much improved (concerning the model of the polarization vector) over the one reported in [54], and the overall agreement between the experimental and EBA results is much better. Only the coupling to the RW mode of the Cu(001) surface was considered. We have observed in our calculations that the overall agreement between the theoretical and experimental results decreases as the deviation of the scattering angle from the specular increases [54] (see figure 9.14). This is not too surprising since the EBA was constructed to work in "close-to-specular" conditions ⁷. Additionally, according to

⁷The term "quasielastic" in inverse space, mentioned many times in *Chapter 8*, means "close-to-specular" in direct space.

reference [56], the effects of correlations neglected in the EBA, become nonnegligible for such high incident projectile energy (113 meV). Also, the static surface corrugation becomes more pronounced as the turning point gets closer to the surface (see figure 3.1) i.e. as the projectile incident energy increases, so that the neglect of static surface corrugation becomes a questionable approximation for very high projectile energies. The calculation represented by the full thick line includes the full exponent $\exp(2W(\tau, \mathbf{R}))$. Dotted thick line represents the EBA calculation with the DWBA contribution subtracted. This means replacing $\exp[2W(\tau, \mathbf{R})]$ in equation (8.53) with $\exp[2W(\tau, \mathbf{R})] - 2W(\tau, \mathbf{R})$. Although the Debye-Waller exponent is quite large $(2W(0,0) = 6.2^{-8})$. the single phonon emission (absorption) peaks corresponding to the RW mode of Cu(001) are still visible, although probably not in the experimental TOF spectrum. This could be due to low energy resolution of $\approx 7 \text{ meV}$ [94, 95] at this high incoming energy. The angular integrated spectrum (as a function of exchanged energy) can be obtained by summing (integrating) the angular resolved TOF spectrum over all lateral wave vectors exchanged ($\Delta \mathbf{K}$). This calculation is presented in figure 9.12

Note that the calculation with the single phonon exchange contribution included becomes identical to the calculation with this contribution excluded beyond $|\Delta \mathbf{E}| = 18.0$ meV which is the maximum frequency of the RW mode throughout the surface Brillouin zone. Note also that the distribution denoted by the full line is quite close to the gaussian distribution, slightly wider on the loss side. Under extreme multiphonon conditions, the EBA can be shown to produce gaussian like spectra (both in $\Delta \mathbf{K}$ and ΔE coordinates) centered around the mean values $\langle E \rangle = \mu_1, \langle \Delta K_x \rangle = 0$ and $\langle \Delta K_y \rangle = 0$ [56].

$9.7.4 \quad \text{He} \rightarrow \text{Xe}(111)$

The angular resolved TOF spectrum in the single-phonon regime for He \rightarrow Xe(111) collision system was shown in figure 6.2. Concerning the present form of numerical procedures for evaluation of multiphonon TOF spectra, this system is not different from the system He \rightarrow Cu(001) except for different interaction potential, maximum RW frequency, the shape of the first Brillouin zone, and for the details of the polarization vector dependence on a wave vector. Since the RW mode

⁸It is often said that the true multiphonon scattering conditions are achieved when 2W(0,0) = 6 [94, 95], although it is not quite obvious (at least not to the author) what it actually means.

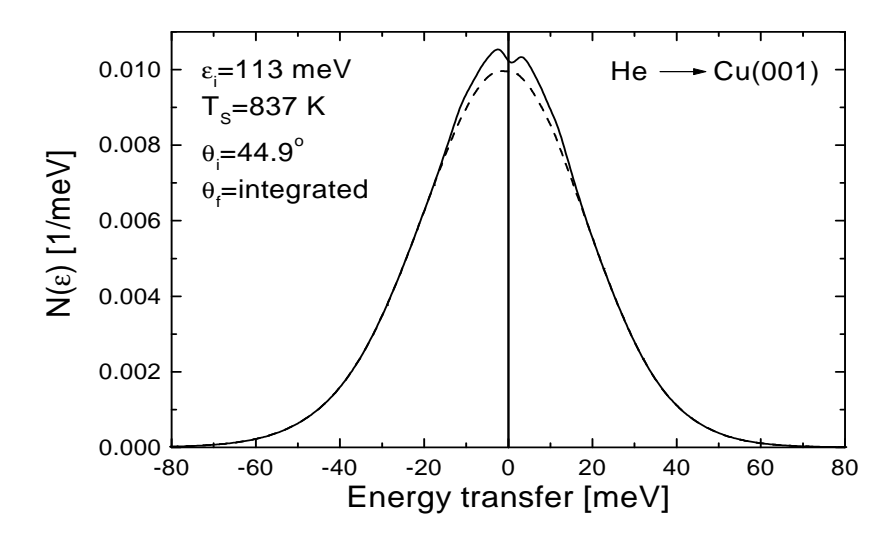


Figure 9.12: Angular unresolved spectrum in the EBA. Full line: EBA. Dashed line: EBA without first Born contributions.

of Xe(111) surface is much softer than the RW mode of the Cu(001) surface, the multiphonon conditions can be achieved at much lower projectile incident energies and the target temperature.

9.8 Mean energy transfer in atom-surface scattering

Mean energy transfer in the EBA can be obtained from equation (8.57). This is the mean energy transferred in the course of a collision irrespective of the final angle in which the scattered atom continues to move. This information cannot be obtained from the typical TOF experiment. However, one can obtain the average energy transferred by the scattered projectile atoms which scatter into the final angle θ_f , both experimentally and theoretically. We call this quantity the angular resolved energy transfer. It is calculated as

$$\mu_r^{EBA}(\epsilon_i, T_S, \theta_i, \theta_f) = \frac{\int_{-\infty}^{\infty} (\Delta E) d(\Delta E) N^{EBA}(\Delta E, \Delta \mathbf{K}(\Delta E))}{\int_{-\infty}^{\infty} d(\Delta E) N^{EBA}(\Delta E, \Delta \mathbf{K}(\Delta E))}$$

$$\mu_r^{exp}(\epsilon_i, T_S, \theta_i, \theta_f) = \frac{\int_{-\infty}^{\infty} (\Delta E) d(\Delta E) N^{exp}(\Delta E, \Delta \mathbf{K}(\Delta E))}{\int_{-\infty}^{\infty} d(\Delta E) N^{exp}(\Delta E, \Delta \mathbf{K}(\Delta E))}, (9.6)$$

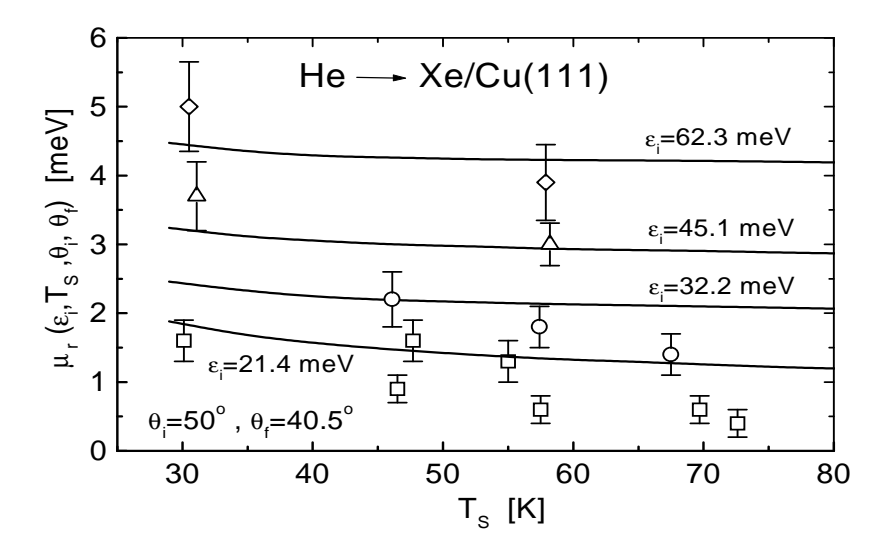


Figure 9.13: Angular resolved energy transfers for the He \rightarrow Xe/Cu(111) collision system as a function of the sample temperature for four different He incident energies. *Symbols*: Experimental data. *Lines*: The EBA calculation.

where $\mu_r^{EBA}(\epsilon_i, T_S, \theta_i, \theta_f)$ and $\mu_r^{exp}(\epsilon_i, T_S, \theta_i, \theta_f)$ are angular resolved energy transfers in the EBA and the experiment, respectively.

$9.8.1 \quad \mathrm{He} \rightarrow \mathrm{Xe/Cu}(111)$

Figure 9.13 displays comparisons of the calculated and measured angular resolved energy transfers for the He \rightarrow Xe/Cu(111) collision system. The results are plotted as a function of the sample temperature for four different He incident energies. The incident and final angles are fixed to $\theta_i = 50^o$ and $\theta_i = 40.5^o$, respectively. The agreement between the experimental and theoretical values for the angular resolved energy transfer is seen to be very satisfactory.

$9.8.2 \quad \mathrm{He} ightarrow \mathrm{Cu}(001)$

Figure 9.14 displays the calculation of the angular resolved energy transfer for the He \rightarrow Cu(001) collision system. The experimental data was taken from reference [94].

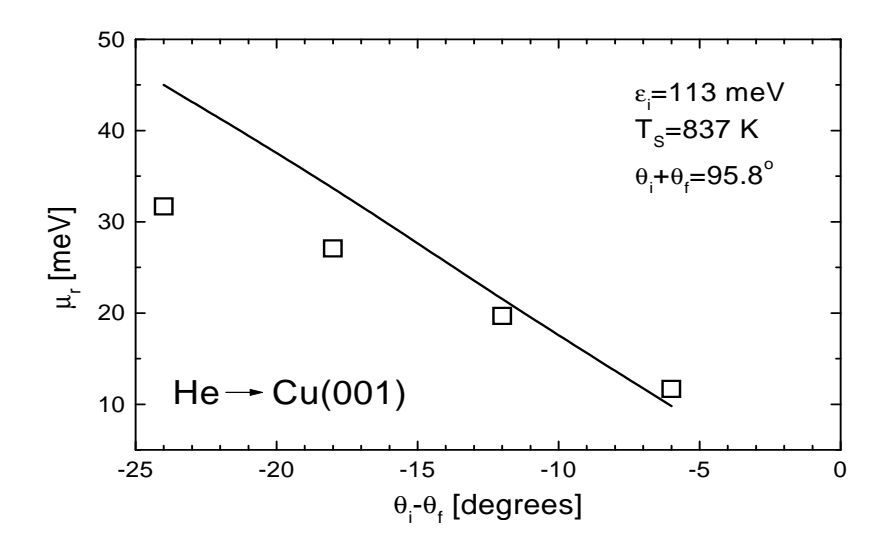


Figure 9.14: Angular resolved energy transfers for the He \rightarrow Cu(001) collision system as a function of the relative angle, $\Delta\theta = \theta_f - \theta_i$. Squares: Experimental data. Line: The EBA calculation.

9.8.3 Ne, Ar, Kr \rightarrow Cu(111)

In this subsection we present the evaluation of equation (8.57) for the Ne, Ar and Kr \rightarrow Cu(111) scattering systems. Although there is no experimental data concerning the mean energy transfer in these scattering systems we have a firm experimental confirmation of the EBA approach which is based on the measurement of the Debye-Waller factor for these systems (see figure 9.6). Figure 9.15 displays the mean energy transfer for Ne, Ar and Kr scattering from Cu(111) surface at zero temperature of the sample $(T_S = 0)$ as a function of the projectile incident energy. The incident angle was set to $\theta_i = 70^{\circ}$. The results are in qualitative agreement with the FOM-TA calculation of the mean energy transfer for Ne, Ar, Kr \rightarrow Ru(001) scattering systems reported in reference [21].

9.9 Comments on the applicability of the EBA to selected scattering systems

The theoretical results obtained by using the EBA and presented in the preceding section have been shown to agree quite satisfactorily with

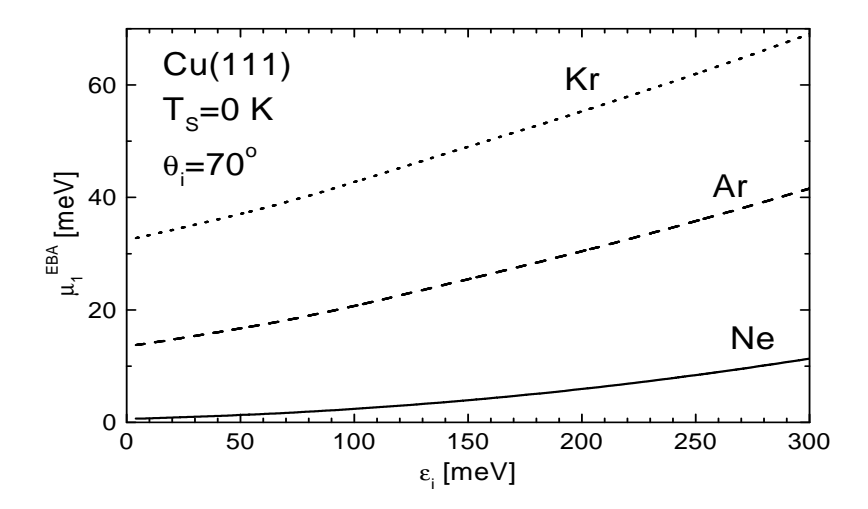


Figure 9.15: Mean energy transfers for the Ne, Ar, Kr \rightarrow Cu(111) collision system as a function of the projectile energy. Full line: The EBA calculation for Ne. Dashed line: The EBA calculation for Ar. Dotted line: The EBA calculation for Kr.

the experimental data, except for very off-specular scattering conditions which lie in the phase space beyond the applicability of the EBA.

In the case of metallic targets (such as Cu(001)), the disagreements between the experimental results and the results produced by the use of the EBA cannot be taken as an evidence of the inappropriateness of the EBA. Namely, the lattice dynamical approach to metallic samples may be even more questionable than the use of the EBA.

Chapter 10

Possible future investigations

Prediction is very difficult, especially of the future.

Niels Bohr

I have seen the future and it is just like the present, only longer.

Kehlog Albran

THEORY OF
THERMAL ENERGY
INERT ATOM
SCATTERING FROM
SURFACE VIBRATIONS

Antonio Šiber

The formalism developed in the preceding chapters to describe inelastic atom-surface scattering was based on several assumptions and approximations which deserve further comments.

- The corrugation of the interaction potential was completely neglected in all the calculations presented. One does not expect this effect to be of crucial importance for the atom-(metal surface) scattering, but it may become important for the systems where the charge delocalization is negligible (e.g. for the He → Xe(111) scattering system). The investigation of the interplay between elastic and inelastic processes in the EBA formalism is in progress [87].
- The approximation of the interaction potential with the Morse potential can be erroneous at extremely low incident projectile energies. This approximation can be easily corrected by introducing numerically calculated wave functions [40]. However this slows down the calculations and restricts the size of the parameter space (temperature of the sample, incident energy, incident angle, projectile atom mass etc.) amenable to examination. The approximation of \mathbf{Q} dependence of $v_{\mathbf{Q}}$, as in equation (6.20), does seem to be quite good, at least for the incident energies higher than 1 meV [40].
- The vibrational dynamics of the target was obtained by assuming the Born-Oppenheimer approximation (BOA) for the electrons of the target atoms. This can be questionable for metallic targets [35] and could be the reason of a failure of the DWBA approximation to describe the so called "anomalous" intensities of longitudinally polarized modes observed on some metal surfaces [35]. However, recent calculations do not support the break down of the BOA in the studied regime [4].
- Anharmonic effects in the vibrations of the target have not been taken into account. This may prove of importance for some calculations reported in *Chapter 6* and *Chapter 8*. Although this effect was approximately accounted for in the earlier publication [7], a nonphenomenological approach of including this effect may be required.
- For the evaluation of the multiphonon TOF spectra in the EBA, a precise information about dispersions and polarization vectors of the modes is needed for *all directions* in the surface Brillouin zone.

This is not the case in the DWBA where we need this information only along the direction of the lateral component of projectile's incident wave vector. For multiphonon TOF spectra presented in this thesis, simple analytical models for the dispersion relations and polarization vectors as a function of the direction in the reciprocal space were used. These models were, however, guided by the lattice dynamics calculations. It would be highly desirable to use the complete output of lattice dynamics calculation as an input for the EBA calculation. This requires a lot of reserved computer memory and CPU time, but some progress in this direction has already been achieved.

• The EBA itself is an approximation. Although the EBA has proven very successful in describing the scattering spectra presented in *Chapter 8*, it would be desirable to theoretically assess the validity of the EBA for every scattering system and every set of scattering parameters studied. These investigations have been carried out for a restricted number of collision systems [56] and for other systems of interest they are under way.

Chapter 11

Summary

If you permit yourself to read meanings into (rather than drawing meanings out of) the evidence, you can draw any conclusion you like.

Michael Keith, "The Bar-Code Beast", The Skeptical Enquirer Vol12(4)

 $A\ conclusion\ is\ the\ place\ where\ you\ got\ tired\ of\ thinking.$

Anonymous

THEORY OF
THERMAL ENERGY
INERT ATOM
SCATTERING FROM
SURFACE VIBRATIONS

Antonio Šiber

In this work I have described all the prerequisites needed to derive the Exponentiated Born Approximation (EBA) and apply it to the atom-surface scattering problems. The validity of the EBA has been tested in numerous comparisons with the existing experimental data. Although the EBA picks up only a selected class of the scattering amplitudes to all order, it is probably the most promising fully quantum formalism of all the previously used to model inelastic scattering of thermal energy inert atoms from surfaces. As the EBA smoothly interpolates between the single-phonon regime of scattering (DWBA) and multi-phonon scattering regime (FOM-TA), it can be used without too many restrictions in a large region of the scattering parameter space. The application of the EBA to the problems of technological interest (e.g. transfer of energy between the interstellar gas and the space vehicles) is currently in progress [57].

Appendix A A simple illustration of the normal modes calculations

For every problem there is one solution which is simple, neat, and wrong.

H.L. Mencken

THEORY OF
THERMAL ENERGY
INERT ATOM
SCATTERING FROM
SURFACE VIBRATIONS

Antonio Šiber

136 APPENDIX A

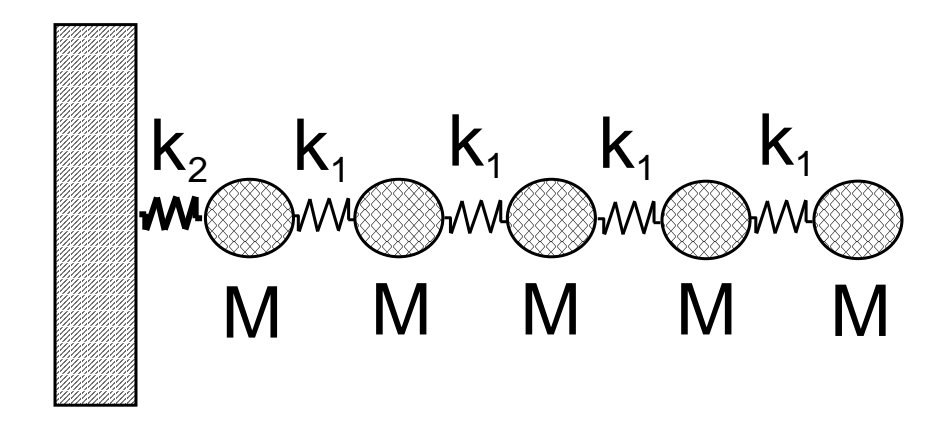


Figure A.1: A simplified vibrational model of epitaxially grown thin film at $\mathbf{Q} = 0$.

The aim of this Appendix is to illustrate a simple application of the normal modes calculation. The example chosen here is directly related to the problem of finding the normal vibrational modes of a thin film epitaxially grown onto a low index surface plane of the substrate.

For small values of the phonon lateral wave vector \mathbf{Q} , a large number of the atoms in a slab (crystal plane) moves coherently i.e. in phase. For $\mathbf{Q} = 0$, the whole slab of atoms moves as a rigid body. Therefore, the forces acting between the atoms in a slab are not of importance in this case. Only the forces acting between the slabs matter. Therefore, we can simplify the geometry of the semi-infinite crystal by introducing a one-dimensional model of the crystal as in figure A.1.

M represents the mass of the adsorbed film slab per slab unit cell, k_1 is the force constant (spring "stiffness") acting between the slabs of the adsorbed film and k_2 is the force constant connecting the substrate material with the slab of the film closest to the substrate. The substrate itself is represented here as completely rigid and infinitely massive supporting material. Therefore, we shall neglect all the degrees of freedom connected with the substrate. For the Lagrangian of the system, L, we can write

$$L = T - V$$

$$= \frac{1}{2} \sum_{n} M(\eta'_{n})^{2}$$

$$- \frac{1}{2} \left[(k_{1} + k_{2})\eta_{1}^{2} + k_{1}\eta_{N}^{2} + \sum_{n=2}^{N-1} 2k_{1}\eta_{n}^{2} \right]$$

APPENDIX A 137

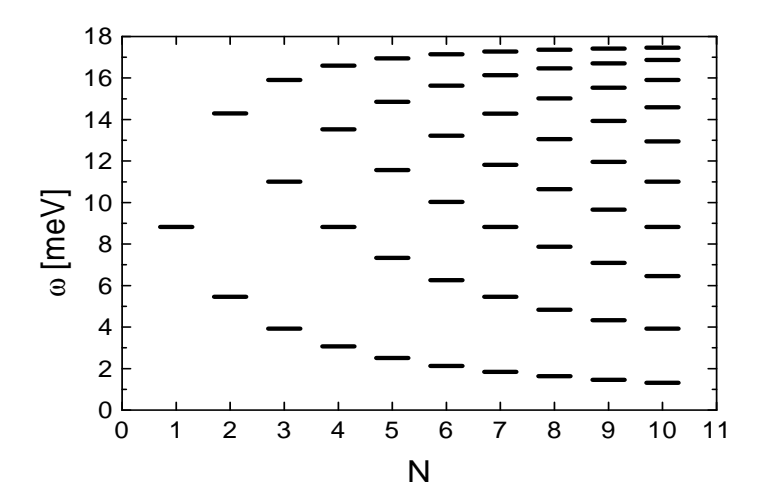


Figure A.2: Eigen-frequencies of adsorbed Ag film as a function of a number of Ag monolayers, N

+
$$\frac{1}{2}k_1\sum_{n=1}^{N-1}(\eta_n\eta_{n+1}+\eta_{n+1}\eta_n).$$
 (A.1)

Here T and V represent the kinetic and potential energy of the system, respectively, η_n is the generalized displacement coordinate of the n-th film slab where n=1 corresponds to the slab closest to the supporting substrate. N is the number of the slabs (monolayers) in the adsorbed film.

Clearly, for the potential and kinetic energy matrices defined in equations (4.4) and (4.5), respectively, we can write ¹:

$$V_{ij} = \begin{bmatrix} k_1 + k_2 & -k_1 & 0 & 0 & \dots & 0 & 0 & 0 \\ -k_1 & 2k_1 & -k_1 & 0 & \dots & 0 & 0 & 0 \\ 0 & -k_1 & 2k_1 & -k_1 & \dots & 0 & 0 & 0 \\ \vdots & \vdots & \ddots & \vdots & \ddots & \vdots \\ 0 & 0 & 0 & 0 & \dots & -k_1 & 2k_1 & -k_1 \\ 0 & 0 & 0 & 0 & \dots & 0 & -k_1 & k_1 \end{bmatrix}$$
(A.2)

¹Of course, special care must of in the cases when N=1 and N=2.

APPENDIX A

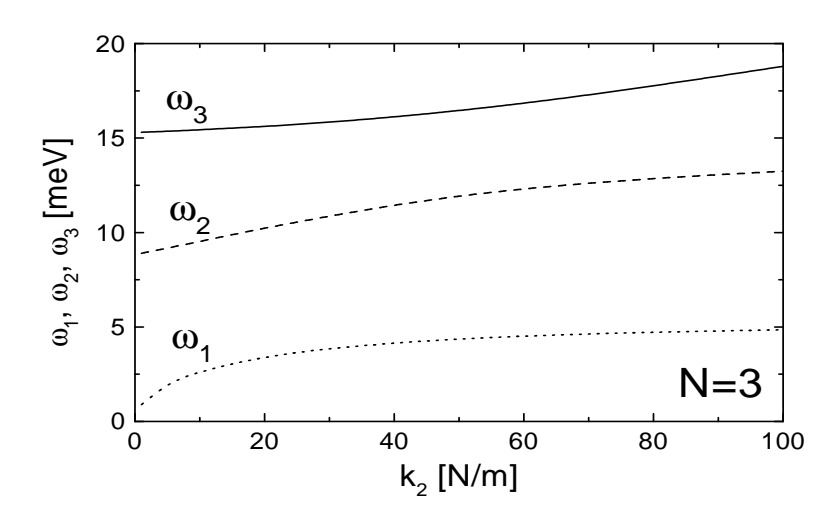


Figure A.3: Eigen-frequencies of three-monolayer Ag film as a function of force constant k_2 .

and

$$T_{ij} = \begin{bmatrix} M & 0 & 0 & \dots & 0 & 0 \\ 0 & M & 0 & \dots & 0 & 0 \\ \vdots & & & \ddots & & \\ \vdots & & & \ddots & & \\ 0 & 0 & 0 & \dots & M \end{bmatrix} = M \cdot 1_{N \times N}, \tag{A.3}$$

where $1_{N\times N}$ is $N\times N$ unit matrix. The normal frequencies of the system can be found by solving equation (4.12) which can be done analytically at least for $N\leq 3$. For larger N's one can numerically solve equation (4.12) by using well known diagonalization techniques [96]. Figure A.2 shows the normal frequencies of the system as a function of the number of slabs N. For this calculation we have taken M=107.87 amu, and $k_1=32.4$ N/m. These parameters correspond to silver slabs and force constant k_1 can be shown to produce a correct speed of sound in silver [81, 51, 97]. Note that for large values of N it becomes sensible to talk about the dispersion (wave vector) of the longitudinal mode of Ag, i.e. sound. The value of force constant k_2 depends on the nature of a supporting material. In figure A.2 we have taken $k_2=k_1$. Figure A.3 displays the normal frequencies of the system with 3 Ag monolayers (N=3) as a function of k_2 force constant.

The modes characterizing the vibrations of thin films at $\mathbf{Q} = 0$ are called *organ pipe modes* and were studied both experimentally (by the

APPENDIX A 139

use of helium atom scattering technique) and theoretically [98, 99].

Bibliography

- [1] A. Lahee and J.P. Toennies, Surface studies on the rebound, Physics World, April 1993, 61
- [2] A. Zangwill, *Physics at Surfaces*, Cambridge University Press, Cambridge, 1988
- [3] N.W. Ashcroft and N.D. Mermin, *Solid State Physics*, Saunders College Publishing, 1976
- [4] G. Santoro, A. Franchini, V. Bortolani, D.L. Mills and R.F. Wallis, to be published
- [5] V. Bortolani and A.C. Levi, *Atom-surface scattering theory*, La Rivisita del Nuovo Cimento **9**(11), 1 (1986)
- [6] V. Celli, Theory of Helium Scattering from Surface Phonons in Surface Phonons, eds W. Kress and F.W. de Wette, Springer-Verlag, Berlin, 1991
- [7] A. Šiber and B. Gumhalter, Debye-Waller factor in $He \to Cu(001)$ collisions revisited: the role of the interaction potentials, Surf. Sci. **385**, 270 (1997)
- [8] L.I. Schiff, Quantum Mechanics, McGraw-Hill, Singapore, 1968
- [9] J.C. Tully, Dynamics of gas-surface interactions: 3D generalized Langevin model applied to fcc and bcc surfaces, J. Chem. Phys. **73**(4), 1975 (1980)
- [10] J.C. Tully, G.H. Gilmer and M. Shugard, Molecular dynamics of surface diffusion. The motion of adatoms and clusters, J. Chem. Phys. **71**(4), 1630 (1979)
- [11] A.S. Davydov, Quantum Mechanics, Pergamon Press, 1976
- [12] G.D. Mahan, Many-Particle Physics, Plenum Press, New York, 1981

- [13] E. Müller-Hartmann, T.V. Ramakrishnan and G. Toulouse, *Localized Dynamic Perturbations in Metals*, Phys. Rev. B **3**(4), 1102 (1971)
- [14] A.C. Levi and H. Suhl, Quantum theory of atom-surface scattering: Debye-Waller factor, Surf. Sci. 88, 221 (1979)
- [15] H.D. Meyer, A semiclassical approach to inelastic scattering from solid surfaces and to the Debye-Waller factor, Surf. Sci. **104**, 117 (1981)
- [16] J. Böheim and W. Brenig, Theory of inelastic atom-surface scattering: examples of energy distributions, Z. Phys. B 41, 243 (1981)
- [17] R. Brako, Energy and momentum transfer in scattering of low-energy atoms on metal surfaces, Surf. Sci. 123, 439 (1982)
- [18] K. Burke and W. Kohn, Finite Debye-Waller factor for "classical" atom-surface scattering, Phys. Rev. B 43, 2477 (1991)
- [19] A. Šiber and B. Gumhalter, Comment on "Quantum scattering of heavy particles from a 10 K Cu(111) surface", Phys. Rev. Lett. 81(8), 1742 (1998)
- [20] D. Himes and V. Celli, *Inelastic scattering in the trajectory approximation and its improvements*, Surf. Sci. **272**, 139 (1992)
- [21] T. Brunner and W. Brenig, Elastic scattering, sticking and accommodation of noble gas atoms at a cold surface, Surf. Sci. 291, 192 (1993)
- [22] C.H. Chen, P.E. Siska and Y.T. Lee, Intermolecular potentials from crossed beam differential elastic scattering measurements, J. Chem. Phys. **59**, 601 (1973)
- [23] K.M. Smith, A.M. Rulis, G. Scoles, R.A. Aziz and V. Nain, J. Chem. Phys., Intermolecular forces in mixtures of helium with the heavier noble gases, 67, 152 (1977)
- [24] R.A. Aziz, U. Buck, H. Jónsson, J.-C. Ruiz-Suárez, B. Schmidt, G. Scoles, M.J. Slaman and J. Xu, Two and three-body forces in the interaction of He atoms with Xe overlayers adsorbed on (0001) graphite, J. Chem. Phys. 91, 6477 (1989)
- [25] D. Farias and K.-H. Rieder, Atomic beam diffraction from solid surfaces, Rep. Prog. Phys. **61**, 1575 (1998)
- [26] V. Celli, D. Eichenauer, A. Kaufhold and J.P. Toennies, Pairwise additive ab initio potential for the elastic scattering of He atoms from the LiF(001) crystal surface, J. Chem. Phys 83(5), 2504 (1985)

- [27] D. Eichenauer and J.P. Toennies, Theory of resonant inelastic onephonon scattering of He atoms from a LiF(001) single crystal surface, J. Chem. Phys. 85(1), 532 (1986)
- [28] D. Eichenauer, U. Harten, J.P. Toennies and V. Celli, *Interaction potential for one-phonon inelastic He-Cu(111) and He-Ag(111) scattering*, J. Chem. Phys. **86**(6), 3693 (1987)
- [29] J.M. Hutson and C. Schwartz, Selective adsorption resonances in the scattering of helium atom from xenon coated graphite: Close-coupling calculations and potential dependence, J. Chem. Phys. **79**(10), 5179 (1979)
- [30] N.D. Lang, Interaction between closed-shell systems and metal surfaces, Phys. Rev. Lett. 46, 842 (1981)
- [31] K. Lenarčič-Poljanec, M. Hodošček, D. Lovrić and B. Gumhalter, Interaction of He atoms with (111) and (100) surfaces of Cu and Ni, Surf. Sci. 251/252, 706 (1991)
- [32] B. Kohler, P. Ruggerone and M. Scheffler, Anomalies in He atom scattering spectra of the H-covered Mo(110) and W(110) surfaces, Surf. Sci. 368, 213 (1996)
- [33] M. Petersen, S. Wilke, P. Ruggerone, B. Kohler and M. Scheffler, Scattering of rare-gas atoms at a metal surface: evidence of anticorrugation of the helium-atom potential energy surface and the surface electron density, Phys. Rev. Lett. **76**(6), 995 (1996)
- [34] B.I. Lundqvist, E. Hult, H. Rydberg, A. Bogicevic, J. Stromquist and D.C. Langreth, Density functionals and Van Der Waals interactions at surfaces, Prog. Surf. Sci. 59, 149 (1998)
- [35] C. Kaden, P. Ruggerone, J.P. Toennies, G. Zhang and G. Benedek, Electronic pseudocharge model for the Cu(111) longitudinal-surface-phonon anomaly observed by helium-atom scattering, Phys. Rev. B 46(20), 13509 (1992)
- [36] A. Franchini, G. Santoro, V. Bortolani, A. Bellman, D. Cvetko, L. Floreano, A. Morgante, M. Peloi, F. Tommasini and T. Zambelli, *Role of the He atom surface potential on the Cu(001) phonon determination*, Surface Review and Letters 1(1), 67 (1994)
- [37] N.S. Luo, P. Ruggerone, J.P. Toennies and G. Benedek, Analysis of inelastic He atom scattering spectra on Cu(001): Evidence for contribution of surface electronic oscillations in Proceedings of the Working Party on Inelastic Energy Transfer in Interactions

- with Surfaces and Adsorbates, eds B. Gumhalter, A.C. Levi and F. Flores, World Scientific, 1993
- [38] J.E. Lennard-Jones and A.F. Devonshire, Proc. Roy. Soc. London, Ser. A 137, 703 (1937)
- [39] A.F. Devonshire, Proc. R. Soc. London, Ser. A 158, 253 (1937)
- [40] G. Gašparović, Utjecaj dugodosežne komponente potencijala na Debye-Wallerov faktor pri raspršenjima atoma na povrsinama, B.Sc. Thesis, University of Zagreb, 1997, unpublished
- [41] C. Carraro and M.W. Cole, Sticking coefficient at ultralow energy: quantum reflection, Prog. Surf. Sci. 57(1), 61 (1998)
- [42] N. Esbjerg and J.K. Norskov, Dependence of the He-scattering potential at surfaces on the surface-electron-density profile, Phys. Rev. Lett. 45, 807 (1980)
- [43] H. Goldstein, Classical mechanics, Addison-Wesley, 1980
- [44] W. Greiner and J. Reinhardt, *Field Quantization*, Springer Verlag, Berlin, 1996
- [45] A. Franchini, Surface phonon linewidth in Proceedings of the Working Party on Inelastic Energy Transfer in Interactions with Surfaces and Adsorbates, eds B. Gumhalter, A.C. Levi and F. Flores, World Scientific, 1993
- [46] F.W. de Wette, Study of Surface Phonons by the Slab Method in Surface Phonons, eds W. Kress and F.W. de Wette, Springer-Verlag, Berlin, 1991
- [47] G. Santoro and V. Bortolani, Theory of inelastic He atom scattering and surface phonons in Proceedings of the Working Party on Inelastic Energy Transfer in Interactions with Surfaces and Adsorbates, eds B. Gumhalter, A.C. Levi and F. Flores, World Scientific, 1993
- [48] J.E. Black, A. Franchini, V. Bortolani, G. Santoro and R.F. Wallis, Surface-phonon dispersion on Cu(110): a comparison of experiment and theory, Phys. Rev. B **36**, 2996 (1987)
- [49] Ch. Kittel, Quantum Theory of solids, John Wiley & Sons, 1963
- [50] V.G. Faires, *Thermodynamics*, The Macmillan Company, New York, 1966

- [51] U. Harten, J.P. Toennies and Ch. Wöll, Helium Time-of-flight Spectroscopy of Surface-phonon Dispersion Curves of the Noble Metals, Faraday Discuss. Chem. Soc. 80, 137 (1985)
- [52] V. Celli, G. Benedek, U. Harten, J.P. Toennies, R.B. Doak and V. Bortolani, Atom-surface interaction in inelastic scattering: He/Ag(111), Surf. Sci. 143, L376 (1984)
- [53] V. Bortolani, A. Franchini, N. Garcia, F. Nizzoli and G. Santoro, Calculation of potential cutoff for one-phonon atom-surface scattering, Phys. Rev. B 28, 7358 (1983)
- [54] A. Šiber, B. Gumhalter and J.P. Toennies, Study of energy transfer in helium atom scattering from surfaces, Vacuum 54, 315 (1999)
- [55] A. Šiber, B. Gumhalter, J. Braun, A.P. Graham, M.F. Bertino, J.P. Toennies, D. Fuhrmann and Ch. Wöll, Combined He-atom scattering and theoretical study of the low-energy vibrations of physisorbed monolayers of Xe on Cu(111) and Cu(001), Phys. Rev. B 59(8), 5898 (1999)
- [56] A. Bilić and B. Gumhalter, Quantum versus semiclassical treatment of multiphonon effects in He-atom scattering from surfaces, Phys. Rev. B 52, 12307 (1995)
- [57] B. Gumhalter, A. Šiber and J.P. Toennies, Recovery temperature for nonclassical energy transfer in atom-surface scattering, Phys. Rev. Lett. 83, 1375 (1999)
- [58] F. Althoff, T. Andersson and S. Andersson, Quantum scattering of heavy particles from a 10 K Cu(111) surface, Phys. Rev. Lett. 79, 4429 (1997)
- [59] N. Cabrera, V. Celli, F.O. Goodman and R. Manson, Scattering of atoms by solid surfaces. I., Surf. Sci. 19, 67 (1970)
- [60] M. Sunjić and A. A. Lucas, Multiple Plasmon Effects in the Energy-Loss Spectra of Electrons in Thin Films, Phys. Rev. B 3(3), 719 (1971)
- [61] J. Idiodi, V. Bortolani, A. Franchini, G. Santoro and V. Celli, Calculation of the Debye-Waller factor for atom-surface scattering: He on Ag(111), Phys. Rev. B 35, 6029 (1987)
- [62] E.P. Gross, Transformation Theory in Mathematical Methods in Solid State and Superfluid Theory, eds R.C. Clark and G.H. Derrick, Oliver and Boyd, Edinburgh, 1969

- [63] D. Dunn, Electron-phonon interactions in an insulator, Canadian Journal of Physics **53**(4) (1975)
- [64] K. Burke, B. Gumhalter and D.C. Langreth, Nearly elastic scattering and the trajectory approximation, Phys. Rev. B 47(19), 12852 (1993)
- [65] B. Gumhalter, K. Burke and D.C. Langreth, Evolution operator and energy spectrum of a quasiclassical particle interacting with bosons: application to atom surface scattering, Surface Review and Letters 1(1), 133 (1994)
- [66] L.H. Ryder, Quantum Field Theory, Cambridge University Press, Cambridge, 1989
- [67] R. Kubo, Generalized Cumulant Expansion Method, J. Phys. Soc. Japan 17(7), 1100 (1962)
- [68] W. Brenig, Comment on "Quantum versus semiclassical treatment of multiphonon effects in He-atom scattering from surfaces", Phys. Rev. B 55(15), 10119 (1997)
- [69] B. Gumhalter and A. Bilić, Multiphonon atom-surface scattering in the collision system $He \rightarrow Cu(001)$, Surf. Sci. **370**, 47 (1997)
- [70] P. Zeppenfeld, K. Kern, R. David, K. Kuhnke and G. Comsa, Lattice dynamics of Cu(110): high-resolution He-scattering study, Phys. Rev. B 38, 12329 (1988)
- [71] A. Chizmeshya and E. Zaremba, The interaction of rare gas atoms with metal surfaces: a scattering theory approach, Surf. Sci. 268, 432 (1992)
- [72] J. Braun, D. Fuhrmann, M.F. Bertino, A.P. Graham, J.P. Toennies, Ch. Wöll, A. Bilić and B. Gumhalter, Multiphonon He atom scattering from Xe overlayers on Cu(111) and Cu(001) surfaces, J. Chem. Phys. 106, 9922 (1997)
- [73] J. Braun, D. Fuhrmann, A. Šiber, B. Gumhalter and Ch. Wöll, Observation of a zone-center gap in the longitudinal mode of an adsorbate overlayer: xenon on Cu(111), Phys. Rev. Lett. 80, 125 (1998).
- [74] A.P. Graham, M.F. Bertino, F. Hofmann, J.P. Toennies and Ch. Wöll, Experimental determination of a longitudinal phonon dispersion curve in a quasi-two-dimensional system, J. Chem. Phys. **106**, 6194 (1997)
- [75] L.W. Bruch, Experimental determination of a longitudinal phonon dispersion curve in a quasi-two-dimensional system - comment, J. Chem. Phys. 107, 4443 (1997)

- [76] L.W. Bruch, A.P. Graham and J.P. Toennies, Vibrations of the commensurate monolayer solid Xe/Pt(111), Molecular Physics 95, 579 (1998)
- [77] J. Ellis, A.P. Graham and J.P. Toennies, Quasielastic helium atom scattering from a two-dimensional gas of Xe atoms on Pt(111), Phys. Rev. Lett. 82(25), 5072 (1999)
- [78] M. Cieplak, E.D. Smith and M.O. Robbins, Molecular origins of friction The force on adsorbed layers, Science 265, 1209 (1994)
- [79] B.N.J. Persson and A. Nitzan, Linear sliding friction on the origin of the microscopic friction for Xe on silver, Surf. Sci. **367**, 261 (1996)
- [80] U. Kleinekathöfer, K.T. Tang, J.P. Toennies and C.L. Yiu, Potentials for some rare gas and alkali-helium systems calculated from the surface integral method, Chem. Phys. Lett. 249, 257 (1996); U. Kleinekathöfer, Ph.D Thesis, University Göttingen, 1996.
- [81] Ch. Wöll, Phonons on surfaces: the importance of structure and adsorbates, Appl. Phys. A Solids and Surfaces **53**, 377 (1991)
- [82] C. Ramseyer, C. Girardet, P. Zeppenfeld, J. Goerge, M. Buchel and G. Comsa, Xe monolayer adsorption on Cu(110): experiments and interaction calculations, Surf. Sci. 313, 251 (1994)
- [83] Andrew Graham, private communication
- [84] R.J. Glauber, Time-Dependent Displacements Correlations and Inelastic Scattering by Crystals, Phys. Rev. 98, 1692 (1955)
- [85] L. van Hove, Correlations in Space and Time and Born Approximation Scattering in Systems of Interacting Particles, Phys.Rev. 95, 249 (1954)
- [86] B. Gumhalter, Different aspects of the Debye-Waller factor in various atom-surface scattering theories, Surf. Sci. **347**, 237 (1996)
- [87] B. Gumhalter and D.C. Langreth, Unified model of diffractive and multiphonon He atom scattering from adsorbates: Holstein renormalization of the interactions and the complete Debye-Waller factor, Phys. Rev. B 60, 2789 (1999)
- [88] F. Althoff, T. Andersson and S. Andersson, Reply to Comment on "Quantum scattering of heavy particles from a 10 K Cu(111) surface", Phys. Rev. Lett. 81(8), 1743 (1998)

- [89] L.D. Landau and E.M. Lifšic, Kvantna mehanika, nerelativistička teorija, Gradjevinska knjiga, Beograd, 1966
- [90] J. Lapujoulade, J. Perreau and A. Karra, The thermal attenuation of elastic scattering of helium from copper single crystal surfaces, Surf. Sci. 129, 59 (1983)
- [91] G. Benedek and J.P. Toennies, Systematic trends in the normal enhancement of the phonon annarmonicity at the surface of metals, Phys. Rev. B 46(20), 13643 (1992)
- [92] G. Benedek, Van Hove singularities of the surface phonon density from inelastic reflection of atoms, Phys. Rev. Lett. **35**, 234 (1975)
- [93] S. Andersson, L. Wilzen, M. Persson and J. Harris, *Sticking in the quantum regime:* H_2 and D_2 on Cu(100), Phys. Rev. B **40**, 8146 (1989)
- [94] F. Hofmann, J.P. Toennies and J.R. Manson, An experimental and theoretical study of the transition from single phonon to multiphonon atom-surface scattering, Surf. Sci. **349**, L184 (1996)
- [95] F. Hofmann, J.P. Toennies and J.R. Manson, A comprehensive experimental study of the dynamical interaction of He atoms with Cu(001) surface phonons, J. Chem. Phys. 101, 10155 (1994)
- [96] Subroutine F0F2DF from the Numerical Algorithm Group (NAG) FORTRAN library
- [97] http://www.shef.ac.uk/chemistry/web-elements/, Web elements
- [98] N.S. Luo, P. Ruggerone, J.P. Toennies, G. Benedek, V. Celli, Intrafilm and interface interaction determination by inelastic helium atom scattering, Journal of Electron Spectroscopy and Related Phenomena, 64-5, 755 (1993)
- [99] D.Fuhrmann, E. Hulpke, W. Steinhögl, Successive multilayer desorption from ultrathin alkali-metal films studied with helium-atom scattering, Phys. Rev. B 57, 4798 (1998)

Acknowledgements

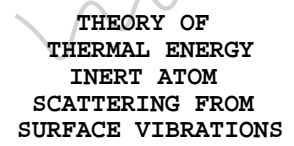
I wish to thank dr. Jens Braun, prof. dr. Christof Wöll and dr. Dirk Fuhrmann for many interesting discussions, especially concerning the experimental aspects of inert atom scattering from surfaces. I thank dr. Andrew Graham and dr. Dirk Fuhrmann for unpublished experimental data which they kindly agreed to share with me. Some of this data was presented in this work (He \rightarrow Xe(111) and He \rightarrow Xe/C(111) systems).

I also enjoyed constructive scientific interference with my colleagues and former coworkers *Ante Bilić* and *Goran Gašparović*. I have been lucky to have an invaluable help from my colleague and friend *Marko Cvitaš* who has taught me a lot about phonons.

Special thanks go to dr. Branko Gumhalter who introduced me to this interesting subject and spent a lot of hours teaching me and working together with me on problems described in this thesis.

My family and friends cannot be thanked enough concerning the form of the thesis.

Antonio Šiber



Antonio Šiber

A. Šiber, Theory of thermal energy inert atom scattering from surface vibrations

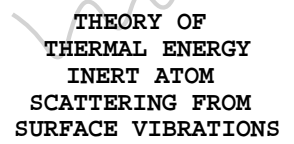
A. Šiber, Teorija neelastičnog raspršenja inertnih atoma na vibracijama kristalnih površina

Životopis

Rodjen sam 27.11.1972. u Zagrebu. Studij fizike pri Prirodoslovnomatematičkom fakultetu Sveučilišta u Zagrebu završio sam 02.07.1996. diplomskim radom "Utjecaj karakteristika potencijala na Debye-Wallerov faktor u raspršenjima atoma na površinama" pod vodstvom dr. Branka Gumhaltera. Tijekom studija osvojio sam Rektorovu nagradu za najbolji studentski rad u godini 1995 za rad "Principi kvantne mehanike na primjeru rezonantnog tuneliranja" koji sam izradio u suradnji sa Hrvojem Buljanom pod mentorstvom prof. dr. Marijana Šunjića. Od 01.02.1997. radim kao znanstveni novak Ministarstva znanosti i tehnologije Republike Hrvatske na temi dr. Gumhaltera pri Institutu za fiziku, Zagreb.

Slijedi popis radova prema Current Contents evidenciji do 01.09.1999.:

- A. Šiber and B. Gumhalter, Surf. Sci. 385, 270 (1997)
- J. Braun, D. Fuhrmann, A. Šiber, B. Gumhalter and Ch. Wöll, Phys. Rev. Lett. **80**, 125 (1998)
- A. Šiber and B. Gumhalter, Phys. Rev. Lett. **81**, 1742 (1998)
- A. Šiber, B. Gumhalter, J. Braun, A.P. Graham, M.F. Bertino, J.P. Toennies, D. Fuhrmann and Ch. Wöll, Phys. Rev. B **59**, 5898 (1999)
- A. Šiber, B. Gumhalter and J.P. Toennies, Vacuum 54, 315 (1999)
- B. Gumhalter, A. Šiber and J.P. Toennies, Phys. Rev. Lett. 83, 1375 (1999)



Antonio Šiber

A. Šiber, Theory of thermal energy inert atom scattering from surface vibrations

A. Šiber, Teorija neelastičnog raspršenja inertnih atoma na vibracijama kristalnih površina

Curriculum Vitae

I was born on 27th of November, 1972 in Zagreb. I finished undergraduate study of physics at The Faculty of Natural Sciences and Mathematics, University of Zagreb on 2nd of July, 1996 with the B. Sc. thesis "The influence of the interaction potential characteristics on the Debye-Waller factor in scattering of atoms from surfaces" under a tutorship of dr. Branko Gumhalter. During the undergraduate study, I won the Rector's award for the best student work in year 1995 for the work entitled "The principles of quantum mechanics in double barrier resonant tunneling" which I made with my colleague Hrvoje Buljan under the supervision of prof. dr. Marijan Šunjić. Since 1st of February, 1997, I work as a research assistant of The Ministry of Science and Technology of Republic of Croatia on dr. Gumhalter's research theme at The Institute of Physics, Zagreb.

The list of papers I published until 1st of September 1999 according to *Current Contents* database follows:

- A. Šiber and B. Gumhalter, Surf. Sci. **385**, 270 (1997)
- J. Braun, D. Fuhrmann, A. Šiber, B. Gumhalter and Ch. Wöll, Phys. Rev. Lett. **80**, 125 (1998)
- A. Šiber and B. Gumhalter, Phys. Rev. Lett. 81, 1742 (1998)
- A. Šiber, B. Gumhalter, J. Braun, A.P. Graham, M.F. Bertino, J.P. Toennies, D. Fuhrmann and Ch. Wöll, Phys. Rev. B 59, 5898 (1999)
- A. Šiber, B. Gumhalter and J.P. Toennies, Vacuum 54, 315 (1999)
- B. Gumhalter, A. Siber and J.P. Toennies, Phys. Rev. Lett. 83, 1375 (1999)